

# **A Surlyn<sup>®</sup> Ionomer as a Self-Healing and Self-Sensing Composite**

**Phillip John Reynolds**  
ID 618 217

**A thesis submitted to the  
University of Birmingham  
for the degree of  
MRes in the Science and Engineering of Materials**

**Department of Metallurgy and Materials  
University of Birmingham  
December 2011**

UNIVERSITY OF  
BIRMINGHAM

**University of Birmingham Research Archive**

**e-theses repository**

This unpublished thesis/dissertation is copyright of the author and/or third parties. The intellectual property rights of the author or third parties in respect of this work are as defined by The Copyright Designs and Patents Act 1988 or as modified by any successor legislation.

Any use made of information contained in this thesis/dissertation must be in accordance with that legislation and must be properly acknowledged. Further distribution or reproduction in any format is prohibited without the permission of the copyright holder.

# **A Surlyn<sup>®</sup> Ionomer as a Self-Healing and Self-Sensing Composite**

## **Abstract**

The ionomer known by its trademark name as Surlyn<sup>®</sup> has recently become an area of interest as it reportedly has the ability to self-heal. In this project, new techniques were employed to investigate three grades of Surlyn<sup>®</sup> (PC2000, 9910 and 1706) with a view to the development of a self-healing and self-sensing composite. The study initially focused on the development of Surlyn<sup>®</sup> plaques and Surlyn<sup>®</sup> fibres; reporting on both the self-healing and self-sensing capabilities of Surlyn<sup>®</sup>. Grade PC2000 fibres were shown to have the highest light transmission results and clearly showed the ability to act as self-sensing light guides. The crack healing ability of Surlyn<sup>®</sup> fibres and Surlyn<sup>®</sup> film was studied during mode I fracture tests and Surlyn<sup>®</sup> was shown to act as a crack arrestor increasing the fracture toughness of carbon-fibre and also suggesting that Surlyn<sup>®</sup> is able to self-heal. Surlyn<sup>®</sup> films and Surlyn<sup>®</sup> fibres were then fabricated with VTM 264 glass-fibre pre-preg with a view to producing a self-healing and self-sensing composite. Further investigation into the self-healing and self-sensing abilities of the fabricated Surlyn<sup>®</sup> composites and Surlyn<sup>®</sup> fibres is discussed.

## **Acknowledgements**

I would like to thank Dr. Stephen Kukureka and Professor Gerard Fernando for their guidance and help during the course of the project and also to Abilash Nair, Dee Harris and Jonathon Burns for their assistance. I would also like to thank my family who have supported me throughout my studies and have always believed in me when I doubted myself. I will always be thankful.

## Table of Contents

	<u>Page</u>
<b>1.0 Introduction.....</b>	<b>1</b>
<b>2.0 Aims.....</b>	<b>3</b>
<b>3.0 Literature Review.....</b>	<b>4</b>
3.1 Ionomers.....	4
3.1.1 Ionomer Definition.....	4
3.1.2 Production of Ionomers.....	4
3.1.3 Ionomer Composition.....	5
3.1.4 Ionomer Morphology.....	5
3.1.4.1 Ionic Aggregate Formation.....	5
3.1.4.2 The Effect of Ionic Aggregate on Thermal, Mechanical and Physical Properties.....	8
3.2 Surlyn <sup>®</sup> .....	10
3.2.1 Surlyn <sup>®</sup> Definition.....	10
3.2.2 Production of Surlyn <sup>®</sup> .....	10
3.2.3 Properties and Applications.....	11
3.3 Self-healing Capacity of Surlyn <sup>®</sup> and other Ionomers.....	12

3.4 Other Self-healing Mechanisms and Systems.....	21
3.4.1 Intrinsic Self-healing Mechanisms.....	22
3.4.1.1 Diels-Alder based polymers.....	22
3.4.1.2 Photodimerization based polymers.....	22
3.4.1.3 Hydrogen bonded and Metal-ligand coordination polymers.....	23
3.4.2 Extrinsic Self-healing Mechanisms.....	24
3.4.2.1 Hollow tubes and Glass fibres.....	24
3.4.2.2 Microcapsules.....	26
3.4.2.3 Microvascular Networks.....	28
3.5 Self-sensing Composites.....	30
<b>4.0 Methodology.....</b>	<b>34</b>
4.1 Materials.....	34
4.1.1 Surlyn Grades <sup>®</sup> .....	34
4.2 Sample Preparation and Preliminary Characterisation.....	34
4.2.1 Preparation of Thin Plaques from Pellets.....	34
4.2.2 Density Measurements.....	35
4.2.3 Differential Scanning Calorimetry.....	36
4.2.4 Fourier Transform Infrared Spectroscopy.....	37
4.2.5 Refractive Index Measurements.....	37

4.3 Production of Surlyn <sup>®</sup> PC2000 and Surlyn <sup>®</sup> 9910 Thick Plaques.....	38
4.3.1 Production of Thick Plaques.....	38
4.3.2 Monitoring the Temperature Profile within a Thick Plaque (Surlyn <sup>®</sup> PC2000 and Surlyn <sup>®</sup> 9910).....	39
4.4 Production of Surlyn <sup>®</sup> Composites (PC2000).....	41
4.4.1 Production of Glass Fibre Reinforced Surlyn <sup>®</sup> Composites.....	41
4.5 Extrusion of Surlyn <sup>®</sup> Fibres.....	42
4.5.1 Development of a Methodology to Extrude Surlyn <sup>®</sup> fibres.....	42
4.6 Characterisation of the Light Transmission.....	44
4.6.1 Light Transmission through the Extruded Surlyn <sup>®</sup> fibres.....	44
4.6.2 Comparison of Light Transmission between Surlyn PC2000 and PMMA fibres.....	45
4.6.3 Effect of Fibre Connection on Light Transmission Measurements.....	45
4.6.4 Light Transmission Distance Measurements for Extruded Thin Surlyn <sup>®</sup> fibres.....	46
4.6.5 Fibre Connection Methods using SMA Connectors.....	46
4.6.6 Light Transmission Measurements through Extruded Thin Surlyn <sup>®</sup> fibres.....	47
4.6.7 Attenuation Experiments.....	49
4.7 Fibre Characterisation.....	50

4.7.1 Fibre Density Measurements.....	50
4.7.2 Differential Scanning Calorimetry.....	50
4.8 Fibre Analysis.....	50
4.9 Sample Storage.....	51
4.10 Surlyn® Composite Development.....	51
4.10.1 Production of Composites.....	51
4.10.1.1 General Pre-preg Lay-up.....	51
4.10.1.2 Vacuum Bagging Procedure.....	52
4.10.1.3 Curing of Composite Samples.....	53
4.10.2 Self-healing Composite Development.....	55
4.10.3 Self-healing/Self-sensing Composite Development.....	57
4.10.4 Crack Arrestor Composites.....	58
4.10.4.1 Crack Arrestors.....	59
4.10.4.2 Composite Set-up.....	60
4.10.4.3 $G_{Ic}$ Sample Preparation.....	61
4.10.4.4 $G_{Ic}$ Test Procedure.....	62
4.10.4.5 $G_{Ic}$ Calculation.....	63
4.10.4.6 Test Specimen Analysis.....	65
<b>5.0 Results and Discussion.....</b>	<b>66</b>



5.1 Preliminary Characterisation.....	67
5.1.1 Density Measurements.....	67
5.1.2 Differential Scanning Calorimetry.....	68
5.1.3 Fourier Transform Infrared Spectroscopy.....	72
5.1.4 Refractive Index Measurements.....	74
5.2 Production of Surlyn <sup>®</sup> PC2000 and Surlyn <sup>®</sup> 9910 Thick Plaques.....	76
5.2.1 Production of Thick Plaques.....	76
5.2.2 Monitoring the Temperature Profile within a Thick Plaque (Surlyn <sup>®</sup> PC2000 and 9910).....	78
5.3 Production <sup>®</sup> of Surlyn <sup>®</sup> Composites.....	80
5.3.1 Production of Glass Fibre Reinforced Composites.....	80
5.4 Extrusion of Surlyn <sup>®</sup> Fibres.....	82
5.4.1 Development of a Methodology to Extrude Surlyn <sup>®</sup> Fibres.....	82
5.5 Characterisation of the Light Transmission.....	89
5.5.1 Light Transmission measurements through extruded thick Surlyn <sup>®</sup> fibres.....	89
5.5.2 Comparison of Light Transmission between Surlyn <sup>®</sup> PC2000 and PMMA fibres.....	93
5.5.3 Effect of Fibre Connection on Light Transmission Measurements.....	95

5.5.4 Light Transmission Distance Measurements for Extruded Thin Surlyn <sup>®</sup> fibres.....	97
5.5.5 Fibre Connection Methods using SMA Connectors.....	100
5.5.6 Light Transmission Measurements through Extruded Thin Surlyn <sup>®</sup> fibres.....	101
5.5.7 Attenuation Experiments.....	105
5.6 Fibre Characterisation.....	108
5.6.1 Density Measurements.....	108
5.6.2 Differential Scanning Calorimetry.....	109
5.7 Self-Healing and Self-sensing Composite Development.....	112
5.7.1 Self-Healing Composite Development.....	112
5.7.2 Self-Healing and Self-Sensing Composite Development.....	114
5.7.3 Crack Arrestor Composites.....	116
5.7.3.1 Reference Samples.....	117
5.7.3.2 Surlyn <sup>®</sup> PC2000 Fibre Samples.....	121
5.7.3.3 Surlyn <sup>®</sup> 1706 Film Samples.....	125
5.7.3.4 Surlyn <sup>®</sup> 1706 Punctured Film Samples.....	130
<b>6.0 Conclusion.....</b>	<b>138</b>
<b>7.0 Future Work.....</b>	<b>140</b>

<b>8.0 Appendices.....</b>	<b>142</b>
A1.1 Figure 1a – Raw data for Surlyn® PC2000 density measurements.....	142
A1.2 Figure 1b - Raw data for Surlyn® 9910 density measurements.....	142
A1.3 Figure 1c – Raw data for Surlyn® 1706 density measurements.....	142
A2.1 Figure 2a – DSC trace of Surlyn® 9910; one cycle.....	143
A2.2 Figure 2b – DSC trace of Surlyn® 1706; one cycle.....	144
A3.1 Figure 3a – DSC trace of Surlyn® 9910; three cycles.....	145
A3.2 Figure 3b - DSC trace of Surlyn® 1706; three cycles.....	147
A4. Figure 4 - (a) Typical Load versus displacement curve and (b) interlaminar fracture toughness ( $G_{Ic}$ ) versus crack length for reference samples two – five.....	149
A5. Figure 5 - (a) Typical Load versus displacement curve and (b) interlaminar fracture toughness ( $G_{Ic}$ ) versus crack length for Surlyn® PC2000 fibre samples two, three and five.....	151
A6. Figure 6 - (a) Typical Load versus displacement curve and (b) interlaminar fracture toughness ( $G_{Ic}$ ) versus crack length for Surlyn® 1706 film, samples one, three, four and five.....	152
A7. Figure 7 - (a) Typical Load versus displacement curve and (b) interlaminar fracture toughness ( $G_{Ic}$ ) versus crack length for punctured Surlyn® 1706 film, samples one, two, four and five.....	154
<b>9.0 References.....</b>	<b>156</b>

## List of Figures

	<b>Page</b>
<b>Figure 1</b> – Proposed conformations of structures of ionomers.....	5
<b>Figure 2</b> – Schematic representation of the Eisenberg-Hird-More model.....	6
<b>Figure 3</b> – Schematic diagram showing the growth of multiplets and the formation of clusters with increases in ionic content.....	8
<b>Figure 4</b> – Diagram showing the model for the order-disorder transition of ionic clusters.....	9
<b>Figure 5</b> – Diagram of EMAA neutralized with sodium.....	11
<b>Figure 6</b> – Schematic diagram of the order-disorder healing theory presented by <i>Fall</i> .....	12
<b>Figure 7</b> – Thermal IR image of React-A-seal® following puncture from a 9 mm bullet (pink area ~ 98 °C and blue area ~ 28 °C).....	13
<b>Figure 8</b> – Image of elastic hinge after sawing of React-A-Seal®.....	15
<b>Figure 9</b> – Image of the peel test sample.....	16

<b>Figure 10</b> – Diagram of healing mechanism in hollow fiber-based self-healing composites.....	26
<b>Figure 11</b> – Diagram of microencapsulated healing system.....	27
<b>Figure 12</b> – S.E.M. image of urea-formaldehyde microcapsules.....	28
<b>Figure 13</b> – Schematic diagram of the self-healing structure composed of a micro vascular substrate and a brittle epoxy coating containing an embedded catalyst.....	29
<b>Figure 14</b> – Schematic diagram of interpenetrating microvascular network.....	30
<b>Figure 15</b> – Picture showing fabrication set-up for producing thick Surlyn <sup>®</sup> plaque incorporating a k-type thermocouple.....	39
<b>Figure 16</b> – Schematic diagram of the location of the thermocouples in the thick Surlyn <sup>®</sup> plaque; thermocouples were spaced 2 mm apart.....	40
<b>Figure 17</b> - Schematic diagram of the custom-made PTFE mould that was used to fabricate the SDOF reinforced Surlyn <sup>®</sup> composites.....	41
<b>Figure 18</b> – A photograph showing the experimental set-up for extruding and hauling off different diameter Surlyn <sup>®</sup> fibres.....	42

<b>Figure 19</b> – Photograph of light transmission intensity measurement set-up.....	45
<b>Figure 20</b> – Photograph of fibre light guide measurement set-up.....	46
<b>Figure 21</b> – Schematic diagram showing the three different methods used to connect thin Surlyn <sup>®</sup> PC2000 fibres with SMA connectors.....	47
<b>Figure 22</b> – Photograph of light transmission intensity measurement set-up.....	48
<b>Figure 23</b> – Schematic diagram of vacuum bagging procedure.....	53
<b>Figure 24</b> – Photograph of autoclave used to cure composite samples.....	54
<b>Figure 25</b> – Schematic diagrams showing different lay-up sequences for the Surlyn <sup>®</sup> 1706 film and glass fibre composite samples.....	56
<b>Figure 26</b> – Schematic diagrams showing different lay-up sequences for the Surlyn <sup>®</sup> PC2000 fibres and glass fibre composite samples.....	58
<b>Figure 27</b> – Photograph of custom made puncture device.....	59
<b>Figure 28</b> – Schematic diagram showing the set-up at the centre of the 16 ply Surlyn <sup>®</sup> film composite plate.....	60

<b>Figure 29</b> – Photograph of $G_{Ic}$ test specimen.....	61
<b>Figure 30</b> – Photograph of Mode I experimental set-up.....	62
<b>Figure 31</b> – Data and geometry for CBT and MCC calculations.....	64
<b>Figure 32</b> – DSC of Surlyn <sup>®</sup> PC2000; one cycle.....	69
<b>Figure 33</b> - DSC of Surlyn <sup>®</sup> PC2000; three cycles.....	71
<b>Figure 34</b> – MFTIR transmission spectrum of Surlyn <sup>®</sup> (a) PC2000, (b) 9910 and (c) 1706.....	74
<b>Figure 35</b> – Heating/Cooling curves for production of thick Surlyn <sup>®</sup> plaques (a) PC2000 and (b) 9910.....	77
<b>Figure 36</b> – Image of thick Surlyn <sup>®</sup> PC2000 plaque containing a k – type thermocouple.....	78
<b>Figure 37</b> – Graphs showing monitored heat flow through thick Surlyn <sup>®</sup> plaques.....	79
<b>Figure 38</b> – Photograph of plaque made from Surlyn <sup>®</sup> PC2000 and small diameter optical fibres.....	81

<b>Figure 39</b> – Photograph demonstrating the Surlyn® composite bleeding light.....	81
<b>Figure 40</b> – Graph showing average diameter of thick Surlyn® PC2000 fibres.....	83
<b>Figure 41</b> – (a) 5x magnification image of extruded Surlyn® PC2000 fibre (10 kg) surface area and (b) SEM image of Surlyn® PC2000 fibre (10 kg) cleaved end.....	84
<b>Figure 42</b> – Graph showing average diameter of thick Surlyn® 9910 fibres.....	85
<b>Figure 43</b> – (a) 5x magnification image of extruded Surlyn® PC2000 fibre (10 kg) surface area and (b) SEM image of Surlyn® PC2000 fibre (10 kg) cleaved end.....	86
<b>Figure 44</b> – Graph showing average diameter of fibres extruded using adapted haul off machine.....	87
<b>Figure 45</b> – (a) 5x magnification image of extruded thin Surlyn® PC2000 fibre (Setting six) surface area and (b) SEM image of Surlyn® PC2000 fibre (Setting six) cleaved end.....	88
<b>Figure 46</b> – (a) Image of curved Fibre and (b) 5x magnification image of fibre Edge.....	90



<b>Figure 47</b> – (a) Image of fibre and (b) 5x magnification image of fibre edge.....	91
<b>Figure 48</b> - (a) Image of fibre and (b) 5x magnification image of fibre edge.....	92
<b>Figure 49</b> – (a) Image of fibre and (b) 5x magnification image of fibre edge.....	92
<b>Figure 50</b> – Photograph of Surlyn <sup>®</sup> PC2000 fibre transmitting light.....	95
<b>Figure 51</b> – 10x magnification image of Surlyn <sup>®</sup> PC2000 fibre transmitting light following method one connection.....	100
<b>Figure 52</b> – Light transmission curves for (a) 40 cm, (b) 30 cm, (c) 20 cm and (d) 10 cm Surlyn <sup>®</sup> PC2000 fibres during the 1 cm cut test.....	104
<b>Figure 53</b> – Light transmission curve for the Surlyn <sup>®</sup> PC2000, 20 cm fibre hailed off using setting one. ....	105
<b>Figure 54</b> – Light attenuation curves for Surlyn <sup>®</sup> PC2000 fibre hailed off using setting 1; (a) 10 g, (b) 50 g , (c) 100 g, (d) 500 g, (e) 1000 g and (f) 2000 g.....	106
<b>Figure 55</b> –DSC of extruded Surlyn <sup>®</sup> PC2000 fibre (setting six); one cycle.....	109
<b>Figure 56</b> - DSC of extruded Surlyn <sup>®</sup> PC2000 fibre (setting six); three cycles.....	111

**Figure 57** – Images and schematic diagrams (not to scale) of 50 mm x 50 mm

(a) single ply, (b) Two ply and (c) four ply glass fibre/Surlyn<sup>®</sup>

(b) 1706 film composites..... 113

**Figure 58** – Images of (a) Surlyn<sup>®</sup> fibres and glass-fibre. (b) Surlyn<sup>®</sup> fibres,

PMMA fibres and glass-fibre. (c) Surlyn<sup>®</sup> Fibres, S2 hollow glass-

fibres and glass-fibre. (d) Surlyn<sup>®</sup> fibres, SDOF and glass-fibre.

(e) Surlyn<sup>®</sup> fibres, standard optical fibres and glass-fibre

composites..... 116

**Figure 59** – Cross-sectional image of  $G_{Ic}$  reference test specimen

(magnification – 10x)..... 118

**Figure 60** – (a) Typical Load versus displacement curve and (b) interlaminar

fracture toughness ( $G_{Ic}$ ) versus crack length for reference sample

one..... 120

**Figure 61** – S.E.M images of reference sample following Mode I fracture

testing..... 121

**Figure 62** - Cross sectional image of  $G_{Ic}$  Surlyn<sup>®</sup> PC2000 fibre test specimen

(magnification – 10x)..... 122

<b>Figure 63</b> – (a) Typical Load versus displacement curve and (b) interlaminar fracture toughness ( $G_{Ic}$ ) versus crack length for Surlyn <sup>®</sup> PC2000 fibres, sample one.....	124
<b>Figure 64</b> – S.E.M images of Surlyn <sup>®</sup> PC2000 fibre sample following Mode I fracture testing.....	125
<b>Figure 65</b> - Cross sectional image of $G_{Ic}$ Surlyn <sup>®</sup> 1706 film test specimen (Magnification – 10x).....	126
<b>Figure 66</b> – (a) Typical Load versus displacement curve and (b) interlaminar fracture toughness ( $G_{Ic}$ ) versus crack length for Surlyn <sup>®</sup> 1706 film, sample two.....	128
<b>Figure 67</b> – S.E.M images of Surlyn <sup>®</sup> 1706 film sample following mode I fracture testing.....	130
<b>Figure 68</b> – S.E.M image of punctured Surlyn <sup>®</sup> 1706 film.....	131
<b>Figure 69</b> - Cross sectional image of $G_{Ic}$ punctured Surlyn <sup>®</sup> 1706 film test specimen (Magnification – 10x).....	131

<b>Figure 70</b> - (a) Typical Load versus displacement curve and (b) interlaminar fracture toughness ( $G_{Ic}$ ) versus crack length for punctured Surlyn <sup>®</sup> 1706 film, sample two.....	133
---	-----

<b>Figure 71</b> – S.E.M images of punctured Surlyn <sup>®</sup> 1706 film sample following mode I fracture testing.....	135
--	-----

## List of Tables

	<u>Page</u>
<b>Table 1</b> – Summary of the Grades of Surlyn <sup>®</sup> used in this study along with selected properties.....	34
<b>Table 2</b> – Table containing a summary of the processing conditions that were used to manufacture the thin film.....	35
<b>Table 3</b> – Table containing temperature ramps used to programme the DSC.....	36
<b>Table 4</b> – Dimensions of the samples used for the MID spectroscopy.....	37
<b>Table 5</b> – Summary of the moulding conditions that were used to produce the thick Surlyn <sup>®</sup> plaques.....	38
<b>Table 6</b> – Summary of the heating ramp sequence that was used to measure the temperature profile around the centre point of the Surlyn <sup>®</sup> plaque.....	40
<b>Table 7</b> – Summary showing weights that were applied to the base of the extruded fibres.....	43
<b>Table 8</b> – Experimentally derived relationship between the setting on the Minimat motor drive and the RPM of the acetyl mandrel.....	44

<b>Table 9</b> – Summary of light transmission procedures carried out on thin Surlyn <sup>®</sup> PC2000 fibres.....	48
<b>Table 10</b> – Weights used during attenuation experiments.....	49
<b>Table 11</b> - Material processing schedule.....	54
<b>Table 12</b> – Surlyn <sup>®</sup> crack arrestors used during Mode I fracture testing.....	59
<b>Table 13</b> – $G_{Ic}$ test procedure with accordance to British Standard BS ISO15024.....	63
<b>Table 14</b> – Density measurement for all three grades of Surlyn <sup>®</sup> .....	67
<b>Table 15</b> – Thermal characteristics of Surlyn <sup>®</sup> PC2000, 9910 and 1706.....	69
<b>Table 16</b> – Refractive Indices for Surlyn <sup>®</sup> PC2000, 9910 and 1706.....	75
<b>Table 17</b> – Average diameter of Extruded Surlyn <sup>®</sup> PC2000 fibres.....	83
<b>Table 18</b> – Average diameter of Extruded Surlyn <sup>®</sup> 9910 fibres.....	85
<b>Table 19</b> – Fibre diameter measurements for Surlyn <sup>®</sup> PC2000.....	87

<b>Table 20</b> – Light transmission measurements through extruded Surlyn®	
PC2000 and 9910 thick fibres.....	89
<b>Table 21</b> – Light intensity and average diameter measurements for Surlyn®	
PC2000 and PMMA fibres.....	94
<b>Table 22</b> – Light transmission, fibre end diameters and fibre diameter for	
Surlyn® PC2000 fibres.....	96
<b>Table 23</b> - Light transmission, fibre end diameters and fibre diameter for	
Surlyn® 9910 fibres.....	96
<b>Table 24</b> – Average diameter and light guide distance for settings	
one - three Surlyn® PC2000 and 9910 fibres.....	98
<b>Table 25</b> - Average diameter and light guide distance for thin Surlyn® PC2000	
fibres.....	99
<b>Table 26</b> – Light transmission readings for test one to three (N/R – no reading).....	101
<b>Table 27</b> – Density measurement results for Surlyn® PC2000 fibre, setting six.....	108
<b>Table 28</b> - Thermal characteristics of extruded Surlyn® PC2000 fibre	
(setting six).....	110

<b>Table 29</b> – Average $G_{Ic}$ , critical energy release rate ( $J/m^2$ ) for reference samples, using both corrected beam (CBT) and modified compliance theory (MCC).....	118
<b>Table 30</b> – Average $G_{Ic}$ , critical energy release rate ( $J/m^2$ ) for Surlyn <sup>®</sup> PC2000 fibre samples, using both corrected beam (CBT) and modified compliance theory (MCC).....	122
<b>Table 31</b> – Average $G_{Ic}$ , critical energy release rate ( $J/m^2$ ) for Surlyn <sup>®</sup> 1706 film samples, using both corrected beam (CBT) and modified compliance theory (MCC).....	126
<b>Table 32</b> – Average $G_{Ic}$ , critical energy release rate ( $J/m^2$ ) for punctured Surlyn <sup>®</sup> 1706 film samples, using both corrected beam (CBT) and modified compliance theory (MCC).....	132



## **1.0 Introduction**

Surlyn<sup>®</sup> is the trademark name given to an ethylene based material known as an ionomer. Surlyn<sup>®</sup> is used for such applications; including food and cosmetics packaging.<sup>1</sup>

Other types of ionomers include styrene, butadiene, urethane and sulfone. Although these materials have been around since the 1960's, it is only recently that this class of material; particularly Surlyn<sup>®</sup> has been studied and observed to contain self-healing properties.

Self-healing is defined as the complete or passive repair of minor damage without the need for detection or any type of manual intervention.<sup>2</sup> Self-healing is classified into two types known as extrinsic and intrinsic healing. Extrinsic healing involves an embedded healing agent and intrinsic healing materials are able to heal by themselves.<sup>3</sup>

Previous studies have subjected Surlyn<sup>®</sup> to different ballistic, indentation and also sawing studies. Surlyn<sup>®</sup> is an example of an intrinsic self-healing material and healing is said to take place due to thermally reversible cross-links and intermolecular interactions helping close the damaged area.<sup>4</sup>

Due to this reported self-healing property, Surlyn<sup>®</sup> shows a potential for future use in a wide variety of unique applications and this is shown by recent developments and research undertaken by both the Navy and N.A.S.A.<sup>5, 6</sup>

Future development and understanding of Surlyn<sup>®</sup> and its self-healing behaviour will allow for the development of materials where damage is detected and repaired in-situ extending their life time and reliability during use.

A number of new techniques were employed during the course of study to further investigate the self-healing and light guide capabilities of three different grades of Surlyn<sup>®</sup> in the interest of developing a self-healing and self-sensing composite material. This then leads to the main aims of the project.

## **2.0 Aims**

- 2.1** To carry out a literature review on the polymer known by its trade names as Surlyn<sup>®</sup> and its self-healing capacity.
- 2.2** To employ different techniques to characterise Surlyn<sup>®</sup> and the three different grades used during this study.
- 2.3** Development of techniques for production of thick and thin Surlyn<sup>®</sup> plaques and extrusion of Surlyn<sup>®</sup> fibres; to a view of developing a self-sensing composite.
- 2.4** To investigate the crack healing capacity of Surlyn<sup>®</sup> and the light transmission (self-sensing) capabilities of Surlyn<sup>®</sup> fibres; to a view of developing a self-healing and self-sensing composite.

## 3.0 Literature Review

### 3.1 Ionomers

#### 3.1.1 *Ionomer Definition*

Ionomers were originally defined as olefin-based polymers containing a relatively small percentage of ionic groups which had strong ionic inter chain forces controlling their properties.<sup>7, 8</sup> As new polymer backbones and more ionic character were being incorporated into ionomers it was clear there were problems with this definition due to the lack of division between such systems and polyelectrolytes and related materials.

Due to this lack of distinction a new definition stated that ionomers are polymers in which the bulk properties are governed by ionic interactions in discrete regions of the material, specifically in materials where the ion group content is  $\sim 15$  mol %.<sup>9, 10</sup> Behaviour of ionomers were therefore attributed to their properties and not their composition enabling a differentiation between an ionomer and a polyelectrolyte.<sup>11</sup>

#### 3.1.2 *Production of Ionomers*

Production of ionomers involves a process known as copolymer neutralization. The process involves ionomers being derived from precursor copolymers containing both ionic and non ionic repeat groups.<sup>4</sup>

The ionic component is then neutralized forming an ionic pair with a metallic cation.<sup>12 - 15</sup> This process produces the ionomer with ionic groups as part of the polymer structure. The

number of acid groups neutralized influences the amount of ionic content present in the ionomer.<sup>4</sup>

### 3.1.3 Ionomer Composition

In general, ionomers are made up of non-ionic and ionic repeat units, making them a low dielectric copolymer. The distribution of these ionic groups along the backbone chain of the ionomer is an important variable. They can be placed randomly or systematically within the primary polymer chain (ionenes), as end groups on polymer chains (monochelics and telechelics), or as segments in a block copolymer (see Figure 1).<sup>10, 16, 17</sup>

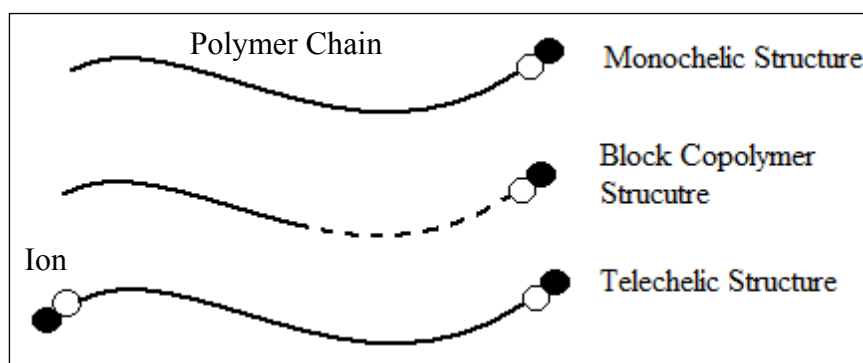


**Figure 1** – Proposed conformations of structures of ionomers.<sup>10</sup>

### 3.1.4 Ionomer Morphology

#### 3.1.4.1 Ionic Aggregate Formation

Ionic aggregate formation takes place when ion pairs aggregate to form quadruplets, sextuplets and higher aggregate formation forming what is known as a multiplet.<sup>18</sup> There are

several factors that govern the formation of multiplets and these include: the dimensions of polymer chains and the tension on the chains that results from ionic aggregation.<sup>19</sup>

In 1990 *Eisenburg, Hird and Moore* developed the EHM model (see Figure 2) that related the morphology of ionomers to mechanical properties. According to the model the ion pairs anchor their attached polymer chains to the multiplet. This creates a region of restricted mobility compared to that of the bulk polymer due to the physical crosslink's present in the vicinity of the multiplet.<sup>18, 20, 21</sup> Also chain extension can occur around the multiplet, which allows more chains to be included in the multiplet formation, again restricting movement.<sup>22</sup>

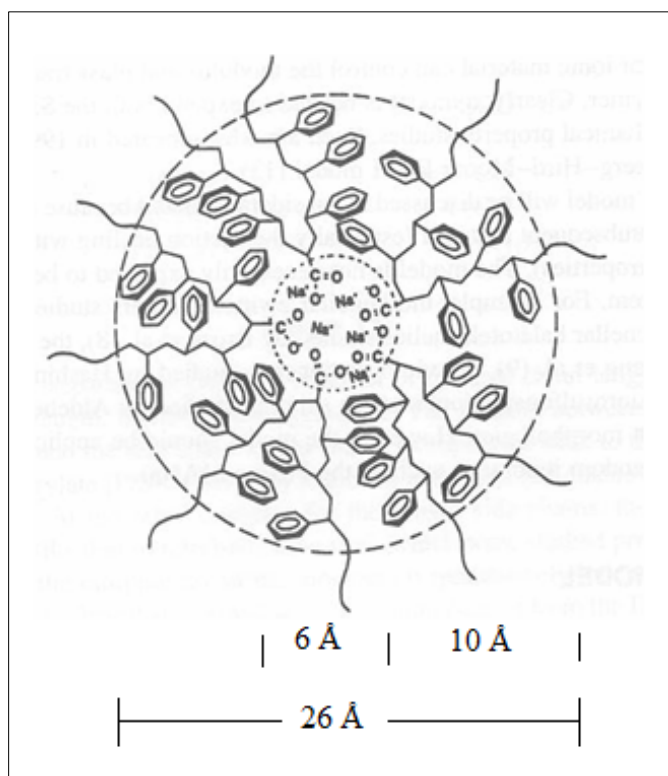


**Figure 2** – Schematic representation of the Eisenberg-Hird-More model.<sup>10</sup>

The next phase involved in the morphology of ionomers involves the term known as an ionic cluster. A cluster is formed when there is an increase in ionic content. This causes increased numbers of multiplets to form. At a certain ion content, the number and size of the regions of restricted mobility begin to increase and eventually overlapping takes place forming a cluster (see Figure 3).<sup>18, 20</sup>

At low levels of ion content, the restricted mobility regions do not overlap one another and only one T<sub>g</sub> is present. As ion levels are increased a large overlap of the restricted mobility regions becomes apparent and thus two T<sub>g</sub>'s are expected; one for the multiplet region and one for the bulk polymer.<sup>10, 18</sup>

Techniques including small angle x-ray scattering, mechanical and dielectric measurements and electron microscopy were responsible for imaging the presence of ionic clusters within ionomers.<sup>23, 24</sup>

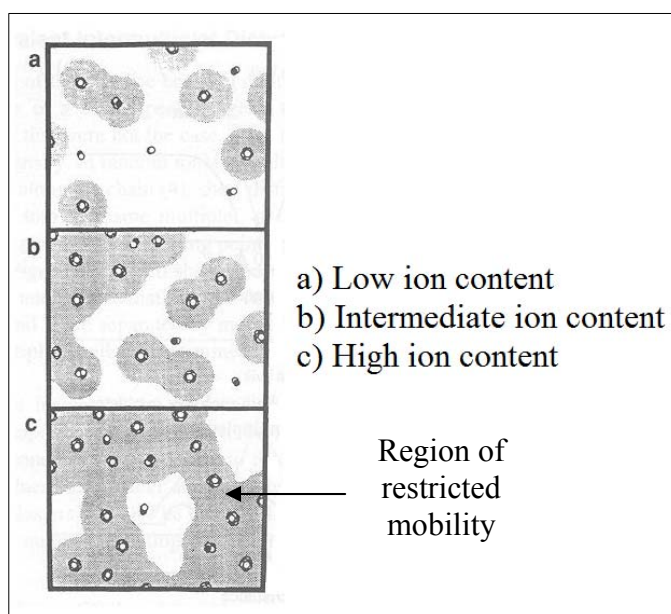


**Figure 3** – Schematic diagram showing the growth of multiplets and the formation of clusters with increases in ionic content.<sup>18</sup>

#### 3.1.4.2 *The Effect of Ionic Aggregate on Thermal, Mechanical and Physical Properties*

The formation of ionic aggregates, which act as physical cross-links, create significant changes in the ionomer properties. Such properties include mechanical and physical changes.<sup>25, 26</sup>

Studies completed by *Bellinger et al.*<sup>27</sup> and *Statz*<sup>28</sup> and *Rees*<sup>29</sup> investigated the effect of ionic content. *Bellinger et al.* found that sodium sulfonated polystyrene ionomers showed an increase of ~ 60 % for tensile strength and ~ 100 % for toughness when ionic content was increased from 0 – 7.5 mol %.<sup>27</sup> *Statz* and *Rees* based there study on EMAA (ethylene-co-



methacrylic acid) materials.<sup>28, 29</sup> They both found a 2:5 fold increase in modulus for ionic content levels up to 40 %.<sup>28, 29</sup>

Formation of ionic aggregates causes morphological changes to occur during heating. The order-disorder transition was discovered by *Tadano et al.*<sup>26</sup> and was used to account for changes that were observed during thermal expansion and calorimetric studies. The model consisted of three phases (see Figure 4).

Phase one was known as the ordered state. This consisted of ordered ionic clusters, polyethylene crystallites and an amorphous region. Once the temperature was increased the order of crystals inside the ionic cluster became disordered (Ti), and with further increases in temperature the crystals would melt (T) whilst still containing the disordered ionic clusters. During cooling (Tc) the re-crystallisation takes place rapidly while the reordering of the ionic clusters occurs more slowly through the relaxation process.<sup>30</sup>

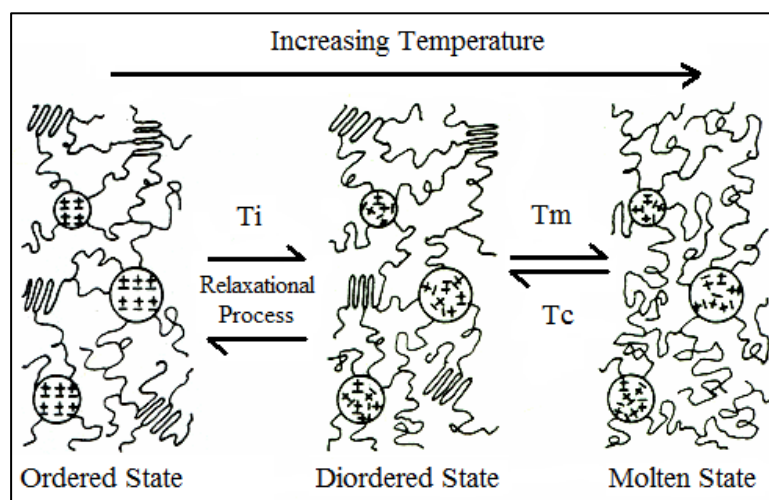


**Figure 4** – Diagram showing the model for the order-disorder transition of ionic clusters.<sup>26</sup>

As discussed the ionic content plays a significant role in controlling the properties of ionomers. The ionomer of interest; known as Surlyn<sup>®</sup>, will be discussed in detail further on in this review.

## **3.2 Surlyn<sup>®</sup>**

### **3.2.1 Surlyn<sup>®</sup> Definition**

Surlyn<sup>®</sup> is a commercial thermoplastic ionomer resin. Surlyn<sup>®</sup> is the trademark name given to the material and was produced by DuPont in the early 1960's. Surlyn<sup>®</sup> is a random copolymer consisting of poly (ethylene-co-methacrylic acid). Surlyn<sup>®</sup> contains 5.4 mol % methacrylic acid and has been neutralized with alkali metals or zinc hydroxide's.<sup>22</sup>

DuPont produces varying different grades of Surlyn<sup>®</sup>. The different grades vary in type of cation used during neutralization.<sup>31</sup>

### **3.2.2 Production of Surlyn<sup>®</sup>**

The production of Surlyn<sup>®</sup> (see Figure 5) involves the copolymerization of ethylene and methacrylic acid via a high-pressure free radical reaction.

Once the copolymer is synthesized, it is then dissolved using tetrahydrofuran. The solvent is then removed leaving the neutralized copolymer (ionomer) as the final product.<sup>32</sup>

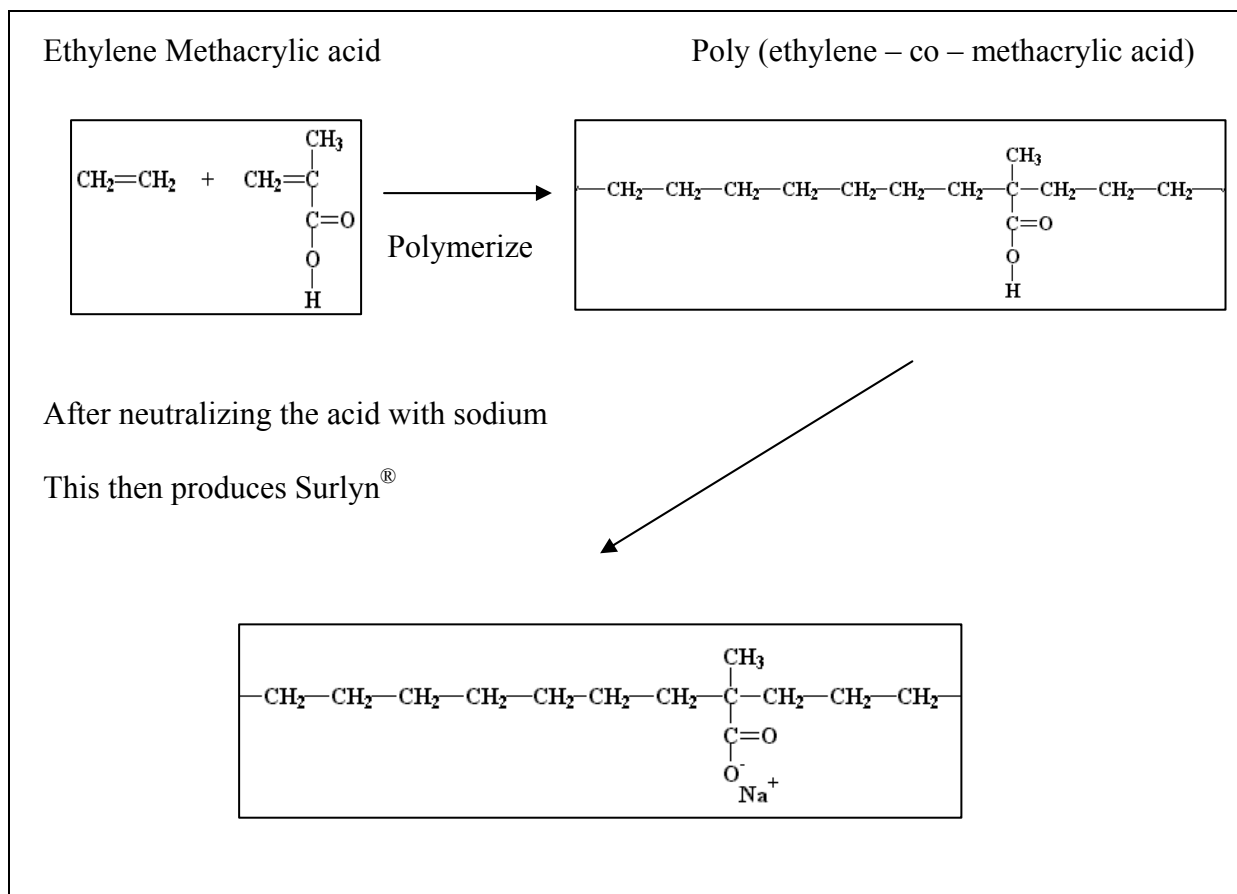


**Figure 5** – Diagram of EMAA neutralized with sodium.

### 3.2.3 Properties and Applications

Properties such as sealing performance, clarity and oil/grease resistance have made them highly suitable for food packaging. The increased clarity; which is a desirable feature needed for packaging such products as food, comes from the reduction of crystallinity present in the copolymer.<sup>30</sup> The material is also used in sporting applications including golf ball covers and ski boots due to its high strength and toughness properties.

### 3.3 Self-Healing Capacity of Surlyn® and other Ionomers

Surlyn® is the most well known ionomer believed to exhibit self-healing properties. The first significant study into the self-healing properties of Surlyn® was carried out by *Fall*.<sup>22</sup> The study carried out bullet-puncture tests on Surlyn® 8920 and 8940. These polymers vary in ionic content and are neutralized with sodium ions.<sup>22</sup>

The study concluded that the presence of the ionic content and order-disorder transition to be the main mechanism for healing after ballistic punctures. It was hypothesized that self-healing would occur if sufficient energy was transferred to the ionomer during the puncture, heating the material above the order-disorder transition and disordering the aggregates. After the puncture has taken place and the heat energy dissipated. The ionic aggregates are said to reorder themselves causing the ionomer to heal (see Figure 6).<sup>22</sup>

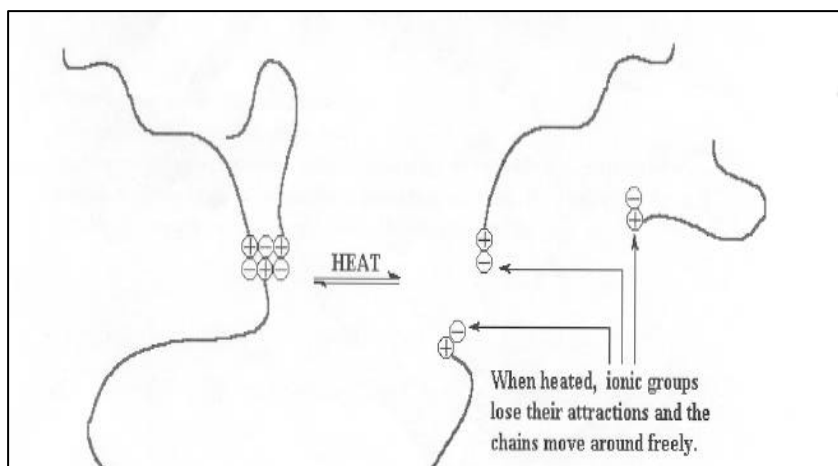


**Figure 6** – Schematic diagram of the order-disorder healing theory presented by *Fall*.<sup>22</sup>

The hypothesis was at first supported by the results collected using a thermal infrared camera during projectile tests using 9 mm bullets (see Figure 7). Results showed that during puncture all samples heated up to  $\sim 98\text{ }^{\circ}\text{C}$ , which was above their melt temperatures. The increase in temperature does produce the disordering effect of the ionic aggregates.<sup>22</sup>

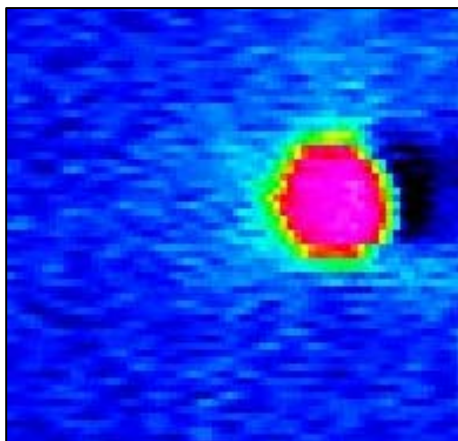


**Figure 7** – Thermal IR image of React-A-seal<sup>®</sup> following puncture from a 9 mm bullet (pink area  $\sim 98\text{ }^{\circ}\text{C}$  and blue area  $\sim 28\text{ }^{\circ}\text{C}$ ).<sup>22</sup>

The study also included puncture tests on two other ionomers, React-a-seal<sup>®</sup> and Nucrel<sup>®</sup> 925. Nucrel<sup>®</sup> 925 contains 0 % ionic content. All four ionomers were able to heal sufficiently to prevent the passage of water through the punctured site. Therefore due to the 0 % ionic content present in Nucrel 925, the initial hypothesis of ionic motivation for healing was inaccurate.<sup>22</sup>

It was then proposed that there were two factors that contribute to the healing process.<sup>22</sup> The first factor indicated by the thermal IR camera suggested that melt flow properties were important for self-healing. The second factor suggested that ionic content is necessary for healing and attributed Nucrel<sup>®</sup> 925's behaviour to the weak aggregation present in the

material. Finally, it was concluded that “the increased elastic character of the melt, due to viscosity, primarily drives the healing phenomenon.”<sup>22</sup>

The next study to focus on the self-healing properties of Surlyn<sup>®</sup> was carried out by *Kalista*.<sup>4</sup> The materials investigated, included two partially neutralized ionomers (Surlyn<sup>®</sup> 8920, 8940) and also two materials without ionic neutralization (Nucrel<sup>®</sup> 925, 960). React-a-seal<sup>®</sup> and a low density polyethylene (LDPE) for comparisons were also investigated.

Projectile impact was the first damage mode used. Films of Surlyn<sup>®</sup> 8940 were impacted with three types of bullets; spherical, flat headed and pointed pellets. The pointed pellet was the only pellet to penetrate and exit the film leaving the sample healed. Due to this, further tests were carried out using the pointed pellet. The mass of the pellet was ~ 0.51 grams and was fired at a velocity of ~ 182 m/s.<sup>4</sup>

Using the pointed pellet, multiple punctures and puncture of multiple films were carried out. Surlyn<sup>®</sup> 8940 was used during the experiments. The films were shown to heal after multiple punctures; however results showed that there would be a limit to healing due to scarring. 100 % LDPE was used as a comparison, and after impact, the samples did not express the healing response that was observed when puncturing Surlyn<sup>®</sup> 8940. It was stated that the lack of self-healing in LPDE indicates the importance of the ionic functionality.<sup>4</sup>

New damage modes were observed. The first being sawing; a sheet of React-A-Seal<sup>®</sup> a quarter of an inch thick was sawed through, using a hack saw. The two halves were seen to

heal leaving an elastic hinge emphasizing the importance of heat energy during healing (see Figure 8).<sup>4</sup>

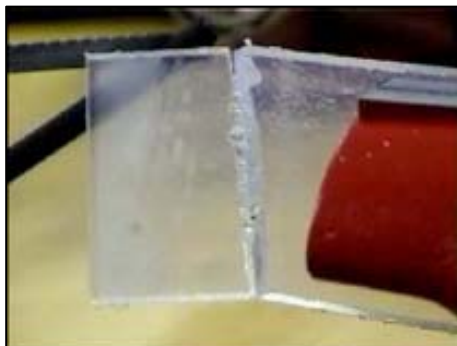


**Figure 8** – Image of elastic hinge after sawing of React-A-Seal<sup>®</sup>.<sup>4</sup>

The final three damage modes investigated were cutting; nail puncture and sewing needle puncture. All three damage modes were tested on films of Surlyn<sup>®</sup> 8940 and no healing behaviour was observed.<sup>4</sup>

Following the studied damage modes, *Kalista* raised the question of whether increased temperatures could be enough to elicit the self-healing response of the materials. Therefore the next stage of the study carried out a peel test (see Figure 9) at specified temperatures and was used to examine the level of bonding and the temperature at which the bonding (self adhesion) took place.<sup>4</sup>

Two 0.8 mm thick Surlyn<sup>®</sup> 8940 laminates were bonded together for 30 minutes at 70, 75, 80, 85 and 90 °C. The laminates were then pulled apart at a rate of 5 cm/min.

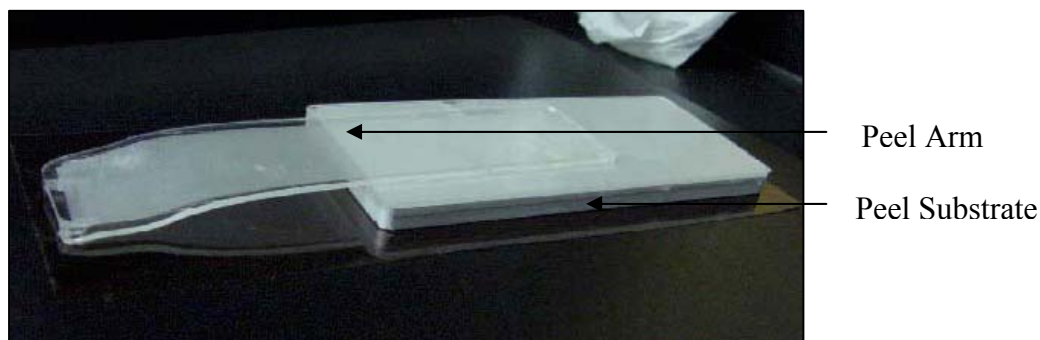


**Figure 9** – Image of the peel test sample.<sup>4</sup>

Results showed that as the temperature approached the melting point of the material the bond strength increased. The bond strength did not increase until temperatures reached  $\sim 85 - 90$  °C.<sup>4</sup>

It was concluded that as temperatures increased to near those measured during projectile impact, the material possessed a potential sealing component which is present in the healing mechanism of punctured films.<sup>4</sup>

The next stage of the study examined the effect of temperature on healing after projectile tests. A novel technique was used to quantify the amount of healing and was called a pressure burst test.<sup>4</sup> Samples were loaded impacted side down via air pressure using nitrogen gas. The other side of the sample was immersed in deionised water. If the sample was able to hold an increase in air pressure without leaking air bubbles through the punctured area, the sample was said to be healed.<sup>4</sup>



Surlyn<sup>®</sup> (8920, 8940) and Nucrel<sup>®</sup> (925, 960) were shot with a pointed pellet. The velocity of the projectile was 182 m/s. Samples were left to equilibrate to test temperatures of 60, 70, 80 and 90 °C for five minutes, prior to the impact tests.<sup>4</sup>

For experiments carried out at room temperature; results revealed that ionic content is not necessary for healing to take place. Samples tested above 70 °C did not heal. Though this was unexpected, room temperature healing was said to take place through an elastic mechanism. This behaviour differed to the viscous response present at elevated temperatures, which distributed impact energy, preventing elastic recovery to take place around the puncture site.<sup>4</sup>

Data collected from the pressurized burst test showed that Nucrel<sup>®</sup> 960 and Surlyn<sup>®</sup> 8920 had the poorest healing behaviour. Nucrel<sup>®</sup> 925 performed the best with no failures and Surlyn<sup>®</sup> 8940 also showed healing of punctured samples. Sample thickness was shown to affect the healing of Surlyn<sup>®</sup> and not Nucrel<sup>®</sup>. It was also stated that ionic content is unnecessary for healing and may even inhibit healing in Surlyn<sup>®</sup> 8920 which contains the most ionic groups.<sup>4</sup>

The final part of the study investigated fabricating carbon nanotubes with Surlyn<sup>®</sup> 8940. This was done to investigate the possibility of producing a composite with both self-healing and enhanced mechanical properties.<sup>4</sup>

Composite samples were subjected to mechanical and projectile tests. During mechanical testing rectangular bars of ~ 1.3 x 6.35 cm were uniaxially deformed in an Instron machine at a rate of 2 mm/min. The young's modulus increased by 21 %, the tensile strength increased by 13 % and finally the toughness increased by 14 % for the composite material. Projectile

puncture showed that the composite material did heal following puncture at room temperature; however that the quality of healing had decreased.<sup>4</sup>

The study concluded that ionic content is not necessary for self-healing properties to be present in the materials. Therefore the two main requirements expected to produce self-healing are a local melt state in the polymer material and sufficient elasticity in the melt to help close the puncture site.<sup>4</sup>

The area of self-healing became a very attractive area for study outside the academic community. The Navy looked into Surlyn<sup>®</sup> for the survivability of aircraft.<sup>5</sup> Surlyn<sup>®</sup> was investigated for lightweight fuel tanks for planes, ships and ground vehicles, taking advantage of the self-healing properties. However results showed that Surlyn<sup>®</sup> degraded once in contact with jet fuel.<sup>5</sup>

The interest in the self-healing capacity of Surlyn<sup>®</sup> was also of interest to NASA. They aimed to understand and generalize the phenomenon of self-healing; therefore the mechanical properties responsible for this ability were explored.<sup>6</sup>

Experimental work involved using a moderate rate impression test. Surlyn<sup>®</sup> 8940 films measuring 6 – 10 mm in thickness were tested. A cylindrical probe; 1.6 – 0.8 mm in diameter was mounted to a 445 N load-cell. Three cross-head speeds were used and the depth of indentation was kept constant at 2.5 mm.

The higher the indentation speed used, resulted in the greater degree of healing. The films also healed more with additional recovery time. Healing was also increased; when room temperature indentions were heated following indentation.

Once indentation tests were carried out at increased temperatures, the degree of healing was shown to decrease (71 % vs. 74 %) and it was concluded that healing at room temperature, related to an elastic recovery of large-strain deformation with relaxation times, ranging from less than a second to several days.<sup>6</sup>

Following *Kalista's* initial work into the self-healing phenomena of ionomers, it was proposed that self-healing occurs through a two-stage process.<sup>6</sup> Stage one involves the polymer elastically rebounding under melt conditions, closing the puncture site. In stage two the puncture site is then sealed through autohesion and interdiffusion of the polymer chains.<sup>4</sup> The following study looked to verify the theory of the two stage model.<sup>33</sup>

Surlyn<sup>®</sup> (8940, 8920) and Nucrel<sup>®</sup> (925, 960) were used during the investigation. *Kalista* and *Ward* performed puncture tests using the same set-up as before; however the ability to puncture films at elevated temperatures and below room temperature were introduced.<sup>33</sup> Films were tested at room temperature, sub-ambient temperatures of 10 °C, - 10 °C and - 30 °C and elevated temperatures of 60 °C, 70 °C, 80 °C and 90 °C. The pressure burst test was employed to quantify the healing response.<sup>33</sup>

Healing did occur at sub-ambient temperatures due to the significant temperature rise into the viscoelastic melt state. Two observations verify this rise in temperature and support the two stage healing model. Stage one, the polymer is believed to elastically retract to close the hole under molten conditions. It is theorized to then weld together (stage two) to produce sealing as verified previously.<sup>33</sup> On a whole, low temperature puncture results have shown that not only does healing persist into low sub ambient temperatures, but may also perform better in some cases given the results for Surlyn<sup>®</sup> 8940 and Nucrel<sup>®</sup> 960. The study concluded that

Surlyn<sup>®</sup> and Nucrel<sup>®</sup> required high energy (increased temperatures) for healing to take place.<sup>33</sup>

A more recent study carried out in 2008 studied the self-healing capacity of Surlyn<sup>®</sup> through three different strategies.<sup>33, 34</sup> The first strategy involved SEM of impact surfaces following ballistic impacts for a range of projectiles at specified velocities. The second strategy investigated the healing mechanism; using a method that mimics the elastic response to impact in a controlled environment. Finally the third strategy investigated the role of the viscous response during impact and found that increased molecular mobility in the melt was critical to achieving optimal healing.<sup>33, 34</sup>

It was confirmed that both elastomeric and viscous behaviour was present around the impact regions. The elastic response which is critical for closure of the hole following impact was shown to be dependent upon ionic content present in the material. The viscous response showed that if there is sufficient molecular mobility and time, polymer chains will diffuse across boundaries and heal.<sup>33, 34</sup>

The self-healing capacity of Surlyn<sup>®</sup> was demonstrated to be repeatable confirming that healing is inherent to the chemical structure and morphology of the ionomer.<sup>33</sup>

The self-healing capacity of Surlyn<sup>®</sup> was shown to heal following ballistic puncture and other damage modes where sufficient heat energy was produced.

Early studies into the self-healing property; accredited it to the ionic aggregate present within the material; however further investigation using ballistic penetration showed that other ionomers (Nucrel<sup>®</sup>) without ionic content also healed.

Healing was then said to be caused by thermally reversible cross-links and intermolecular interactions, which were present in the melt state, helping close the punctured area.

Surlyn<sup>®</sup> shows huge potential for application, and as this class of material develops and the exact cause of the healing is uncovered, this will allow for the design of a new polymeric material possessing the self-healing property.

### **3.4 Other Self-healing Mechanisms and Systems**

The application of a self-healing polymeric material is a very advantageous concept; therefore other self-healing systems have been studied. Many new concepts have been inspired by biological systems, where healing is triggered and completed in an autonomic fashion.<sup>35, 36</sup>

Other materials and systems with the ability to self-heal are classified into two categories. They are divided into intrinsic and extrinsic, where intrinsic materials are able to heal by themselves and extrinsic materials where a healing agent is embedded in the material.<sup>37</sup> These categories have also been termed as reversible and non-reversible systems.<sup>38</sup>

### **3.4.1 *Intrinsic Self-healing Mechanisms***

The self-healing properties present in these materials are unable to heal autonomically and therefore require stimulation for healing to take place (generally heating). The reversible systems work by the polymer reverting back to its constituents following damage, repairing itself. The reversible bonds or cross-links present within the polymer are categorized as covalent and non-covalent bonds.<sup>38</sup>

Covalently bound systems include; diels-alder based polymers and photodimerization based polymers. Non-covalently bound systems include hydrogen bonded polymers and metal-ligand coordination polymers.<sup>38</sup>

#### **3.4.1.1 *Diels-Alder based polymers***

Work carried out by *Chen et al.* designed a polymer with a matrix containing weak chemical bonds which break when damaged and reform when heated.<sup>37-42</sup> The matrix is produced by a thermally reversible Diels-Alder (DA) cycloaddition of multi-furan and multi-maleimide. Healing takes place through covalent bonds and was shown to be fully reversible and could be used to restore damaged areas multiple times.<sup>37-42</sup>

#### **3.4.1.2 *Photodimerization based polymers***

The application of photo-induced reversible polymers is very advantageous, as the use of light is clean, cheap and readily available. A study presented by *Chung et al.* focused on an ethane

based polymer that under went photodimerization to produce a highly cross-linked matrix.<sup>43</sup> However after tests were carried out on an original and then a damaged and healed sample; strength measurements had decreased raising doubts over the self-healing ability of the polymer.<sup>34, 41</sup>

#### **3.4.1.3 *Hydrogen bonded and Metal-ligand coordination polymers***

Non-covalently bound polymers cross-link when intermolecular interactions of the monomer units takes place. The reversibility of these bonds allows the polymer to change in length, extent of cross-links present, constitution and structure. This results in one of their inherent traits being the ability to self-heal.<sup>38, 41</sup>

Hydrogen bonding is the most popular way of achieving a reversible supramolecular polymer and the main challenge involved in producing the material is finding the right balance between the association constant and the reversible system.<sup>41</sup>

Another way of producing these supramolecular polymers is to use metal-ligand coordination. The ligands are introduced into the system in three ways; copolymerization of functionalized monomer, functionalization of end or side groups of preformed polymers, or by using functionalized initiators and/or end cappers in living or controlled polymerizations.<sup>38, 40</sup>

### **3.4.2 *Extrinsic Self-healing Mechanisms***

Some polymers do not have the ability to self-heal; therefore a healing agent is embedded into the material.<sup>40</sup> Healing occurs when damage in the form of cracks causes the release of the encapsulated healing agent into the crack planes.

There are two types of healing agent; single and two-component. Single-component healents are able to cure under the induction of air and therefore make them unsuitable for damage that occurs deep inside the material. The two-component healent consists of a resin and a hardener. Damage causes the two-components too meet causing polymerisation and bonding of the damaged material.<sup>44</sup>

For healing to take place, certain conditions are required. The liquid agent must be compatible with the encapsulation method. The catalyst must be tolerant of the matrix it is embedded in and once damage occurs, polymerisation must occur quickly at room temperature. Finally the ratio of monomer and catalyst must be relatively insensitive due to the random distribution of microcapsules within the matrix material.<sup>45</sup> Healing agent storage methods include hollow glass tubes, glass-fibres, microcapsules and microvascular networks.

#### **3.4.2.1 *Hollow tubes or Glass fibres***

The use of hollow glass tubes (see Figure 10) was first proposed by *Dry* who identified them as a possible container for a repair system.<sup>46</sup> They were initially studied as part of a repair



system for damaged concrete.<sup>47</sup> *Dry* also looked at using the system in a polymeric matrix and used a single part cyanoacrylate resin encapsulated in glass pipette tubes.<sup>48</sup>

A study carried out by *Bleay et al.* argued that previous work used hollow glass fibres that were too large and may cause the material to fail.<sup>49</sup> Therefore the focus of their study was to use hollow fibres which acted as both structural reinforcement and as a container for repair resins.<sup>49</sup> An epoxy resin system was used and results showed that following impact testing, potential improvements were present after the application of heat and vacuum to the impacted panel.

*Bond* and other researchers continued the work based on producing polymer composites including hollow fibres.<sup>50 – 54</sup> The studies investigated using epoxy based healing agents and UV dye with hollow fibres. This would then allow self-healing and in-situ damage detection.

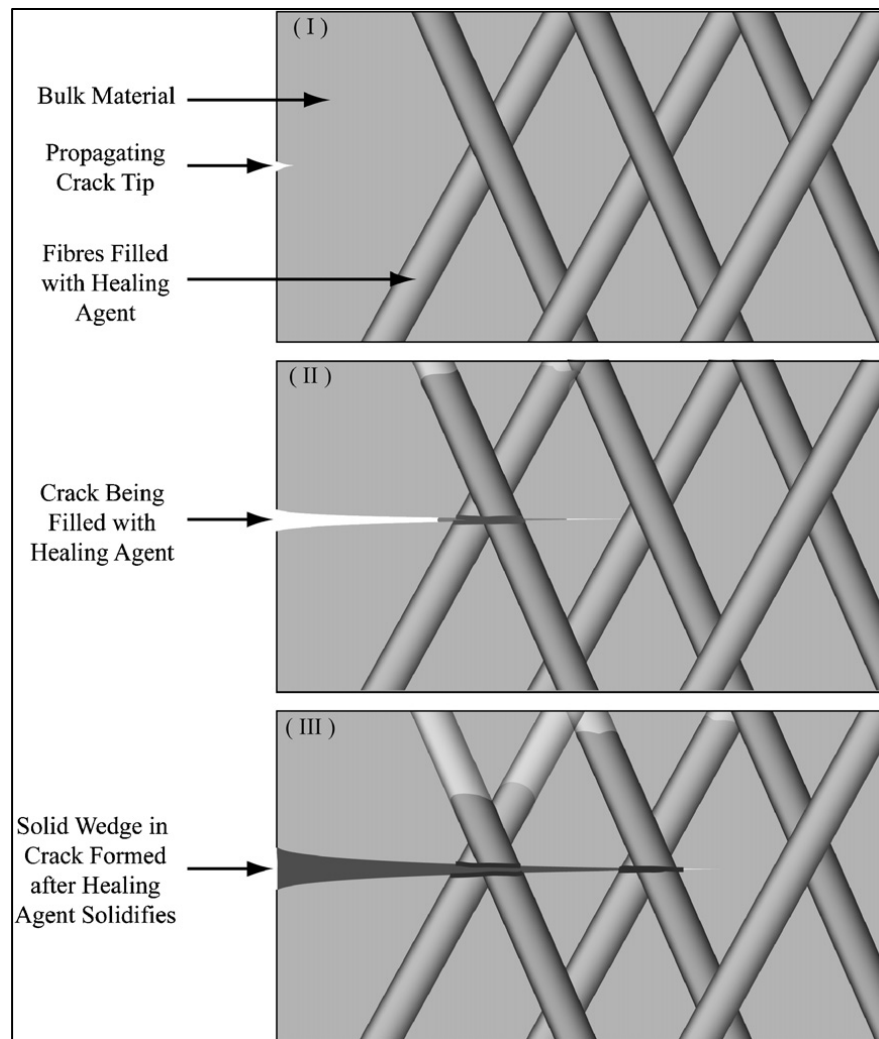


**Figure 10** – Diagram of healing mechanism in hollow fibre-based self-healing composites.<sup>55</sup>

### 3.4.2.2 Microcapsules

Another self-healing system involves embedding a microencapsulated healing agent and a catalytic chemical trigger within a polymer matrix (see Figure 11). Once damaged, the capsules release the healing agent into the crack. Once in contact with the catalyst, polymerisation is initiated and the crack is repaired.<sup>56</sup>

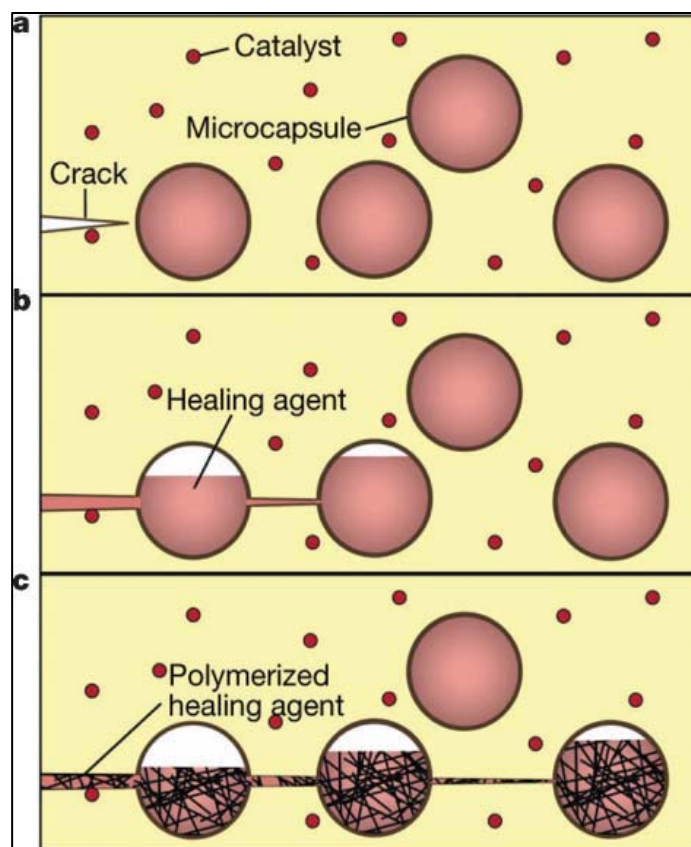


**Figure 11** – Diagram of microencapsulated healing system.<sup>38</sup>

This system was first reported by *White et al.* and consisted of a liquid healing agent dicyclopentadiene (DCPD), a urea-formaldehyde microcapsule (see Figure 12) and a solid catalyst (Grubbs first generation catalyst).<sup>56</sup> Healing took place via ring opening polymerization (ROMP).<sup>56 - 59</sup>

Since the encapsulation system was first demonstrated further studies have taken place to improve the method. These involve the development of the microcapsules, improved catalysts and different healing agents.<sup>41, 60-68</sup>

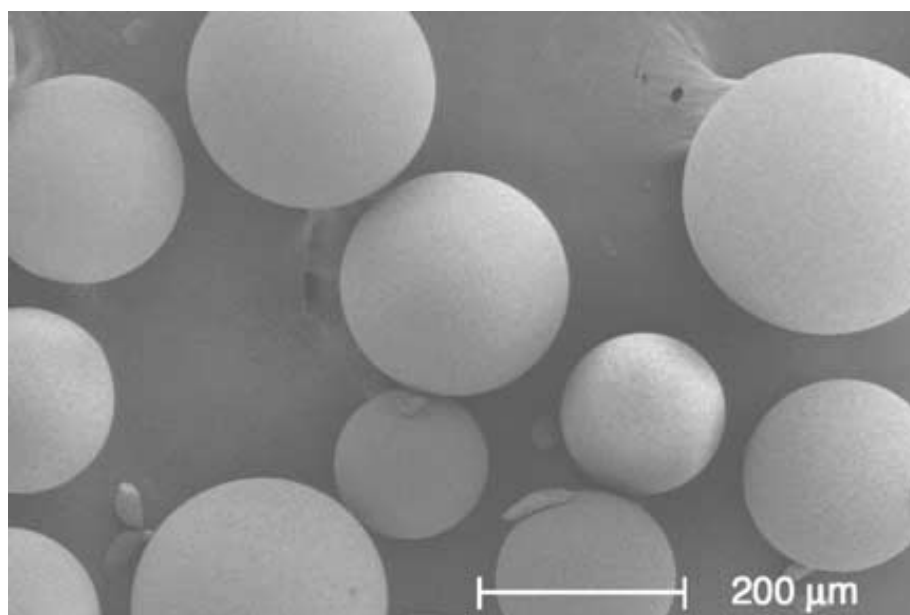


**Figure 12** – S.E.M. image of urea-formaldehyde microcapsules.<sup>60</sup>

#### **3.4.2.3** *Microvascular Networks*

The previously described autonomic systems are limited due to the ability of only single damage repair. A new type of system involves a bio- inspired coating – substrate design that delivers healing agent to cracks in a polymer coating via a three-dimensional microvascular network (see Figure 13) embedded in the substrate, allowing for repeatable healing.<sup>69</sup> Dicyclopentadiene (DCPD) was used as the healing agent as it was successful during the microencapsulated studies previously reported.

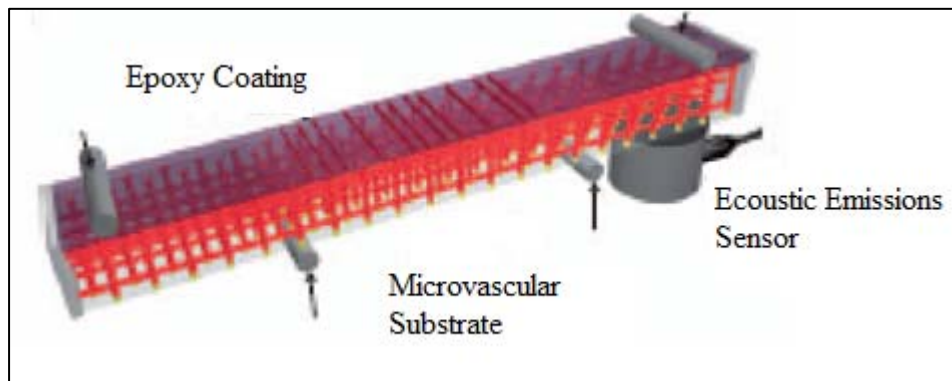


**Figure 13** – Schematic diagram of the self-healing structure composed of a micro vascular substrate and a brittle epoxy coating containing an embedded catalyst.<sup>69</sup>

*Williams et al.* have also demonstrated a network design which involved a sandwich composite with either a single or dual network.<sup>70, 71</sup> The single network involved 1.5 mm channels that were filled with an epoxy resin and hardener and allowed full mechanical recovery to take place during a single cycle.<sup>70</sup> The dual network involved samples being infiltrated with unmixed pressurized fluid and showed significant healing results.<sup>71</sup>

Further work undertaken by *Toohey et al.* modified his initial design by photolithographically patterning four isolated regions within the embedded microvascular network.<sup>72</sup> The study showed that 16 repairs out of 23 were achieved. However difficulties involved the healing agents having to migrate over long distances.

More recently a new biomimetic coating/substrate design was developed.<sup>73</sup> This incorporated a three-dimensional interpenetrating microvascular network that was embedded to enable repeated healing (see Figure 14).

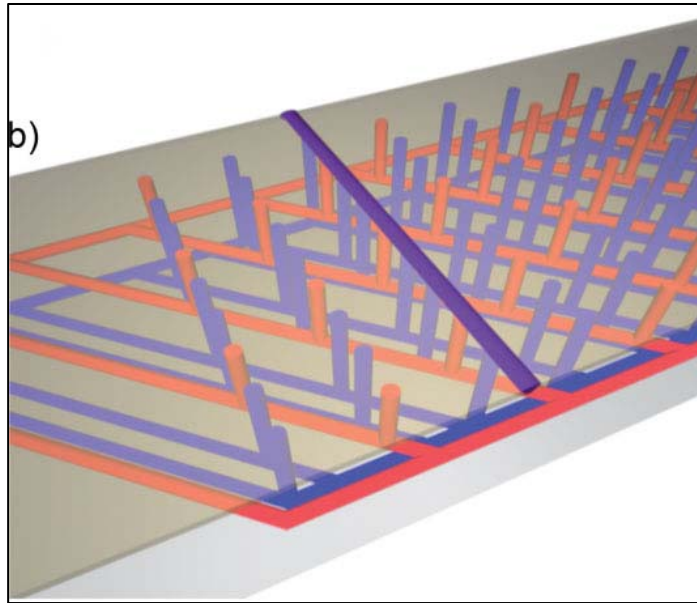


**Figure 14** – Schematic diagram of interpenetrating microvascular network.<sup>73</sup>

### 3.5 Self-sensing Composites

The application of composite materials has increased significantly in recent years. They exhibit increased strength, stiffness and light weight properties making them suitable for use in the aeronautical, aerospace and sporting industries.

The structure of a fibre reinforced composite is comprised of three components: reinforced fibres (generally carbon, glass or aramid fibres), matrix resin and an interfacial region that joins the fibre and the resin. The type of properties present in the material can be tailored by altering the types and ratios of fibres and matrices used in the composite material.<sup>74</sup>

During the lifetime of a fibre reinforced composite, the structure may suffer from damage due to aging, mechanical fatigue, corrosion, thermal stress and other environmental factors. Therefore the monitoring and detection of damage is of paramount importance, allowing repair or replacement of the structure.<sup>75</sup>

Damage monitoring known also as structural health monitoring involves the use of damage sensors. Conventional methods involve embedding the sensors (fibre optic sensors) in the material or attachment of the sensor onto the surface of the material (piezoelectric sensors). These methods are high in cost, show poor durability and also affect the mechanical properties of the structures.<sup>75</sup>

Recent development within the field of fibre reinforced composite materials has focused on the structural material itself acting as the sensor, therefore removing the need for an embedded or attached sensor to monitor damage. The term is known as “self-sensing” and alleviates the issues previously described with embedding and attaching sensors.<sup>75</sup>

In 1997 *Hayes et al.* used a commercially available quartz reinforcing fibre (9 µm in diameter) to develop a novel composite system in which the fibre used acted as a light guide. During manufacture, the fibre coating was de-sized and recoated with a silicon resin. The resultant light guide was termed a “self-sensing” fibre. These fibres were then embedded inside a 16 ply carbon-fibre reinforced composite panel. These panels were subjected to impact testing investigating whether these fibres could act as a damage detection system.<sup>76</sup>

In comparison to three types of conventional optical fibre (30, 50 and 125  $\mu\text{m}$  in diameter) the results indicated that the self-sensing fibres were more sensitive to impact damage and capable of detecting damage as low as 2 J from impacts carried out using a 20 mm hemispherical tup.<sup>76</sup>

Due to the high costs of quartz fibres, in 2004 *Kister et al.* used conventional reinforcing E-glass fibres to detect impact damage. The fibres were converted into light guides by applying an appropriate cladding material (epoxy and polyurethane based resin system). The E-glass fibres were embedded within a 16 ply glass-fibre reinforced composite. Results demonstrated that the concept could be used to study in-situ and in real time the failure processes in the composite material. Damaged areas on the self-sensing composites were highlighted by bleeding light from the damaged E-glass fibres.<sup>77</sup>

Another type of self-sensing composite was reported by *Wang et al.* Self-sensing was attained in a carbon-fibre polymer matrix composite by using the interlaminar interface as a sensor. The interlaminar interface was used as a thermistor, a thermocouple junction, a stress sensor, a damage sensor and a moisture sensor.<sup>78</sup> *Wang et al.* also demonstrated the self-sensing of damage in a carbon-fibre polymer matrix composite by measurement of the electrical resistance or potential away from the damaged region. It was demonstrated in the laminates of a quasi-isotropic continuous carbon-fibre epoxy matrix composite under impact.<sup>75</sup>

The reported studies show how composite materials are able to sense damage. However these smart materials only have the ability to sense and not repair the damage, highlighting the



importance of the following study investigating Surlyn<sup>®</sup> as a self-healing and self-sensing composite material.

## 4.0 Methodology

### 4.1 Materials

#### 4.1.1 *Surlyn<sup>®</sup> Grades*

Three grades of EMAA (ethylene-co-methacrylic acid) random copolymers from DuPont were used in this study. The trade name for this ionomer is Surlyn<sup>®</sup>. A summary of the materials and selected properties are presented in table one.

**Table 1** – Summary of the Grades of Surlyn<sup>®</sup> used in this study along with selected properties.

Surlyn <sup>®</sup> Grade	Metal Salt	Properties	Applications	Form
PC2000	Sodium	Good toughness, abrasion resistance, tear resistance and high stiffness	Golf ball covers	Pellet
9910	Zinc	High clarity, stiffness and abrasion resistance	Golf ball covers	Pellet
1706	Zinc	High clarity 0.06 mm in thickness	Pharmaceuticals, food packaging and medical packaging	Film

### 4.2 Sample Preparation and Preliminary Characterisation

#### 4.2.1 *Preparation of Thin Plaques from Pellets*

A Hydraulic press (Moore, serial number E1127, George. E. Moore and Son LTD, Birmingham, England) was used to compression mould thin plaques of Surlyn<sup>®</sup> PC2000 and

9910. The pellets were placed into the metal mould, which was sandwiched by two metal backing plates and two PTFE sheets and placed into the press. The mould dimensions were 100 mm x 100 mm x 1 mm. Surlyn<sup>®</sup> 1706 was tested in as received film form.

**Table 2** – Table containing a summary of the processing conditions that were used to manufacture the thin film.

Material	Weight of Polymer	Press Temperature	Press Force	Stabilisation Time	Pressing Time	Cooling Time
Surlyn <sup>®</sup> PC2000	60 g	165 °C	10 Ton	5 mins	3 mins	30 mins
Surlyn <sup>®</sup> 9910						
During cooling the sample was kept under the press force.						

#### 4.2.2 Density Measurements

Density measurements were determined using a microbalance that had a density kit incorporated into the set-up. Five 10 mm x 10 mm samples were tested for each grade. Samples were weighed in atmospheric air and then in the less dense liquid (n-heptane). The following equation was then used to determine the density:

$$\text{Sample Weight in Air} / \text{Sample Buoyancy} \times \text{Density of Liquid (n-heptane)} \text{ (1)}$$

#### 4.2.3 Differential Scanning Calorimetry (DSC)

A DSC (DSC 7, The Perkin-Elmer Corp, Norwalk, Conn) was used to examine the thermal characteristics of the ionomers. Each experiment used 15 – 20 mg of material. Samples were heated at a rate of 10 °C per minute and were subjected to temperatures ranging from -10 – 150 °C. The DSC temperature ramp is presented in table three:

**Table 3** – Table containing temperature ramps used to programme the DSC.

<b>Ramp No.</b>	<b>Temperature Ramp</b>
1	Hold at – 10 °C for one minute.
2	Heat to 150 °C at 10 °C/min.
3	Hold at 150 °C for two minutes.
4	Cool to – 10 °C at 5 °C/min.
5	Hold at – 10 °C for two minutes.
6	Heat to 150 °C at 10 °C/min.

This cycle was repeated once for one set of experiments and three times for the second set of experiments. The DSC power and temperature calibrations were carried out before testing. The power calibration was carried out by using the known heat of fusion for Indium (Heat of fusion of 99.999 % purity Indium = 28.45 J/g). The temperature calibration was carried out by running standard materials, with accurately known melting points. In this case Indium and Tin were used (Melting points of 99.999 % Indium = 156.60 °C and 99.999 % Tin = 233.91 °C).

#### 4.2.4 Fourier Transform Infrared Spectroscopy (FTIR)

The ionomers were characterised using a mid infrared spectrometer. The MID-FTIR spectra were obtained using a (MAGNA 760, Nicolet Instrument Corporation). A golden gate ATR (attenuated total reflection) accessory was used during testing. Three samples were tested for each grade of Surlyn<sup>®</sup>. Each experiment comprised of 100 scans. Also a spectral range of 4000 – 650 cm<sup>-1</sup> and a resolution of 4 cm<sup>-1</sup> were used during the experiment.

**Table 4** – Dimensions of the samples used for the MID spectroscopy.

FTIR	Sample Size
MFTIR	20 mm x 20 mm

#### 4.2.5 Refractive Index (RI) Measurements

An Abbe Refractometer (Model 60/ED, Bellingham and Stanley Ltd) was used to measure the RI of the three grades of Surlyn<sup>®</sup>. The RI was measured in transmission mode and two samples were tested for each grade. The sample dimensions were 40 mm x 20 mm x 1 mm.

### 4.3 Production of Surlyn<sup>®</sup> PC2000 and Surlyn<sup>®</sup> 9910 Thick Plaques

#### 4.3.1 Production of Thick Plaques

Fabrication of thick Surlyn<sup>®</sup> plaques was carried out using a similar procedure to that described in section 4.2.1. However in this instance, the mould dimensions were 100 mm x 100 mm x 5 mm. K-type thermocouples were used to monitor heat flow during fabrication.

**Table 5** – Summary of the moulding conditions that were used to produce the thick Surlyn<sup>®</sup> plaques.

Material	Weight of Polymer	Press Temperature	Press Force	Stabilisation Time	Pressing Time	Cooling Time
Surlyn <sup>®</sup> PC2000	60 g	165 °C	10 Ton	5 mins	3 mins	30 mins
Surlyn <sup>®</sup> 9910						
During cooling the sample was kept under the press force.						

The thermocouple was introduced into the plaque by drilling a hole through the mould and was secured using high-temperature proof tape. The temperature was monitored from when both plates were in contact with the press, until the sample was ready to remove.

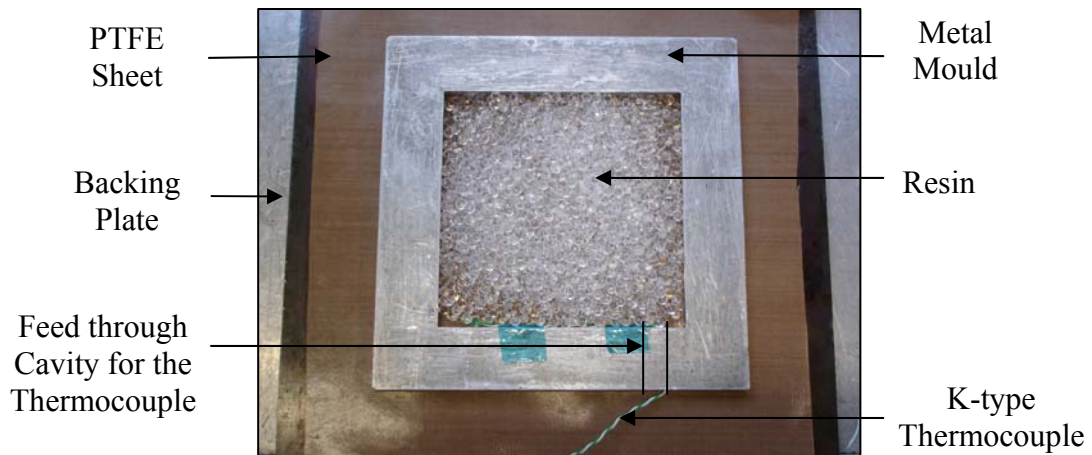


**Figure 15** – Picture showing fabrication set-up for producing thick Surlyn<sup>®</sup> plaque incorporating a k-type thermocouple.

#### **4.3.2** *Monitoring the Temperature Profile within a Thick Plaque (Surlyn<sup>®</sup> PC2000 and 9910)*

The calibration of the plaques with regard to monitoring the temperature profile at specified locations was undertaken. This was carried out as the intention at a later date was to subject these plaques to indentation and ballistic impact. It was not possible to undertake these tests for various reasons that were outside the control of the author. With reference to figure 16, eight thermocouples were attached to the plaque around the centre point using high temperature proof tape.

Key:

● - Centre point

○ - K-type thermocouple

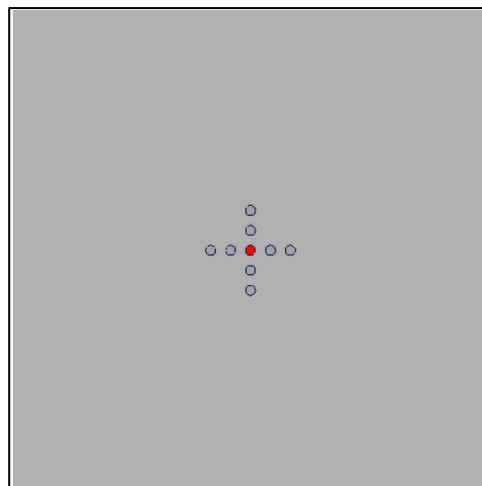


**Figure 16** – Schematic diagram of the location of the thermocouples in the thick Surlyn<sup>®</sup> plaque; thermocouples were spaced 2 mm apart.

Additional thermocouples were placed in the centre and on the side wall of the oven. Once the plaque was secured in the oven the following temperature ramp was used:

**Table 6** – Summary of the heating ramp sequence that was used to measure the temperature profile around the centre point of the Surlyn<sup>®</sup> plaque.

Temperature (°C)	Stabilisation Time (Mins)
Without oven cover	10
With oven cover	10
30	30
40	30
50	30
60	30
70	30
80	30



#### 4.4 Production of Surlyn® Composites (PC2000)

##### 4.4.1 Production of Glass Fibre Reinforced Surlyn® Composites

The main focus was to develop a methodology to fabricate self-sensing and self-healing composites. The term self-sensing is used to describe the situation where the reinforcing fibres act as light guides. Surlyn® as a material that is capable of self-healing was discussed in the literature review section. Here custom-made small diameter optical fibres (SDOF) with a diameter of 17  $\mu\text{m}$  were used as reinforcing fibres.

A diagram of the fabrication set-up is shown in figure 17. The SDOF were sandwiched between two layers of 50 mm x 50 mm x 1 mm layers of the Surlyn® PC2000 thin plaque. Samples were fabricated using the parameters found in table two.

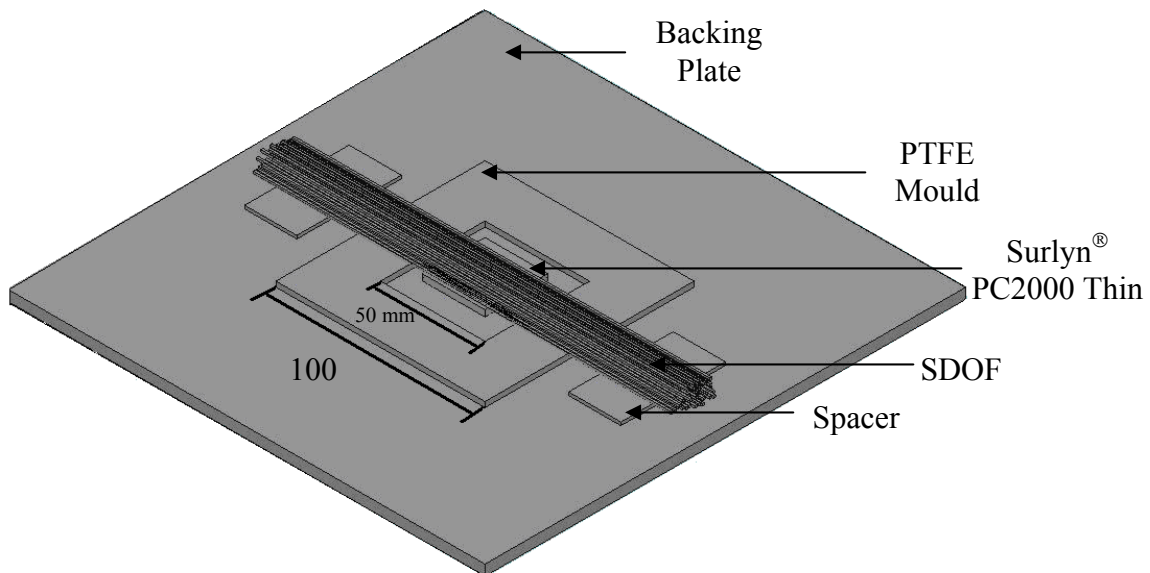


**Figure 17** - Schematic diagram of the custom-made PTFE mould that was used to fabricate the SDOF reinforced Surlyn® composites.

## 4.5 Extrusion of Surlyn® Fibres

### 4.5.1 Development of a Methodology to Extrude Surlyn® Fibres

The aim of this part of the research was to design a methodology to extrude Surlyn® fibres. This was investigated to establish if Surlyn® could be used as a self-sensing light guide. The intention was to investigate if the light guide properties of the Surlyn® fibre could be used to study fibre damage and healing in-situ.

An MFI (Melt flow index, Serial number E1197, Davenport LTD, Welwyn Garden City, England) and a Minimat (Miniature Materials Tester) (Polymer Laboratories, Loughborough, LE11 0QE, UK) were adapted to enable extrusion and drawing of fibres respectively. An Acetal mandrel was fitted to the Minimat drive unit enabling fibres to be hauled off at specified speeds. A photograph of the fibre extrusion set-up is shown in figure 18.

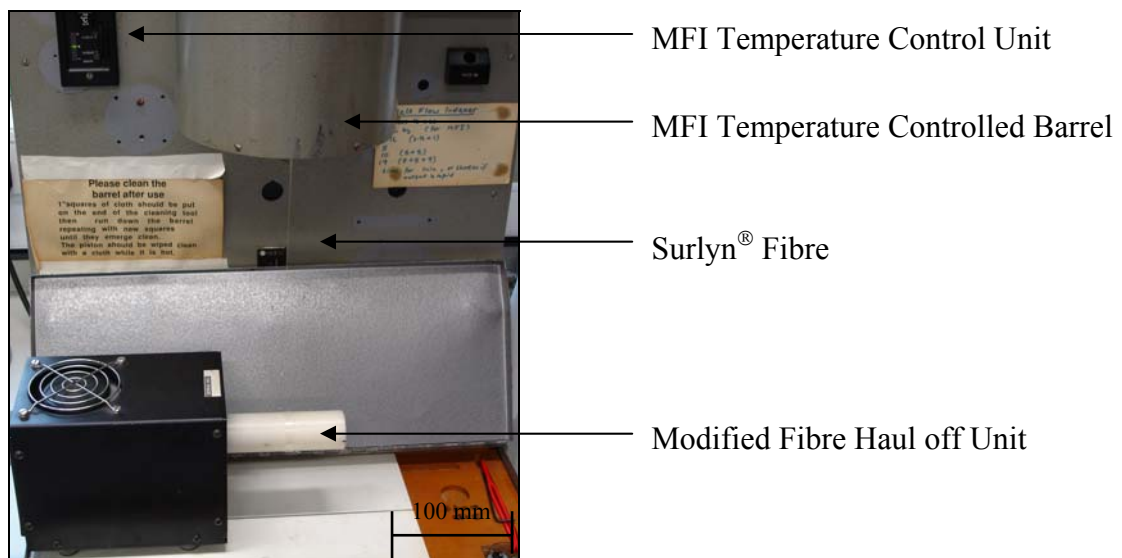


**Figure 18** – A photograph showing the experimental set-up for extruding and hauling off different diameter Surlyn® fibres.

The polymers used in this study were Surlyn<sup>®</sup> PC2000 and 9910. The extrusion of Surlyn<sup>®</sup> fibres was as follows:

The barrel was set to 165 °C for both grades of Surlyn<sup>®</sup>. Approximately five grams of Surlyn<sup>®</sup> pellets were packed into the barrel with a 2 mm diameter die. A 10 kg weight was applied to the piston to extrude the fibres. Different diameter fibres were extruded by applying specified weights to the base of the fibres. The specified weights are summarised in table seven.

**Table 7** – Summary showing weights that were applied to the base of the extruded fibres.

Surlyn <sup>®</sup> PC2000	Surlyn <sup>®</sup> 9910
3 g	7 g
5 g	10 g
7 g	20 g

Once approximately 200 mm of the fibre was extruded, it was cleaved off at the exit of the barrel with a razor blade. Smaller diameter fibres were extruded by using the previously mentioned haul off unit. The settings on the haul off machine were correlated to the revolutions per minute of the acetal mandrel; a summary of this relationship is presented in table eight.

**Table 8** – Experimentally derived relationship between the setting on the Minimat motor drive and the RPM of the acetyl mandrel.

Setting	RPM
1	33
2	48
3	62
4	77
5	92
6	116
7	122
8	137
10	168

## **4.6 Characterisation of the Light Transmission**

### **4.6.1** *Light Transmission through the Extruded Surlyn<sup>®</sup> fibres*

The aim here was to develop a simple technique to characterize the light transmission intensity through both Surlyn<sup>®</sup> PC2000 and 9910 fibres. With reference to the ‘thicker’ fibres (diameter range 1.886 – 2.772 mm), 12 x 200 mm length Surlyn<sup>®</sup> PC2000 and 9910 fibres were illuminated using a white-light source (Bentham Instruments LTD, serial number 68792, Reading, Berkshire, RG2 ONH) and the respective light intensities were determined using a light intensity meter (Thorlabs LTD, Cambridgeshire, CB7 4EX). A photograph of the set-up is presented in figure 19.

As the fibres were too large to be connected with SMA connectors, a 10 mm mark from each end of the fibres was made ensuring that all fibres were lined up consistently within the light source and detector. The light source was left to stabilise for 20 minutes and all light transmission experiments were carried out in a dark room.

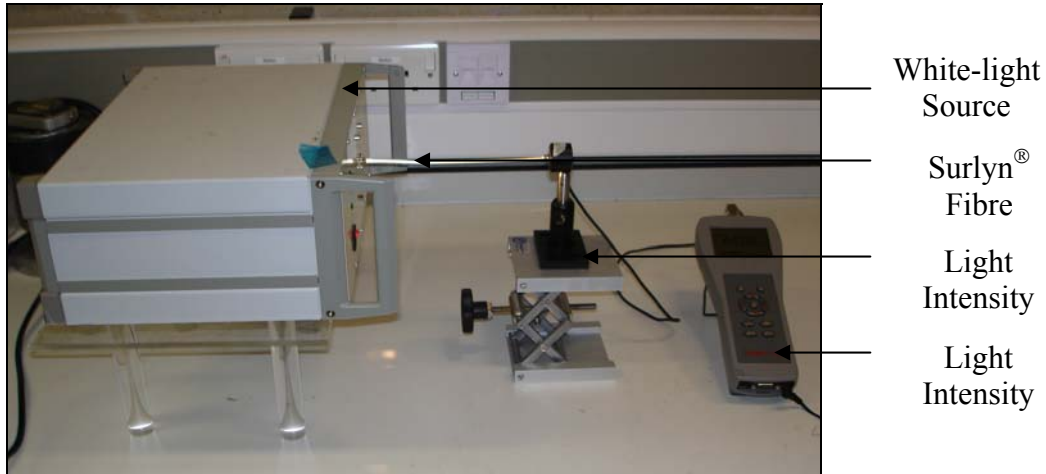


**Figure 19** – Photograph of light transmission intensity measurement set-up.

#### **4.6.2.** *Comparison of Light Transmission between Surlyn® PC2000 and PMMA fibres*

A study was undertaken to enable a comparison of the light transmission characteristics of the Surlyn® fibres and as-received PMMA optical fibres. Twelve fibres were tested for each type of fibre using the method described in section 4.6.1.

#### **4.6.3** *Effect of Fibre Connection on Light Transmission Measurements*

Initial light transmission experiments were carried out without connecting the fibres with SMA connectors. This study was undertaken to investigate whether the connection with the light source and detector had an effect on the light intensity. Twelve fibres of Surlyn® PC2000 and 9910 were tested using the method described in section 4.6.1.

#### **4.6.4** *Light Transmission Distance Measurements for Extruded Thin Surlyn<sup>®</sup> fibres*

As Surlyn<sup>®</sup> PC2000 and 9910 fibres could be extruded in longer lengths and smaller diameters, the light guide distance was measured for each setting used to haul off the fibres. This study was used to investigate whether the smaller diameter fibres possess the ability to act as light guides. Each fibre was placed 10 mm into the light source (Intralux 4000-1, Volpi, USA). The other end was visually observed and cleaved in 10 mm increments until light was observed. A photograph of the experimental set-up is presented in figure 20.

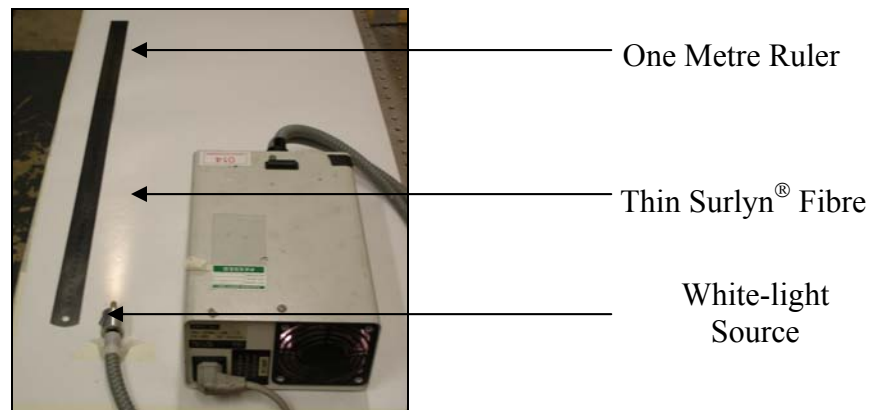


**Figure 20** – Photograph of fibre light guide measurement set-up.

#### **4.6.5** *Fibre Connection Methods using SMA Connectors*

Following the initial light transmission studies, this section investigated the development of three different methods for connecting the thin Surlyn<sup>®</sup> PC2000 fibres with SMA connectors (0.5 mm). A diagram of the three different methods is presented in figure 21.

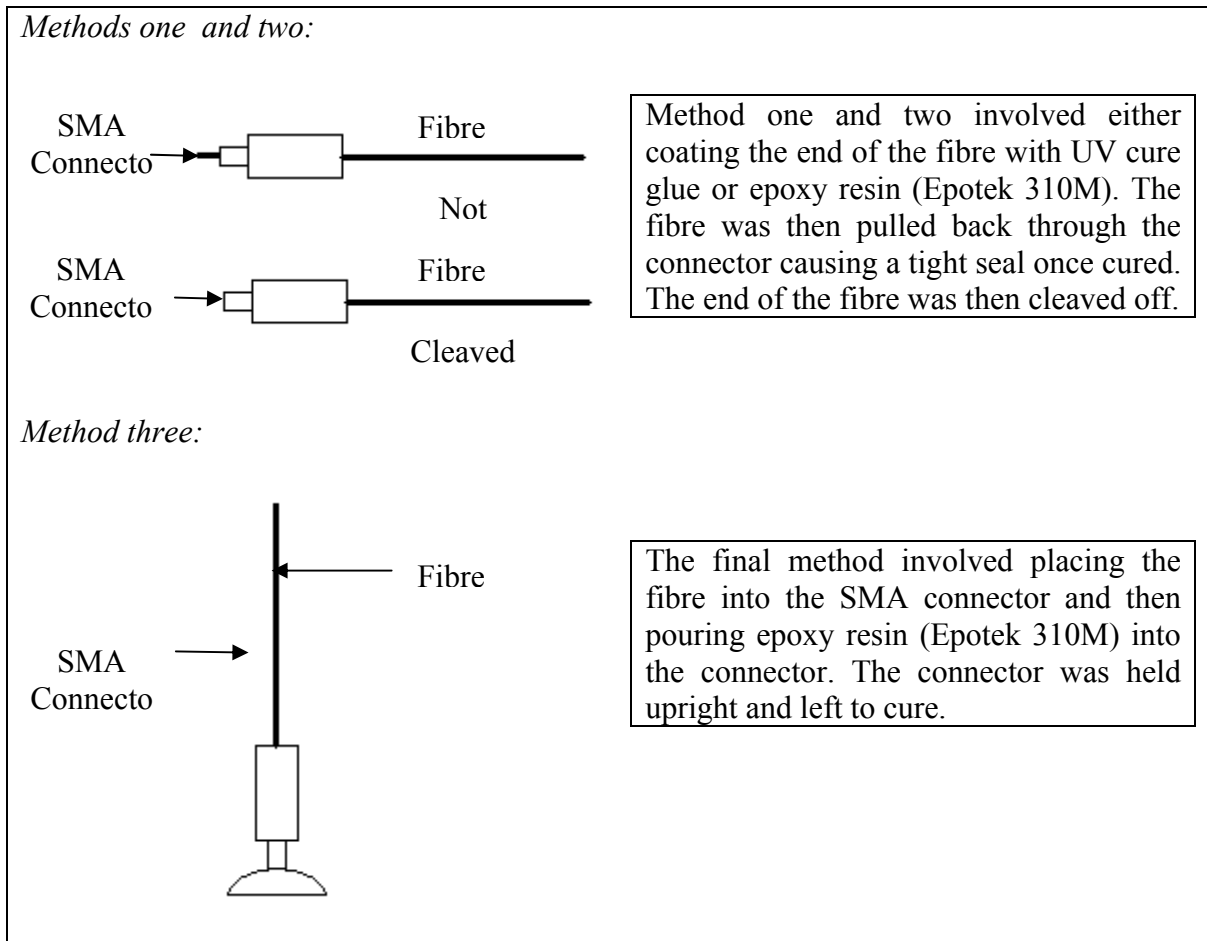


**Figure 21** – Schematic diagram showing the three different methods used to connect thin Surlyn<sup>®</sup> PC2000 fibres with SMA connectors.

#### **4.6.6** *Light Transmission Measurements through Extruded Thin Surlyn<sup>®</sup> fibres*

As a method to connect the thin Surlyn<sup>®</sup> PC2000 fibres with SMA connectors had been developed, this study was undertaken to characterize the light transmission and self-sensing capabilities of the hauled off Surlyn<sup>®</sup> PC2000 fibres.

Four different lengths of fibre (40 cm, 30 cm, 20 cm and 10 cm) were tested for each hauled off fibre. Measurements were carried out using a white light source (Intralux 4000-1) and a light intensity meter (Thorlabs LTD, Cambridgeshire, CB7 4EX). The experimental set-up is presented in figure 22. Four different procedures were carried out for each light transmission reading and are presented in table nine.

**Table 9** – Summary of light transmission procedures carried out on thin Surlyn<sup>®</sup> PC2000 fibres.

	<b>Experimental Procedure</b>
<b>1</b>	Measurements were taken after the fibre was fully connected to both light source and detector.
<b>2</b>	Measurements were taken after both ends of the fibre were disconnected and then reconnected to both light source and detector.
<b>3</b>	Measurements were taken after each SMA connector was disconnected half-way from both the light source and detector.
<b>4</b>	Light transmissions were recorded whilst fibres were cut 1 cm away from the detector.

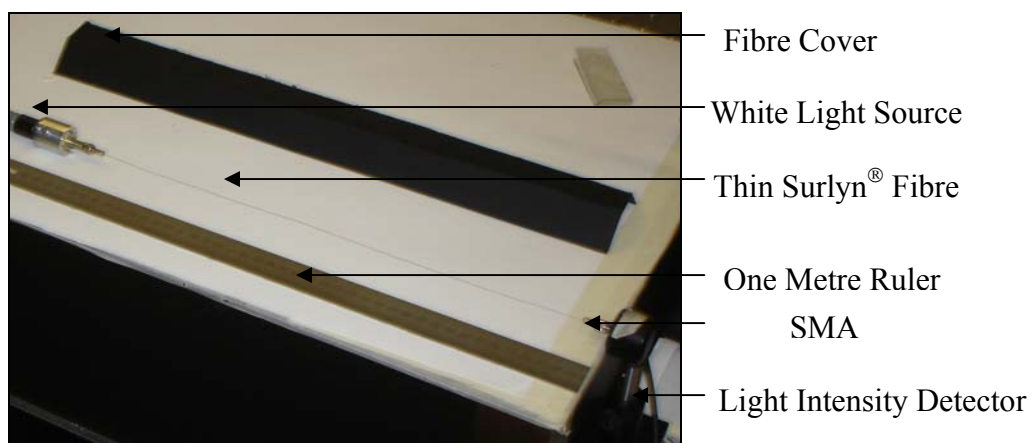


**Figure 22** – Photograph of light transmission intensity measurement set-up.



#### **4.6.7 Attenuation Experiments**

The following experiments were undertaken to establish the attenuation characteristics of the thin Surlyn<sup>®</sup> PC2000 fibres. These experiments were carried out to establish whether the process of embedding the Surlyn<sup>®</sup> fibres in an autoclave would attenuate the light transmission characteristics through the fibres.

Using the experimental set-up shown previously in figure 22; weights were placed on the centre of the fibre to study their affect on light transmission. The weights that were used during testing are presented in table 10. The 20 cm, setting one hauled off fibre was used throughout testing. Each experiment lasted 30 seconds and the weight was applied to the fibre from 11-20 seconds enabling the attenuation characteristics to be established.

**Table 10** – Weights used during attenuation experiments.

<b>Applied Weight (g)</b>
10
50
100
500
1000
2000

## **4.7 Fibre Characterisation**

Following the preliminary characterisation of both Surlyn<sup>®</sup> PC2000 and 9910 plaques, this section was carried out to investigate whether extruding the fibre has caused any changes in such properties as the density and crystallinity.

The Surlyn<sup>®</sup> PC2000 fibre (setting six) was studied as this fibre was shown to have the best light guide distance and was involved during further testing.

### **4.7.1 Fibre Density Measurements**

Using the procedure that was previously described in section 4.2.2, density measurements were carried out on five 20 mm samples.

### **4.7.2 Differential Scanning Calorimetry (DSC)**

Using the temperature ramps previously described in section 4.2.3, the thermal characteristics of the fibre were studied.

## **4.8 Fibre Analysis**

Both image analysis and scanning electron microscopy were used to analyse the surface area and cleaved area of chosen fibres.

## **4.9 Sample Storage**

All samples were handled with surgical gloves and stored inside a desiccator until needed for testing.

## **4.10 Surlyn® Composite Development**

The main focus of this section was to develop and fabricate Surlyn® composites with both self-healing and self-sensing capabilities. Both Surlyn® PC2000 fibres (setting six) and Surlyn® 1706 film were incorporated with glass-fibre pre-preg. The intention was to subject samples to both indentation and ballistic experiments investigating their capabilities, however it was not possible to undertake these tests due to various reasons that were outside the control of the author.

### **4.10.1 *Production of Composites***

#### **4.10.1.1 *General Pre-preg Lay-up***

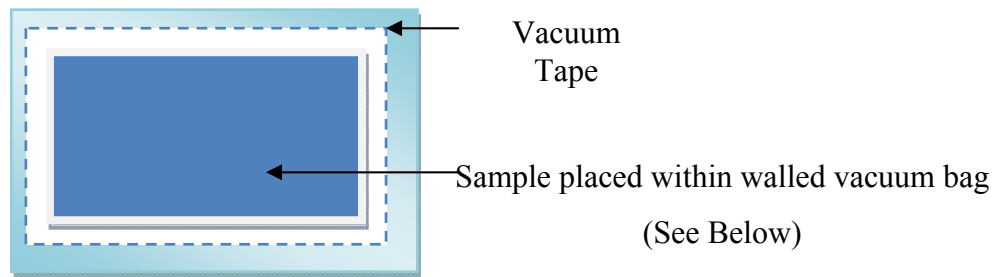
Each laminate was cut to size using a Stanley knife. The laminates were then laid on top of each other at the required orientation. A custom made tool was designed to assist with the alignment of the laminates and consolidation of the laminates was carried out using a wooden roller.

#### **4.10.1.2 *Vacuum Bagging Procedure***

Before the samples could be consolidated using an autoclave, the sample has to go through a procedure known as ‘vacuum bagging’. This allows both pressure and vacuum to be applied resulting in greater interlaminar bonding and lower void content.

Before carrying out the procedure a release agent (Chem Trend Monocoat 1367L) was applied to the aluminium tooling plate allowing the sample to be easily removed from the autoclave following consolidation. The vacuum bagging procedure and materials required are presented in figure 23.

*Plan View:*



*Cross Sectional View:*

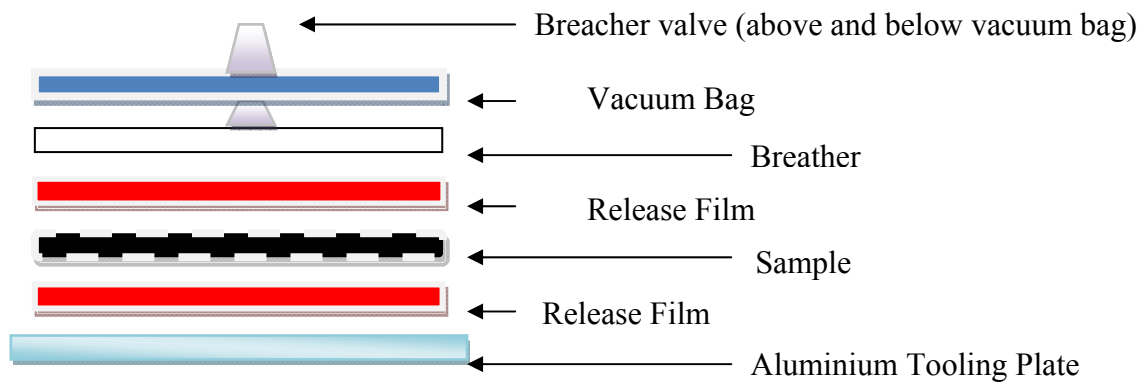


**Figure 23** – Schematic diagram of vacuum bagging procedure.

#### **4.10.1.3** *Curing of Composite Samples*

All composite samples were cured using an autoclave (99/20; Leeds and Bradford Boiler Company UK). The autoclave was controlled via a personal computer which used a commercially available package (SV32 Version 2; Specview Ltd, UK). A photograph of the autoclave is presented in figure 24.

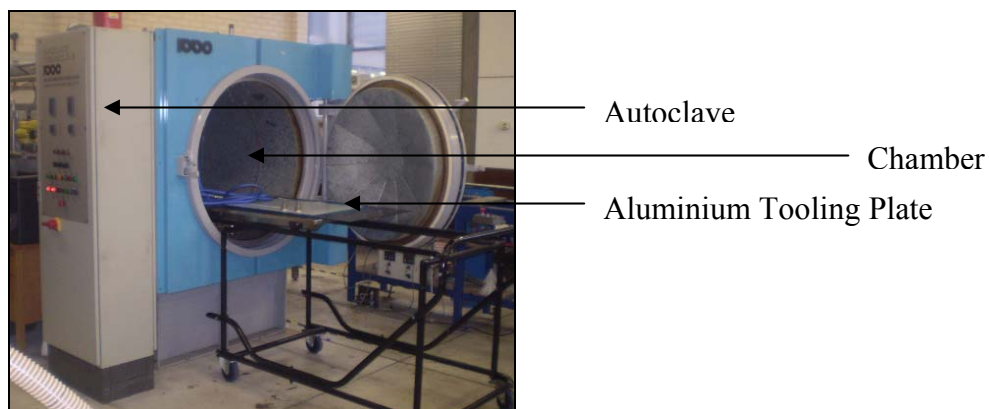


**Figure 24** – Photograph of autoclave used to cure composite samples.

The autoclave was equipped with temperature, vacuum and pressure control capabilities. All samples were cured under the same processing schedule shown in table 11.

**Table 11** - Material processing schedule.

TEMPERATURE CONTROL					PRESSURE CONTROL				
Profile segment	Ramp rate (°C/minute)	Target temperature (°C)	Time (mins)	Cycle end command	Profile segment	Ramp rate (MPa/minute)	Target pressure (MPa)	Time (mins)	Vacuum command
1	2	65		On	1	0.00 <sub>7</sub>	0.007		On
2			1.0	On	2			20	On
3	2	120		On	3	0.02 <sub>1</sub>	0.138		On
4			60.0	On	4			1	Off
5	2	50		On	5	0.02 <sub>1</sub>	0.482		Off
6			2.0	On	6			67	Off
7	1	25		Off	7	0.01 <sub>4</sub>	0		On

#### **4.10.2 *Self-healing Composite Development***

The development of a self-healing composite involved fabricating Surlyn<sup>®</sup> 1706 film, with VTM 264 glass-fibre (Unidirectional glass fibre/epoxy pre-impregnated material, Advanced Composites Group, UK). The average thickness of the Surlyn<sup>®</sup> film was 0.06 mm. Single ply, two ply and four ply unidirectional samples were produced. All samples were 50 mm x 50 mm in dimension and the different sample lay-up sequences are presented in figure 25.

Key:

 Glass fibre pre-preg       Surlyn<sup>®</sup> 1706 film

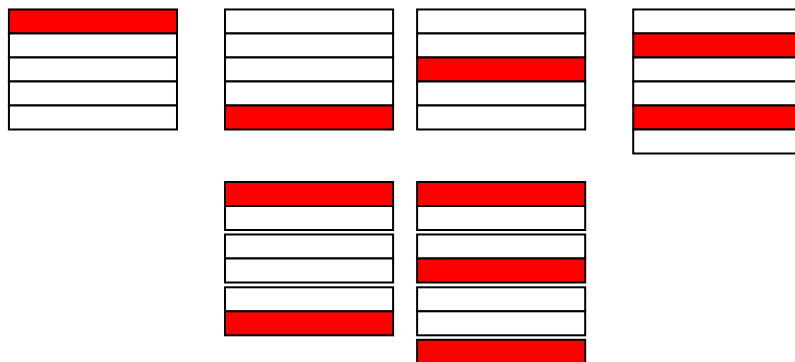
*Single Ply:*



*Two Ply:*



*Four ply:*



*One, two and four ply reference samples:*

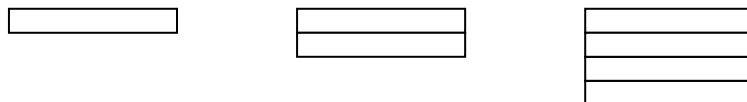




**Figure 25** – Schematic diagrams showing different lay-up sequences for the Surlyn<sup>®</sup> 1706 film and glass fibre composite samples.



#### 4.10.3 Self-healing/Self-sensing Composite Development

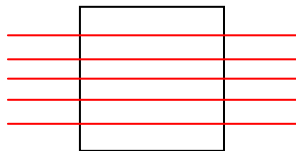
Composites were fabricated using VTM 264 glass-fibre and five different types of fibre. Surlyn<sup>®</sup> PC2000 fibres (setting six) were added to all composite samples. The aim of this aspect of the research was to develop a composite with both self-healing and self-sensing capabilities, where Surlyn<sup>®</sup> with its reputation for self-healing could also be used to sense fibre damage.

All five samples were 50 mm x 50 mm and single ply. All fibres were 150 mm in length. The composite set-up and different fibres used during fabrication of the samples is presented in figure 26.

Key:  VTM 264 glass-fibre  Surlyn<sup>®</sup> PC2000 fibre

*Sample 1:*

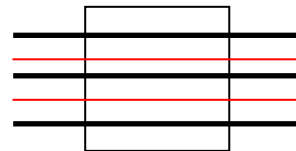
33 Surlyn<sup>®</sup> PC2000 fibres



*Sample 2:*

10 Surlyn<sup>®</sup> PC2000 fibres

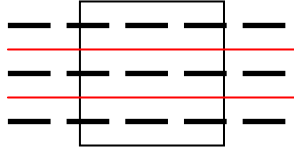
11 PMMA fibres



*Sample 3:*

8 Surlyn<sup>®</sup> PC2000 fibres

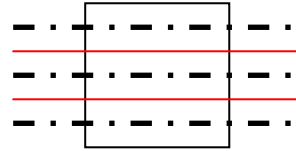
9 bundles of S2 hollow glass-fibres



*Sample 4:*

9 Surlyn<sup>®</sup> PC2000 fibres

9 bundles of small diameter optical fibres



*Sample 5:*

10 Surlyn<sup>®</sup> PC2000 fibres

11 Stripped standard optical fibres

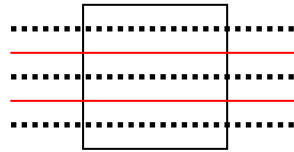


**Figure 26** – Schematic diagrams showing different lay-up sequences for the Surlyn<sup>®</sup> PC2000 fibres and glass-fibre composite samples.

#### **4.10.4 Crack Arrestor Composites**

The main focus of this part of the study was to investigate whether Surlyn<sup>®</sup> would act as a crack arrestor when incorporated into a carbon-fibre composite. Mode I fracture tests were carried out and were used to determine the  $G_{Ic}$ , the critical energy release rate, of the fibre reinforced composites.

#### 4.10.4.1 Crack Arrestors

Three carbon-fibre (VTM 264 unidirectional carbon fibre/epoxy material, Advanced Composites Group, UK) reinforced composites were made with Surlyn<sup>®</sup> acting as a crack arrestor. The three different Surlyn<sup>®</sup> crack arrestors are presented in table 12.

**Table 12** – Surlyn<sup>®</sup> crack arrestors used during Mode I fracture testing.

Plate	Crack Arrestor
1	87 Surlyn <sup>®</sup> PC2000 setting six Fibres
2	Surlyn <sup>®</sup> 1706 Film
3	Surlyn <sup>®</sup> 1706 Punctured Film

The film was punctured using a custom made device (see Figure 27). Punctures were introduced to increase resin flow through the film. A 16 ply carbon-fibre reference plate was also produced, enabling a comparison to be made against the Surlyn<sup>®</sup> crack arrestors.

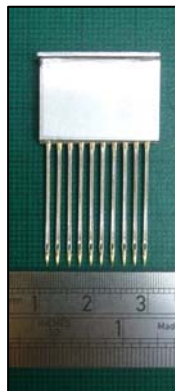


**Figure 27** – Photograph of custom made puncture device.

#### 4.10.4.2 Composite Set-up

Each composite plate was 16 ply and 300 mm x 300 x 5 mm in size. The Surlyn<sup>®</sup> crack arrestors and PTFE strip were placed in the centre between the eighth and ninth plies. The PTFE strip was used to produce the pre-crack which was required for the Mode I test. An example of the composite set-up for the Surlyn<sup>®</sup> film plates is presented in figure 28. For the samples containing fibres they were placed vertically where the film is shown in figure 28.

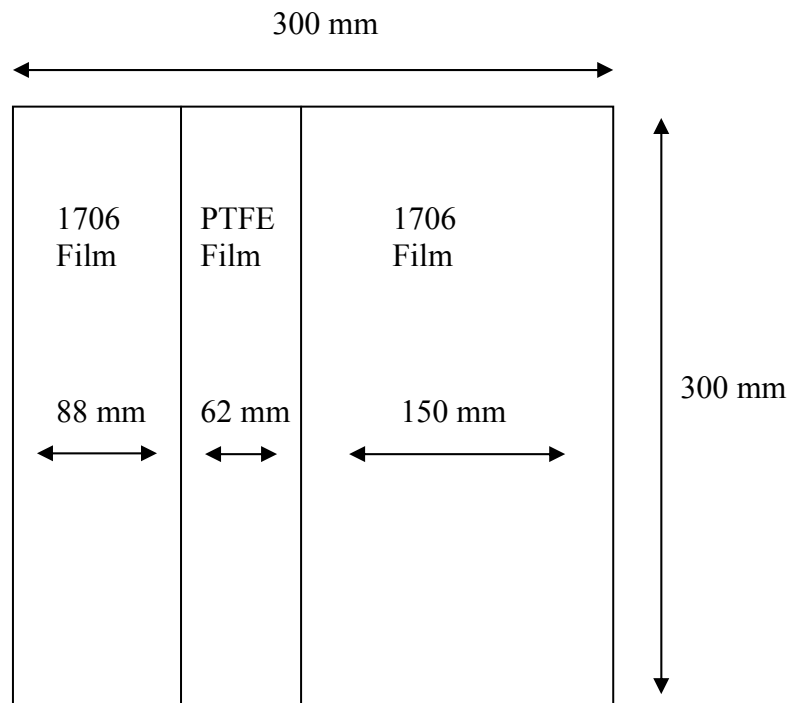


**Figure 28** – Schematic diagram showing the set-up at the centre of the 16 ply Surlyn<sup>®</sup> film composite plate.

#### 4.10.4.3 $G_{Ic}$ Sample Preparation

Five samples were produced from each composite plate. Samples were cut to size (length – 125 mm, width – 20 mm) using a diamond cutting wheel and inspected to ensure the PTFE had initiated a pre-crack.

Blocks which hold the specimen in the fixture were then fitted. One block was fitted to each side of the pre-crack end of the specimen. The blocks were fitted to the sample using scotch weld (two part B/A structural adhesive) and cured for two hours at 66 °C.

Finally the PTFE section was identified and the rest of the specimen was labelled. At the end of the PTFE section marks were drawn at 5 mm intervals along the edge, extending to 55 mm. The first 10 mm and last 5 mm were marked with 1 mm intervals. A photograph of a  $G_{Ic}$  specimen is presented in figure 29.

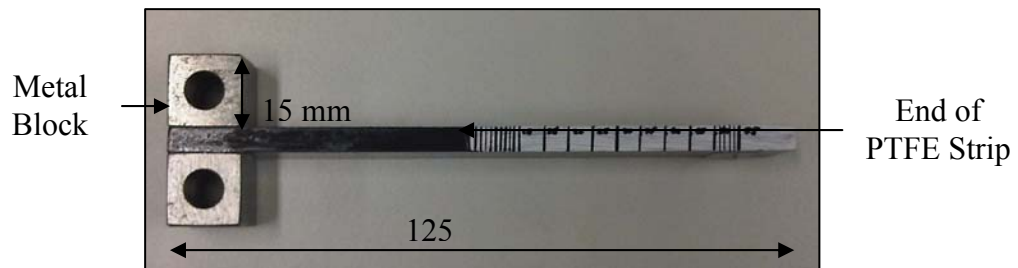


**Figure 29** – Photograph of  $G_{Ic}$  test specimen.

#### 4.10.4.4 $G_{Ic}$ Test Procedure

An Instron machine (Model 5566, Serial no. H1529) was used to carry out the mode I fracture toughness tests. The  $G_{Ic}$  test specimen was fitted into the Instron using a custom made fixture. A photograph of the Mode I set-up is presented in figure 30.

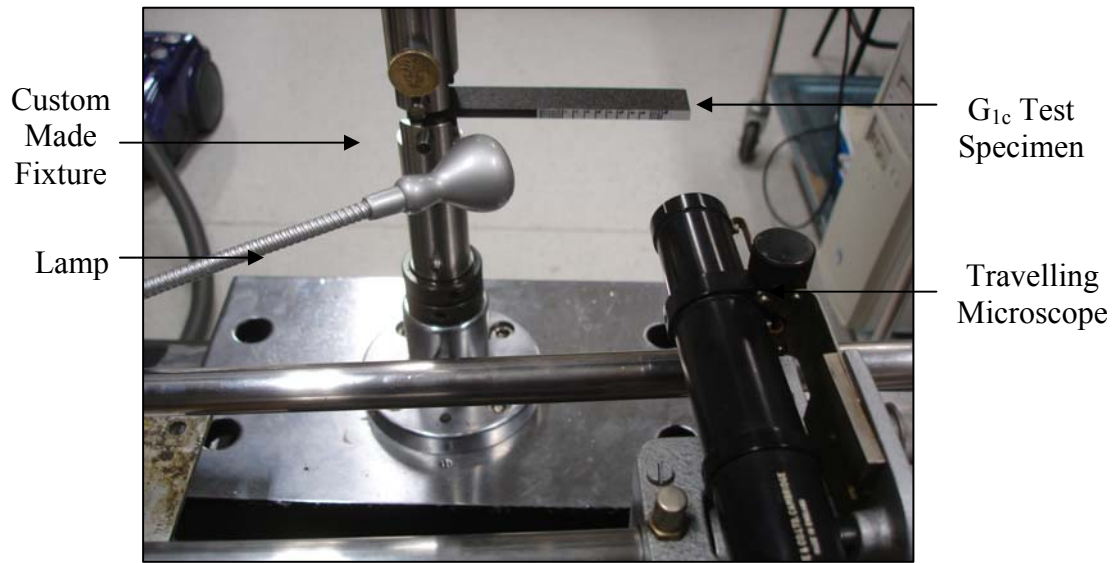


**Figure 30** – Photograph of Mode I experimental set-up.

The Mode I tests were carried out in accordance with the British Standard BS ISO15024.<sup>79</sup> The experimental procedure that was used for each test specimen is presented in table 13.

**Table 13** –  $G_{Ic}$  test procedure with accordance to British Standard BS ISO15024.<sup>79</sup>

	<b>Procedure – With accordance to British Standard BS ISO15024</b>
<b>Test Set-up</b>	The $G_{Ic}$ test specimen was fitted into the fixture ensuring that the beam was perpendicular with direction of the applied load.
<b>Initial Loading (Pre-crack)</b>	The specimen was loaded at 1 mm/min to produce a pre-crack of 3 mm. The specimen was then unloaded at 5 mm/min.
<b>Re-loading</b>	The specimen was re-loaded at 1 mm/min without stopping until the final delamination increment was reached or the specimen failed. The specimen was then unloaded at 5 mm/min.
<b>Data</b>	Throughout the test the load and displacement values were recorded continuously by the Instron. A microscope was used to monitor crack propagation and AE Win software was used to manually trigger the delamination increments which were then matched up with the displacement and load from the Instron data.

#### 4.10.4.5 $G_{Ic}$ Calculation

Using the data collected and a database (Excel spreadsheet); fracture toughness  $G_{Ic}$  values were determined from the corresponding points on the load-displacement curve. From this curve a value of (P) is calculated as the onset of crack growth. This point is also calculated as the point at which delamination is visually observed (VIS). The corrected beam theory (CBT) (A) and modified compliance calibration (MCC) (B) were the two data reduction methods used to calculate the critical energy release rate  $G_{Ic}$ . Figure 31 presents the data required to carry out both analysis methods.

$A_0$	Initial delamination length
-------	-----------------------------

A	Total delamination length
P	Load
$\Delta$	Load line displacement
C	Load line compliance $\delta / P$
B	Width of specimen
2h	Thickness of specimen

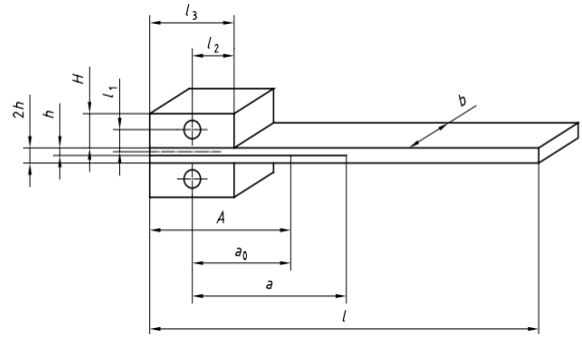


**Figure 31** – Data and geometry for CBT and MCC calculations.<sup>79</sup>

The two data reduction methods CBT and MCC used to calculate  $G_{IC}$  are presented below:

*Method A* - Corrected beam theory (CBT):

$$G_{IC} = \frac{3P\delta}{2b(a + |\Delta|)} \times F \quad (3)^{79}$$

F – Large displacement factor

N – Load block correction

*Method B* – Modified Compliance Calibration (MCC):

$$G_{IC} = \frac{3m}{2(2h)} \times \left(\frac{P}{B}\right)^2 \times \left(\frac{bC}{N}\right)^{2/3} \times F \quad (4)^{79}$$

F – Large displacement factor

N – Load block correction



#### **4.10.4.6 $G_{Ic}$ Test Specimen Analysis**

Before testing image analysis was carried out on one sample from each crack arrestor type. Following testing S.E.M was carried out on the fracture surface of one of the failed samples from each type of investigated crack arrestor.

## **5.0 Results and Discussion**

The focal point of the study was to develop Surlyn<sup>®</sup> as a self-healing and self-sensing composite. The ability of Surlyn<sup>®</sup> (8940) as a self-healing material was discussed during the literature review section. The following results aim to investigate the self-healing ability of Surlyn<sup>®</sup> and establish the self-sensing ability of Surlyn<sup>®</sup>.

Initial characterisation experiments were employed to obtain information about the three grades of Surlyn<sup>®</sup> used during the study.

The development of thick Surlyn<sup>®</sup> plaques was studied for self-healing aspects, whilst the self-sensing capabilities of Surlyn<sup>®</sup> were investigated through the development of Surlyn<sup>®</sup> fibres which were subjected to various light transmission studies.

Surlyn<sup>®</sup> film and fibres were then incorporated with glass-fibre and carbon-fibre pre-impregnated materials.

The crack healing capacity of Surlyn<sup>®</sup> was studied along with the development of a Surlyn<sup>®</sup> composite, with a view to developing a self-sensing and self-healing Surlyn<sup>®</sup> composite.

## 5.1 Preliminary Characterisation

### 5.1.1 Density Measurements

Table 14 presents the five density measurements; average density and standard deviation for all three grades of Surlyn<sup>®</sup> (see Appendix Figure 1 for raw data).

**Table 14** – Density measurement for all three grades of Surlyn<sup>®</sup>.

	Surlyn <sup>®</sup> Grade		
	Surlyn <sup>®</sup> PC 2000	Surlyn <sup>®</sup> 9910	Surlyn <sup>®</sup> 1706
Sample No.	Density (g/cm <sup>3</sup> )		
1	0.967	0.973	0.987
2	0.968	0.974	0.985
3	0.967	0.973	0.977
4	0.969	0.974	0.977
5	0.968	0.973	0.942
<b>Average</b>	<b>0.968</b>	<b>0.973</b>	<b>0.974</b>
S.D	0.0008	0.0005	0.02

The average density for Surlyn<sup>®</sup> PC2000 and 9910 was recorded at 0.97 g/cm<sup>3</sup> matching the data found on DuPont's data sheets.<sup>80, 81</sup> The standard deviation was very low showing a high consistency for the measurements recorded.

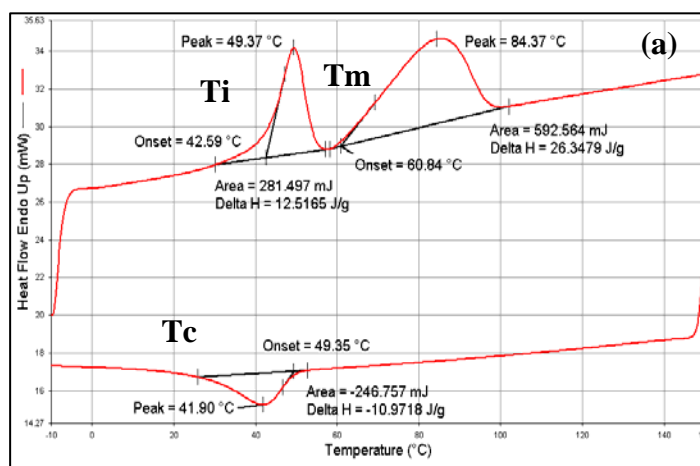
The average density for Surlyn<sup>®</sup> 1706 was 0.97 g/cm<sup>3</sup>. This was slightly higher than the 0.95 g/cm<sup>3</sup> found on the material data sheet.<sup>82</sup> The standard deviation was also higher showing a wider spread of data. The results may be due to changes in temperature and humidity.

The results show that the three grades of Surlyn<sup>®</sup> are amorphous. This is due to high branching present in the material. The amorphous nature of the material makes them transparent in film form.

The low density and transparency make Surlyn<sup>®</sup> ideal for a composite material. This is due to the low density of Surlyn<sup>®</sup> making it lightweight and as reported the primary advantage of a composite is their lightweight property. The transparency also suggests that Surlyn<sup>®</sup> maybe able to guide light and is further examined later on in the report.

### 5.1.2 Differential Scanning Calorimetry (DSC)

Two different temperature ramps (one cycle and three cycles) were employed to study the thermal characteristics of Surlyn<sup>®</sup> PC2000, 9910 and 1706. Temperatures ran from – 10 °C up to 150 °C. Figure 32 shows an example of a one cycle temperature ramp for Surlyn<sup>®</sup> PC2000 (see Appendix Figure 2 for Surlyn<sup>®</sup> 9910 and 1706).



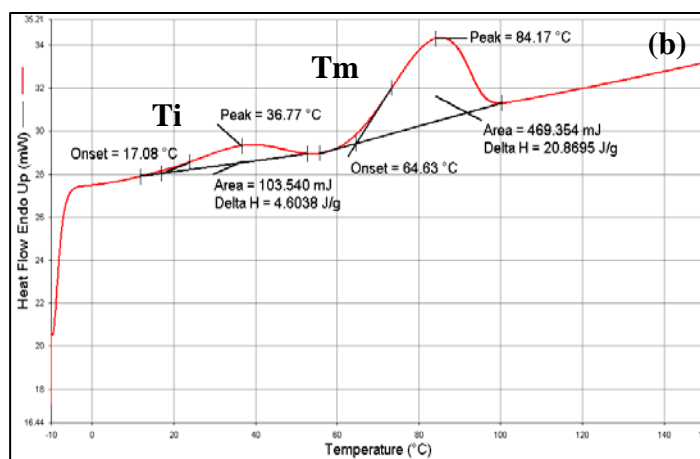


**Figure 32** – DSC of Surlyn<sup>®</sup> PC2000; one cycle.

From the DSC results; the thermal transitions including the order-disorder transition ( $T_i$ ), melt transition ( $T_m$ ), crystallization transition ( $T_c$ ) and crystallinity % were determined for each material (Table 15). The order-disorder is a thermal transition found in ionomers and is discussed below. Material crystallinity was determined using the following equation:

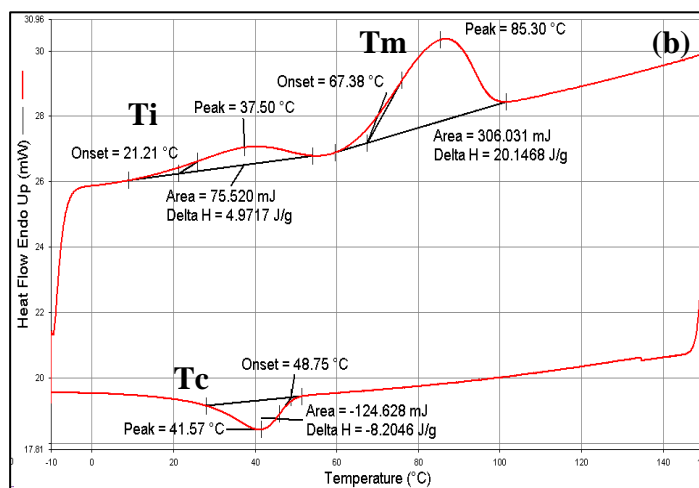
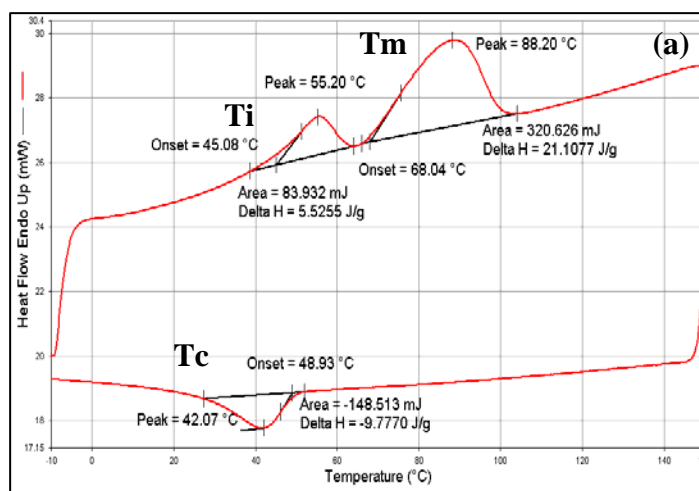
$$\text{Heat of fusion for sample} / \text{Heat of fusion of 100 \% crystalline material} \times 100 \quad (5)$$

**Table 15** – Thermal characteristics of Surlyn<sup>®</sup> PC2000, 9910 and 1706.

Surlyn <sup>®</sup> Grade	$T_i$ (°C)	$T_m$ (°C)	$T_c$ (°C)	Crystallinity (%)
PC2000	49.37	84.37	41.9	9
9910	51.87	91.37	54.9	11
1706	60.67	90	61.9	10

The same trend was shown for all grades of the material. Referring back to figure 32a the first peak is known as the order-disorder transition and for Surlyn<sup>®</sup> PC2000 once a temperature of

~ 50 °C is reached the ionic aggregates become disordered. Upon the second heat shown in figure 32b the transition Ti has been suppressed and the temperature causing this transition has decreased.<sup>26, 83</sup> For all three grades, all samples have low crystallinity corresponding to the low density measurements previously reported. The amount of crystallinity present in the material is controlled by the amount of branching. Only segments between the branches can crystallise and if the number of branch points is high the crystallinity and density of the material is low.



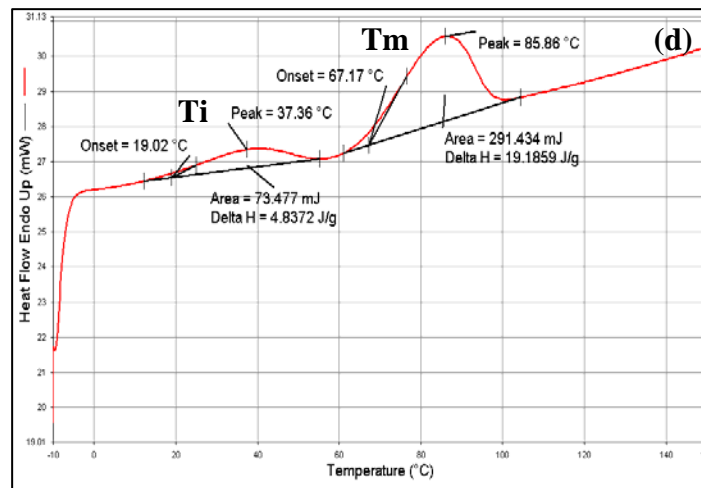
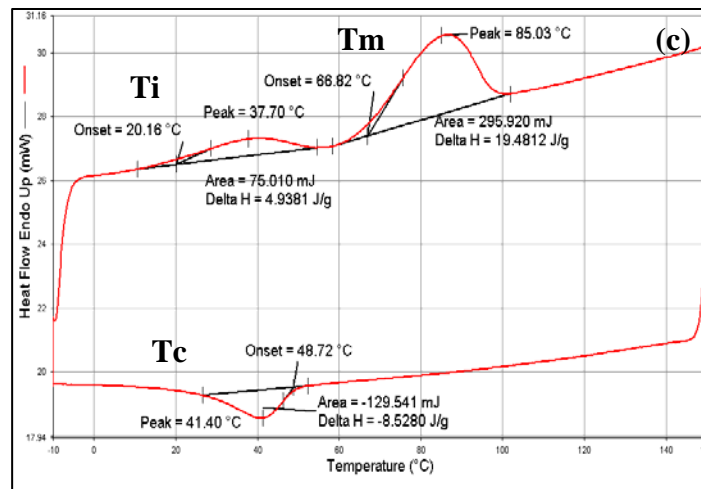


**Figure 33** - DSC of Surlyn<sup>®</sup> PC2000; three cycles.

Figure 33 is an example of a three cycle temperature ramp for Surlyn<sup>®</sup> PC2000 (see Appendix Figure 3 for Surlyn<sup>®</sup> 9910 and 1706). All grades followed the same trends, where the order-disorder transition (Ti) was suppressed. The temperature for the transition is also shown to drop.

Further studies have shown that when the sample (Surlyn<sup>®</sup> 8940) is left for a short period of time (one hour) the ionic aggregates are said to re-order and the suppressed Ti peak return.<sup>26</sup>

Overall a clear link is shown between the DSC results and density measurements suggesting that Surlyn<sup>®</sup> is a low density, amorphous material. Information obtained will enable further understanding and development during the study.

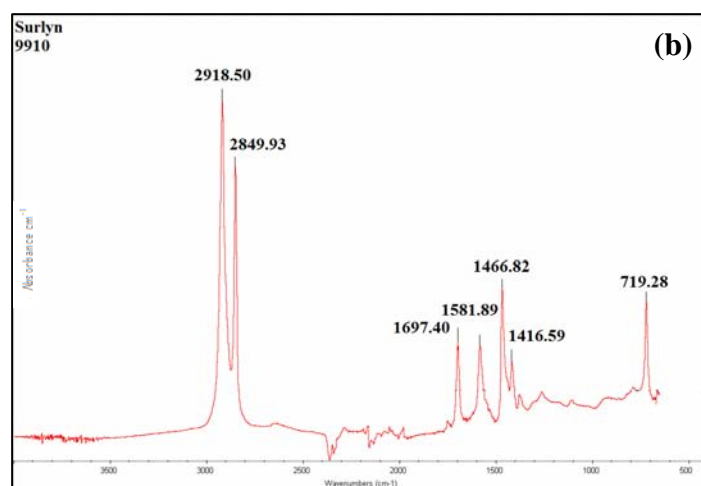
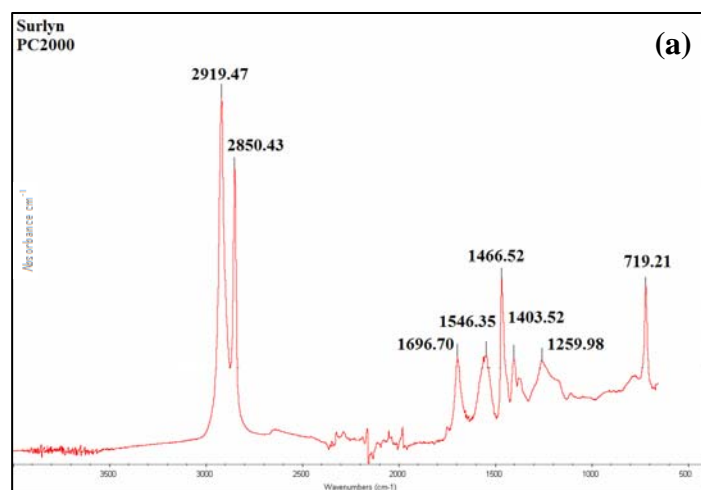
### **5.1.3 Fourier Transform Infrared Spectroscopy (FTIR)**

MFTIR was used to examine the molecular structures of Surlyn<sup>®</sup> PC2000, 9910 and 1706. Figure 34 contains spectra for all three grades of Surlyn<sup>®</sup>. The MFTIR had a spectral range of 4000 – 700 cm<sup>-1</sup>.

From the spectra collected for all three grades of Surlyn<sup>®</sup> analysis showed that the sharp band at ~ 720 cm<sup>-1</sup> is caused by methylene rocking in the pendant backbone.<sup>84</sup> The ~ 1260 cm<sup>-1</sup> peak found on the PC2000 spectra is due to C-O stretching vibrations of COOH groups in the hydrogen bonded dimers.<sup>85</sup> The other bands found between ~ 1400 – 1550 cm<sup>-1</sup> are due to CO<sub>3</sub> groups.<sup>86</sup>

The peak with a wavelength of ~ 1700 cm<sup>-1</sup> is due to C=O stretching vibrations in H bonded carboxylic acid dimers where both C=O groups are in H bands.<sup>87</sup> Finally the two large peaks are present due to CH<sub>3</sub> groups (~ 2850 cm<sup>-1</sup>) and methyl groups (~ 2920 cm<sup>-1</sup>) present in the materials.<sup>88, 89</sup>





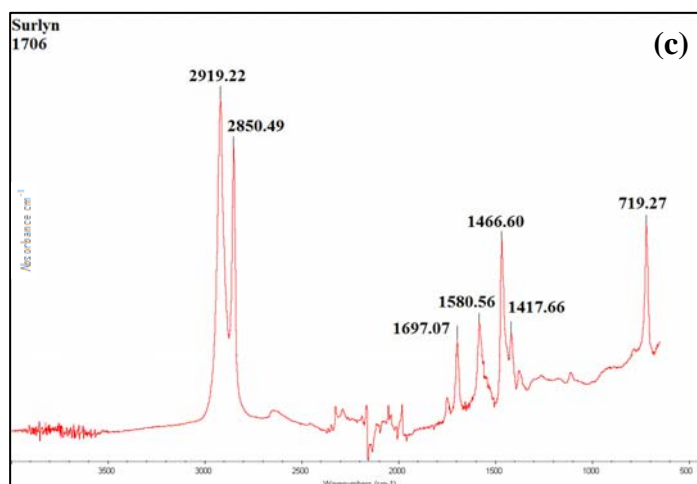


**Figure 34** – MFTIR transmission spectrum of Surlyn<sup>®</sup> (a) PC2000, (b) 9910 and (c) 1706.

All recorded spectra show that all three grades of Surlyn<sup>®</sup> contain the same structures. These results are expected as the polyethylene based materials differ only in the metallic cation with which they are neutralized with (sodium and zinc).

#### **5.1.4 Refractive Index (RI) Measurements**

The refractive indices (RI) of all three Surlyn<sup>®</sup> grades were taken in transmission mode with contact liquid (monobromonaphthalene).

**Table 16** – Refractive Indices for Surlyn<sup>®</sup> PC2000, 9910 and 1706.

<b>Surlyn<sup>®</sup> PC2000</b>	RI	Temperature (°C)	RT (°C)
Sample 1	1.51	26.7	25.3
Sample 2	1.51	27.3	25.4

<b>Surlyn<sup>®</sup> 9910</b>	RI	Temperature (°C)	RT (°C)
Sample 1	1.51	26.4	24.2
Sample 2	1.51	27	25

<b>Surlyn<sup>®</sup> 1706</b>	RI	Temperature (°C)	RT (°C)
Sample 1	1.51	27.4	25
Sample 2	1.51	26.3	24.9

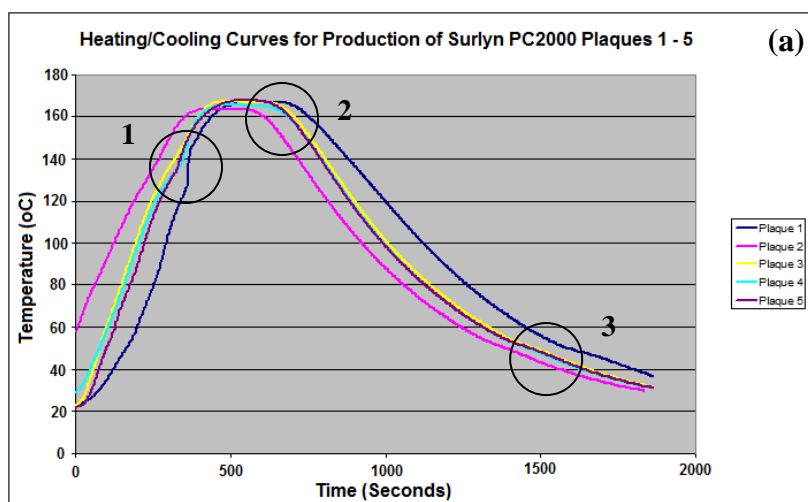
A low RI of 1.51 was measured for all three grades and matches the indices given by DuPont.<sup>90</sup> The RI for Surlyn<sup>®</sup> is said to be between 1.51 and 1.52.

The greater the index of refraction, the slower light travels through the material. The RI of a typical optical fibre is 1.48. The RI of the material also increases with density.<sup>91</sup> With these details and with reference to the known RI of Surlyn<sup>®</sup> and the transparency of the material, the use of Surlyn<sup>®</sup> as a light guide is promising and is investigated further during the course of the study.

## 5.2 Production of Surlyn® PC2000 and Surlyn® 9910 Thick Plaques

### 5.2.1 Production of Thick Plaques

The next stage of the experimental work employed a novel way of fabricating thick Surlyn® plaques, whilst monitoring heat flow through the material using a k-type thermocouple. Figure 35 contains the heating/cooling curves produced during fabrication of Surlyn® PC2000 and 9910 thick plaques (see Figure 36).



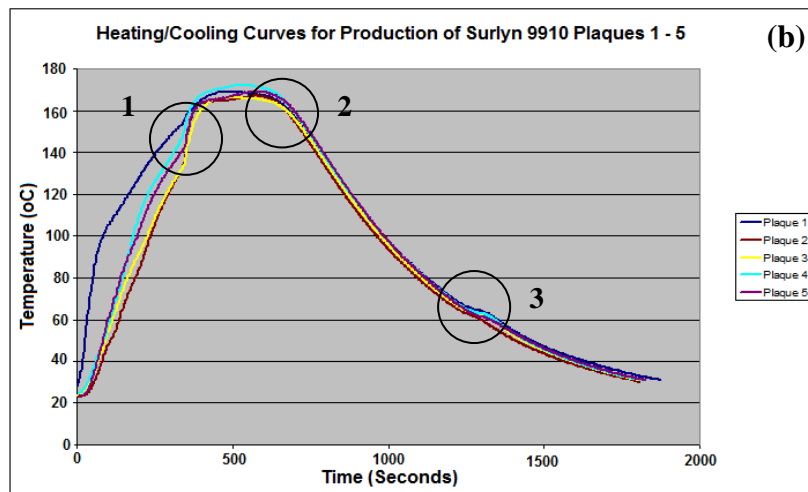


**Figure 35** – Heating/Cooling curves for production of thick Surlyn<sup>®</sup> plaques

(a) PC2000 and (b) 9910.

Both graphs contain all five curves for each plaque fabricated. The beginning of each curve shows the temperature increase during stabilisation time in the press. Area one circled on the graph indicates where pressure was then applied to the samples causing a steep rise towards the fabrication temperature (165 °C).

The curves then plateau off as the fabrication temperature is reached. Area two indicates the start of the cooling period as a gradual decline in temperature is visible. The crystallisation transition of the plaque is indicated on the graph by section three. Fabrication of the Surlyn<sup>®</sup> plaques showed that heat flow through the samples was stable.

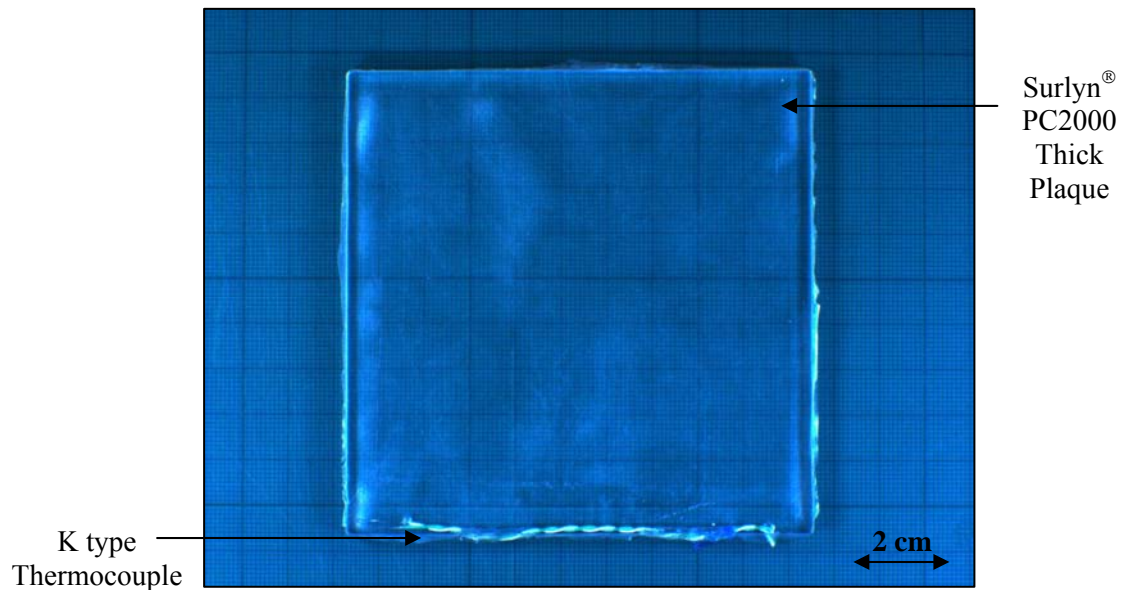


**Figure 36** – Image of thick Surlyn® PC2000 plaque containing a k – type thermocouple.

### **5.2.2** *Monitoring the Temperature Profile within a Thick Plaque (Surlyn® PC2000 and 9910)*

The calibration experiment involved monitoring heat flow through the fabricated thick plaques when heated to known temperatures. This initial experiment was carried out, as future work involved monitoring heat flow through the sample whilst subjected to indentation and ballistic impact experiments. Due to circumstances outside of the authors control indentation and ballistics experiments were not carried out and are further discussed in the future work chapter 7.0.

Eight thermocouples were attached to each plaque and a further two thermocouples were attached to the oven. Figure 37 contains the temperature curves for both monitored plaques.

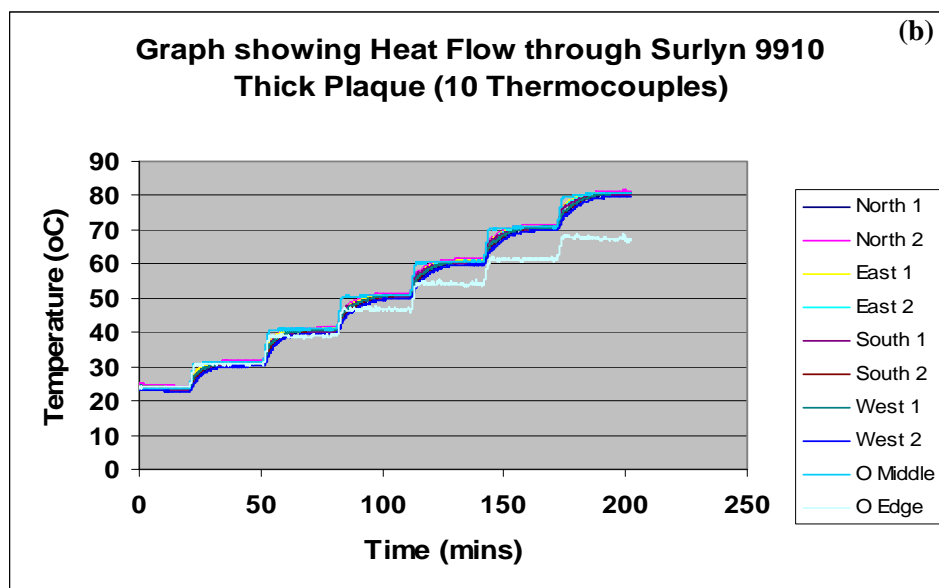
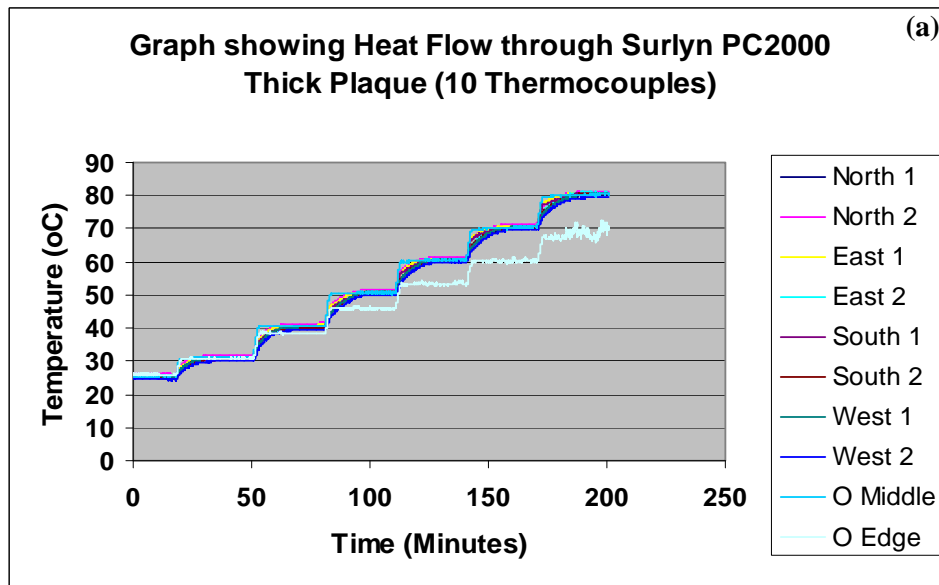


**Figure 37** – Graphs showing monitored heat flow through thick Surlyn<sup>®</sup> plaques.

Both graphs show a uniform trace; showing that heat flow through the plaques is stable. This would enable the temperature to be monitored during the future indentation and ballistics experiments, uncovering the optimum temperatures needed for self-healing.

The non-uniform trace present on both graphs is caused by a slight temperature loss occurring on the outer edges of the oven.

### **5.3 Production of Surlyn<sup>®</sup> Composites**

#### **5.3.1 *Production of Glass-Fibre Reinforced Composites***

After developing a method to fabricate Surlyn<sup>®</sup> plaques, the next step involved using these plaques to develop the novel idea of a Surlyn<sup>®</sup>, self-healing and self-sensing composite. However during this section the initial research aimed to create a composite where the Surlyn<sup>®</sup> thin plaque would act as the self-healing matrix and small diameter optical fibres would act as the self-sensing reinforcing fibres.

Figure 38 shows a photograph of the fabricated composite, with the small diameter optical fibres guiding light. Causing damage to the composite causes bleeding light from the composite and is shown in figure 39. The idea is then for the Surlyn<sup>®</sup> to self-heal, mending the composite material.



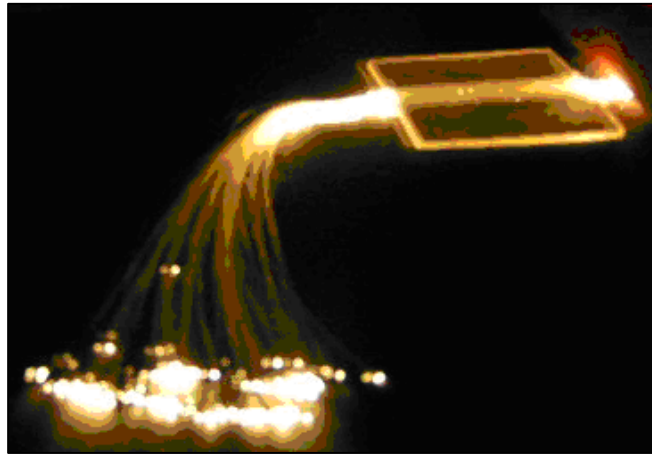


**Figure 38** – Photograph of plaque made from Surlyn® PC2000 and small diameter optical fibres.

Although bleeding light provides a low cost approach to damage detection, the use of small diameter optical fibres enables temperature and pressure to also be used. As ballistic and indentation tests were unable to be carried out, the measurement of the reported self-healing capabilities of Surlyn® are further discussed in the future work chapter 7.0.



**Figure 39** – Photograph demonstrating the Surlyn® composite bleeding light.

## **5.4 Extrusion of Surlyn<sup>®</sup> Fibres**

### **5.4.1 *Development of a Methodology to Extrude Surlyn<sup>®</sup> fibres***

Two methods were developed to extrude Surlyn<sup>®</sup> fibres. This was investigated to establish if Surlyn<sup>®</sup>, with its reported self-healing reputation, could be used as a light guide and at the same time sense as self-healing fibres.

The first method produced Surlyn<sup>®</sup> fibres ranging from ~ 0.3 mm to ~ 3.5 mm in diameter. Specified weights were suspended from the base of the fibre with the intention of extruding fibres with uniform diameter.

Surlyn<sup>®</sup> PC2000 and 9910 fibres were produced. Twelve fibres measuring 200 mm in length were produced for each weight used.

**Table 17** – Average diameter of Extruded Surlyn® PC2000 fibres.

<b>Surlyn®PC2000</b>	<b>Average Fibre Diameter (mm)</b>			
Fibre No.	10 Kg	3 g	5 g	7 g
1	2.105	0.724	0.503	0.509
2	2.070	0.734	0.49	0.548
3	2.555	0.754	0.551	0.541
4	2.510	0.705	0.541	0.532
5	1.885	0.707	0.592	0.586
6	2.753	0.737	0.669	0.465
7	2.772	0.673	0.649	0.559
8	2.694	0.698	0.546	0.549
9	2.591	0.75	0.57	0.578
10	2.390	0.79	0.648	0.669
11	2.668	0.725	0.638	0.53
12	2.734	0.731	0.692	0.582
<b>Average (mm)</b>	<b>2.477</b>	<b>0.727</b>	<b>0.591</b>	<b>0.554</b>
S.D	<b>0.301</b>	<b>0.03</b>	<b>0.067</b>	<b>0.049</b>

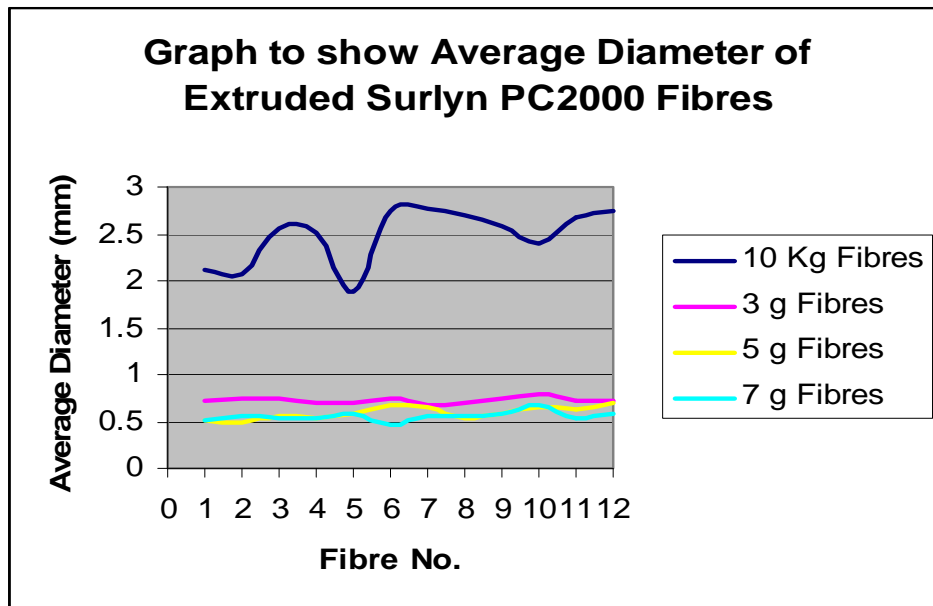


**Figure 40** – Graph showing average diameter of thick Surlyn® PC2000 fibres.

The first set of fibres was extruded using a 10 kg weight applied to the piston. The average diameter of the fibres was 2.477 mm and the standard deviation was 0.301. Figure 40 shows

the curve for the extruded fibre using the 10 kg weight, which has poor uniformity in diameter over the 12 fibres extruded. As the weight was increased, the diameter of the fibres decreased and the uniformity of extruded fibres became more consistent.

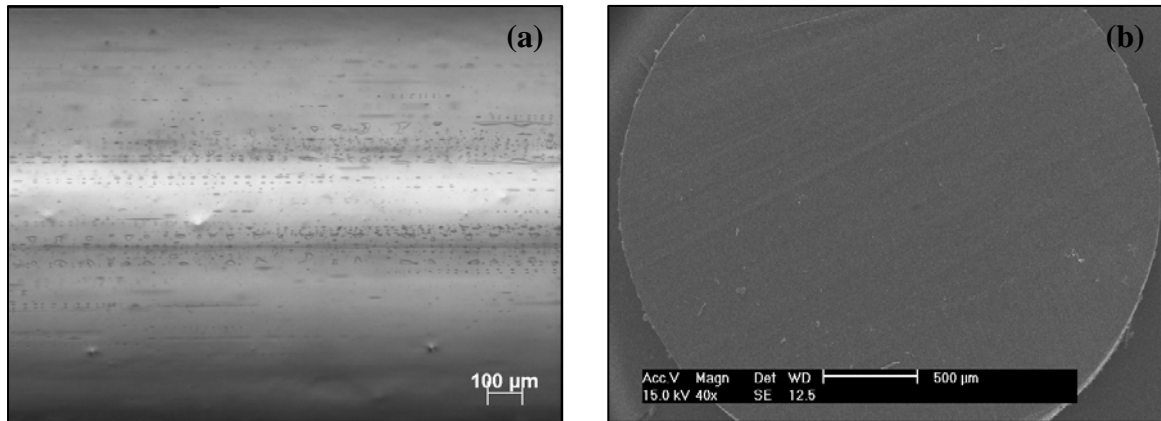


**Figure 41** – (a) 5x magnification image of extruded Surlyn® PC2000 fibre (10 kg) surface area and (b) SEM image of Surlyn® PC2000 fibre (10 kg) cleaved end.

The first set of Surlyn® 9910 fibres were also extruded using a 10 kg weight applied to the piston.

**Table 18** – Average diameter of Extruded Surlyn® 9910 fibres.

<b>Surlyn® 9910</b>	<b>Average Fibre Diameter (mm)</b>			
Fibre No.	10 Kg	7 g	10 g	20 g
1	3.555	2.018	0.578	0.236
2	3.290	2.026	0.574	0.249
3	3.551	2.071	0.554	0.255
4	3.586	2.075	0.569	0.264
5	3.573	1.905	0.579	0.252
6	3.615	1.953	0.563	0.262
7	3.467	1.888	0.57	0.275
8	3.609	1.909	0.571	0.266
9	3.530	1.919	0.553	0.246
10	3.598	1.904	0.552	0.257
11	3.383	1.886	0.565	0.274
12	3.585	1.975	0.572	0.271
<b>Average</b>	<b>3.528</b>	<b>1.961</b>	<b>0.567</b>	<b>0.259</b>
S.D	0.1	0.07	0.009	0.012

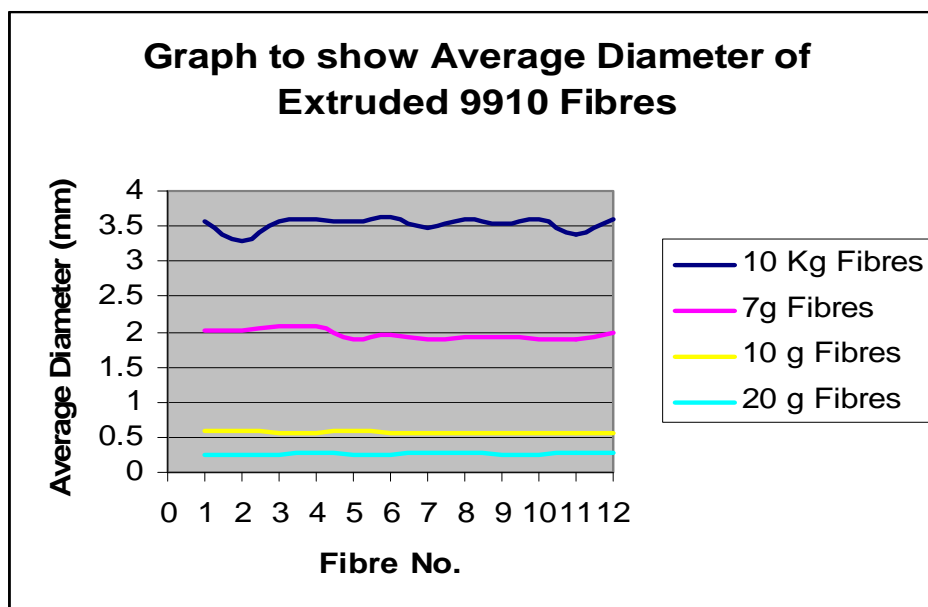


**Figure 42** – Graph showing average diameter of thick Surlyn® 9910 fibres.

The average diameter of the fibres is 1.051 mm thicker than that of the PC2000 fibres. The fibres were shown to have a more uniform diameter. This is due to the different viscosities of the two materials.

Surlyn<sup>®</sup> PC2000 has a melt flow rate of 4.5 g/10 min and Surlyn<sup>®</sup> 9910 has a melt flow rate of 0.7 g/10 min.<sup>80, 81</sup> Surlyn<sup>®</sup> 9910 has a higher viscosity than the other grade causing a slower rate of extrusion. The fibre would then be able to solidify, keeping a more uniform diameter. Due to the higher viscosity heavier weights were used to extrude the fibres. The average diameters of the fibres are shown to decrease when the applied weight is increased.

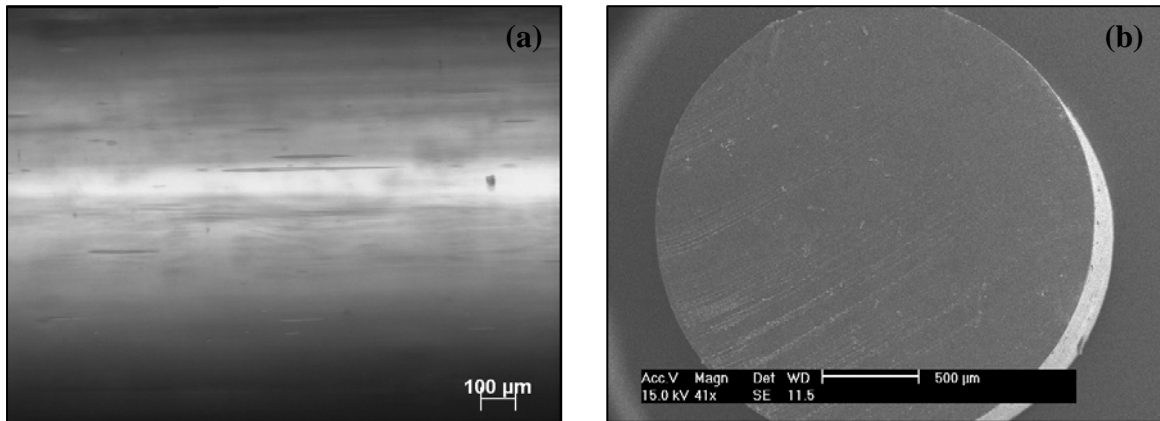


**Figure 43** – (a) 5x magnification image of extruded Surlyn<sup>®</sup> PC2000 fibre (10 kg) surface area and (b) SEM image of Surlyn<sup>®</sup> PC2000 fibre (10 kg) cleaved end.

The second method developed to extrude fibres, involved the production of a device to haul off longer lengths of fibre. The aim was to enable production of longer lengths of fibre with a smaller diameter, with a view to using the fibres as a self-healing and self-sensing reinforcing fibre.

Nine different settings were used to haul off fibres. Table 19 contains the average diameter of Surlyn® PC2000 fibres extruded using each extrusion speed setting.

**Table 19** – Fibre diameter measurements for Surlyn® PC2000.

<b>PC2000</b>	Measurement Point (mm)											
Setting	1	2	3	4	5	6	7	8	9	10	<b>Av.</b>	<b>SD.</b>
1	0.473	0.481	0.479	0.462	0.47	0.484	0.485	0.454	0.463	0.473	<b>0.472</b>	0.01
2	0.443	0.45	0.43	0.438	0.418	0.396	0.411	0.417	0.437	0.437	<b>0.428</b>	0.017
3	0.255	0.276	0.249	0.274	0.28	0.278	0.278	0.271	0.28	0.275	<b>0.272</b>	0.011
4	0.357	0.356	0.363	0.352	0.374	0.346	0.358	0.356	0.364	0.347	<b>0.357</b>	0.008
5	0.343	0.308	0.306	0.285	0.294	0.285	0.295	0.295	0.286	0.286	<b>0.298</b>	0.018
6	0.258	0.281	0.277	0.258	0.251	0.272	0.27	0.267	0.274	0.276	<b>0.268</b>	0.01
7	0.262	0.272	0.279	0.278	0.27	0.273	0.273	0.247	0.279	0.278	<b>0.271</b>	0.01
8	0.25	0.242	0.26	0.238	0.247	0.228	0.224	0.257	0.237	0.253	<b>0.244</b>	0.012
10	0.231	0.229	0.223	0.236	0.229	0.229	0.225	0.211	0.222	0.22	<b>0.226</b>	0.007

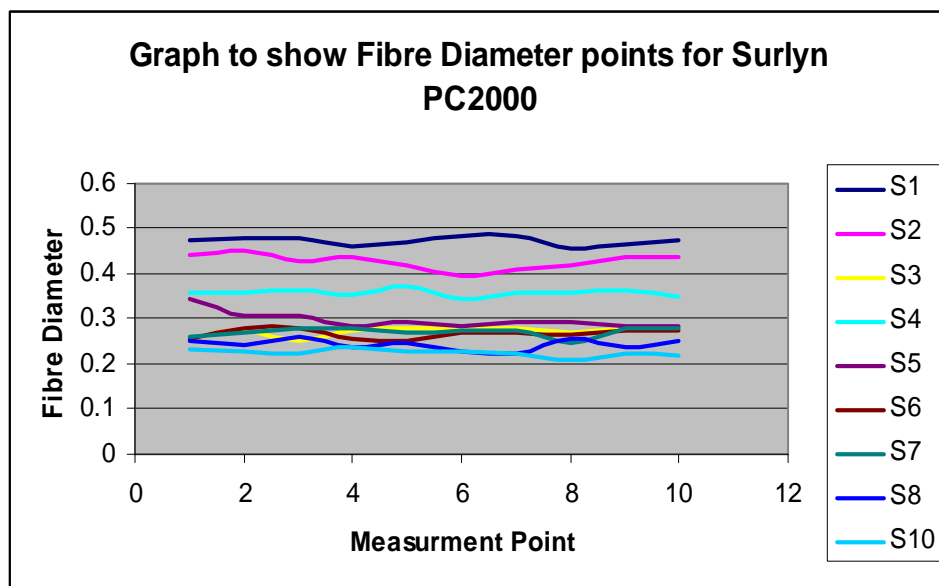


**Figure 44** – Graph showing average diameter of fibres extruded using adapted haul off machine.

The main trend shows that as the speed of the machine extruding fibres increases, the diameter of the fibres decreases. The diameters of the fibres ranged from 0.472 mm to 0.226 mm.

The speed and amount of fibre that can be hauled off is very advantageous in enabling a quick and efficient way of collecting fibres of required lengths and diameters. Method two enables smaller diameter fibres to be extruded with a view to incorporating them into a composite material. The standard deviation results and the curves present in figure 44, show that the uniformity of the fibres is more consistent than those fibres that were extruded using weights.

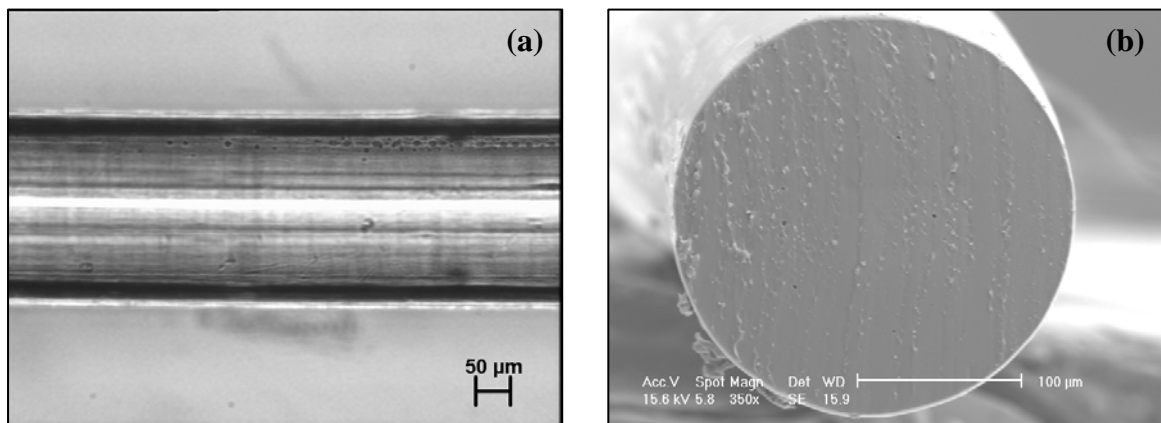


**Figure 45** – (a) 5x magnification image of extruded thin Surlyn® PC2000 fibre (Setting six) surface area and (b) SEM image of Surlyn® PC2000 fibre (Setting six) cleaved end.



## 5.5 Characterisation of the Light Transmission

### 5.5.1 Light Transmission measurements through extruded thick Surlyn<sup>®</sup> fibres

Following the extrusion of Surlyn<sup>®</sup> fibres, light transmission measurements were carried out to investigate whether the fibres could be used as self-sensing light guides. Initial light intensity measurements were carried out on Surlyn<sup>®</sup> PC2000 and 9910 large diameter fibres.

Fibres of approximately the same diameter were chosen. Measurements were conducted on 200 mm fibres. Due to the diameter of the fibres they were not connected with SMA connectors.

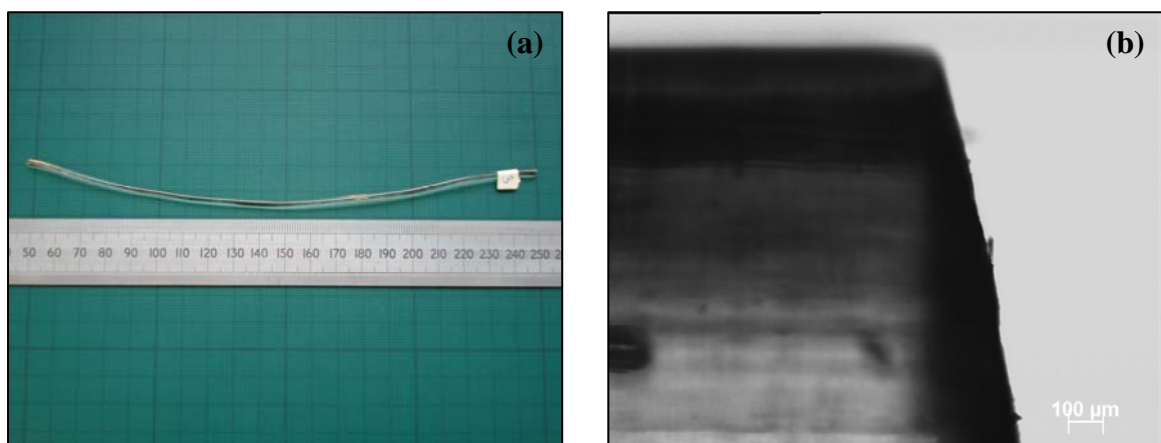
**Table 20** – Light transmission measurements through extruded Surlyn<sup>®</sup> PC2000 and 9910 thick fibres.

	Surlyn <sup>®</sup> PC2000		Surlyn <sup>®</sup> 9910	
Fibre No.	Av. Diameter	Wavelength (mW)	Av. Diameter	Wavelength (mW)
1	2.105	28.26	2.018	39.22
2	2.07	19.47	2.026	37.02
3	2.555	<b>8.54</b>	2.071	25.18
4	2.51	44.16	2.075	<b>20.72</b>
5	1.885	43.2	1.905	44.33
6	2.753	40.64	1.953	47.08
7	2.772	24.77	1.888	<b>51.98</b>
8	2.694	60.77	1.909	39.02
9	2.591	51.67	1.919	38.74
10	2.39	50.97	1.904	35.42
11	2.668	60.74	1.886	44.82
12	2.734	<b>61.47</b>	1.975	29.53
<b>Average</b>	2.477	<b>41.22</b>	1.961	<b>37.76</b>
S.D	0.301	17.503	0.07	9.091

Both fibres were able to transmit light. Surlyn<sup>®</sup> PC2000 had the maximum light intensity reading of 61.47 mW and also the lowest of 8.54 mW. The standard deviation showed that Surlyn<sup>®</sup> 9910 had the most consistent light intensity readings.

Surlyn<sup>®</sup> PC2000 is neutralized with sodium ions whilst Surlyn<sup>®</sup> 9910 is neutralized with zinc ions. Zinc ions cross-link Surlyn<sup>®</sup> whilst the sodium ions do not cross-link Surlyn<sup>®</sup>. The cross-linking within the Surlyn<sup>®</sup> 9910 could be a factor resulting in the lower light transmission results.

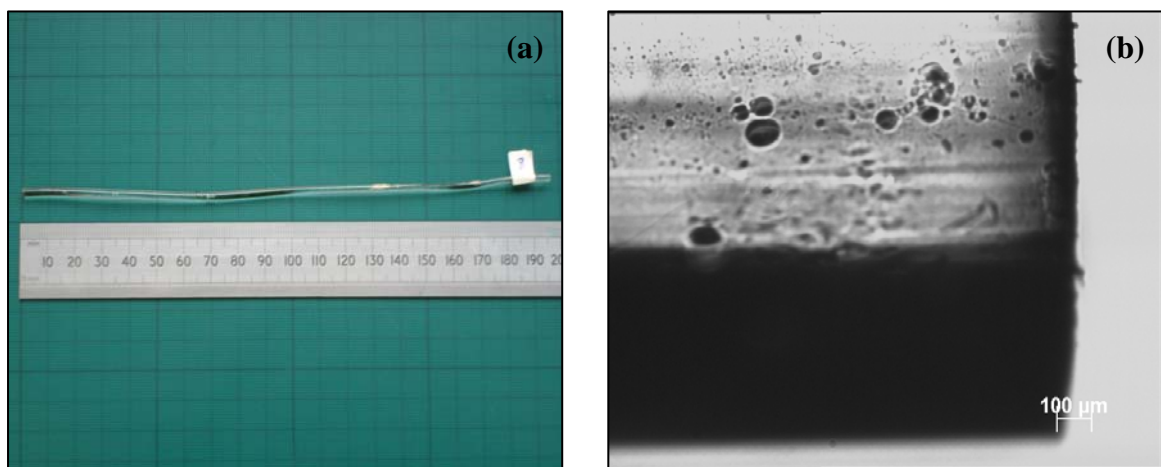
Image analysis was carried out on the fibres highlighted in table 20 characterising the low and high light transmission fibres. Figure 46 contains images of Surlyn<sup>®</sup> PC2000, fibre three which had a light transmission reading of 8.54 mW.



**Figure 46** – (a) Image of curved fibre and (b) 5x magnification image of fibre edge.

The lowest transmission reading may have been caused by the fibre curvature present in figure 46a. Figure 46b highlights the angled cleave of the fibre end also contributing to the lower reading.

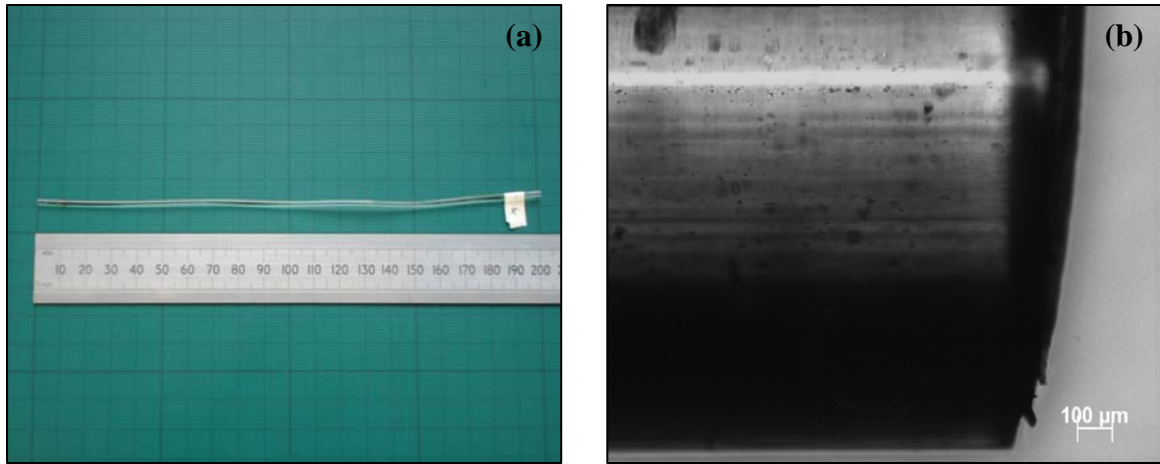
Figure 47 contains images of the highest light transmitting fibre. Surlyn<sup>®</sup> PC2000 fibre number 12 had a recorded reading of 61.47 mW.



**Figure 47** – (a) Image of fibre and (b) 5x magnification image of fibre edge.

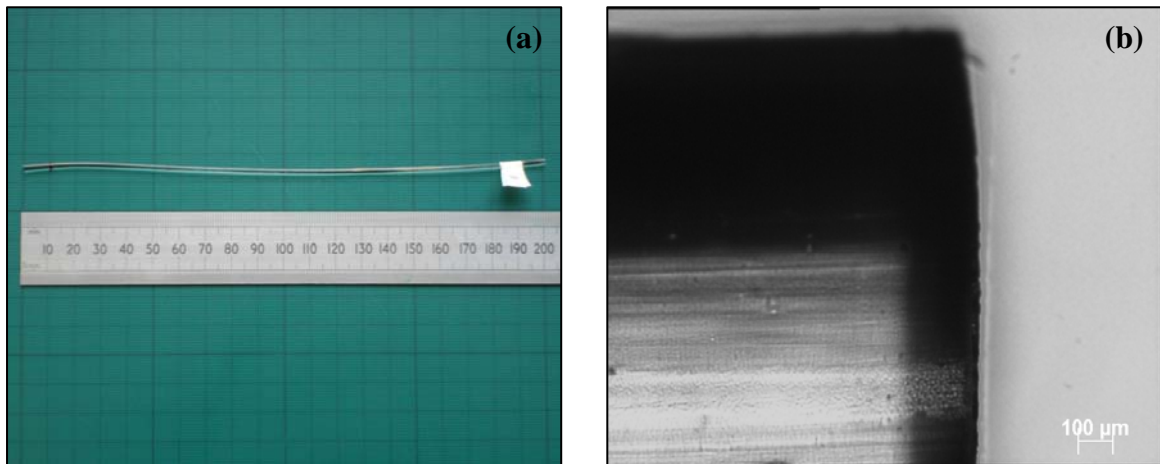
Overall the fibre is far straighter than fibre three. Each end of the fibre had a much better cleave which can be observed in figure 47b. The difference in diameter between the two fibres was 0.179 mm showing the diameter may also have an effect on the light intensity.

Figure 48 contains images taken of Surlyn<sup>®</sup> 9910 fibre number four. This fibre had a reading of 20.72 mW.



**Figure 48** - (a) Image of fibre and (b) 5x magnification image of fibre edge.

The fibre is shown to be relatively straight; however both ends of the fibre show a poor angle of cleave on each edge. The diameter of the fibre was 2.075 mm. This may also be a factor resulting in a lower light intensity reading. The final characterised fibre had a measured reading of 51.98 mW. Figure 49 contains images of the Surlyn<sup>®</sup> 9910 fibre seven.



**Figure 49** – (a) Image of fibre and (b) 5x magnification image of fibre edge.

Figure 49a shows that the fibre is relatively straight. Figure 49b contains an image of the cleaved edge which was straight on both ends of the fibre. The fibre diameter was 1.888 mm showing that the diameter of the fibre may not be as significant as the fibre quality, cleave and cation in contributing to the light transmission reading measured.

The light transmission results showed that Surlyn<sup>®</sup> is able to act as a light guide. Further studies were carried out on the light transmission abilities of Surlyn<sup>®</sup> and are reported in the following sections.

#### ***5.5.2 Comparison of Light Transmission between Surlyn<sup>®</sup> PC2000 and PMMA fibres***

As initial light transmission results had been collected for Surlyn<sup>®</sup>, a comparison against Poly (methyl methacrylate), a commercially available fibre was undertaken to further investigate the light guide capabilities of Surlyn<sup>®</sup> fibres.

PMMA optical fibres are used for short distance communication lines. They are very flexible and installation is very economical compared to that of glass-fibre.<sup>92</sup> Surlyn<sup>®</sup> PC2000 fibres were chosen as they had the highest average recorded light transmission.

Standard PMMA fibre was used and had an average diameter of 0.864 mm. Surlyn<sup>®</sup> PC2000 fibres were extruded using a three gram weight (method one) and had an average diameter of 0.852 mm.

**Table 21** – Light intensity and average diameter measurements for Surlyn<sup>®</sup> PC2000 and PMMA fibres.

Fibre Type	PMMA	Surlyn <sup>®</sup> PC2000	PMMA	Surlyn <sup>®</sup> PC2000
Fibre No.	Wavelength (mW)	Wavelength (mW)	Average Width (mm)	Average Width (mm)
1	1.9	6.32	0.866	0.822
2	4.2	6.58	0.868	0.884
3	3.21	4.64	0.871	0.814
4	2.71	6.49	0.862	0.876
5	1.8	7.8	0.867	0.848
6	3.72	5.28	0.869	0.877
7	2.27	5.78	0.867	0.868
8	2.59	5.58	0.861	0.852
9	2.09	6.69	0.859	0.862
10	3.17	4.3	0.858	0.841
11	2.27	7.94	0.859	0.847
12	1.75	5.97	0.859	0.837
<b>Average</b>	<b>2.64</b>	<b>6.11</b>	<b>0.864</b>	<b>0.852</b>
S.D	0.788	1.107	0.005	0.021

Results showed that the average light intensity measurements for Surlyn<sup>®</sup> PC2000 were nearly three times that of the PMMA fibres. The highest measurement for the Surlyn<sup>®</sup> PC2000 fibres was 7.94 mW. The Surlyn<sup>®</sup> PC2000 fibres were on average 0.010 mm smaller in diameter than the PMMA fibres. The standard deviations show that both the fibre diameters and light transmission measurements were consistent for all fibres.

The comparison between the fibres shows that Surlyn<sup>®</sup> PC2000 does have the potential as a light guide enabling self-sensing capabilities and the reported self-healing potential to be utilized.



**Figure 50** – Photograph of Surlyn® PC2000 fibre transmitting light.

### **5.5.3** *Effect of Fibre Connection on Light Transmission Measurements*

So far, all light transmission studies have been carried out on thick Surlyn® fibres without connecting the ends of the fibres with SMA connectors. Therefore this study was undertaken to investigate whether the connection with the light source and detector had an effect on the measured light intensity.

Two sets of 12 fibres, 200 mm in length were extruded for both Surlyn® PC2000 and 9910. The fibre ends were large enough so that a tight seal was formed between the fibre, light source and detector.

**Table 22** – Light transmission, fibre end diameters and fibre diameter for Surlyn® PC2000 fibres.

<b>Surlyn® PC2000</b>	Light Source Diameter - ~ 3.20 mm			
	Light Intensity Meter Diameter - ~ 2.50 mm			
Fibre No.	Light Source End (mm)	Measurement End (mm)	Wavelength (mW)	Average Width (mm)
1	3.063	2.387	25.81	2.650
2	3.061	2.387	22.9	2.602
3	2.926	2.366	20.64	2.602
4	2.937	2.304	45.94	2.505
5	3.081	2.303	40.5	2.609
6	2.973	2.329	58.55	2.537
7	2.95	2.396	63.99	2.540
8	3.091	2.386	57.84	2.610
9	2.982	2.39	27.32	2.541
10	3.025	2.349	68.36	2.607
11	<b>3.145</b>	<b>2.454</b>	<b>90.38</b>	<b>2.647</b>
12	<b>3.173</b>	<b>2.386</b>	<b>93.76</b>	<b>2.681</b>

**Table 23** - Light transmission, fibre end diameters and fibre diameter for Surlyn® 9910 fibres.

<b>Surlyn® 9910</b>	Light Source Diameter - ~ 3.18 mm			
	Light Intensity Meter Diameter - ~ 2.50 mm			
Fibre No.	Light Source End (mm)	Measurement End (mm)	Wavelength (mW)	Average Width (mm)
1	2.54	2.44	73.72	2.381
2	2.724	2.439	56.85	2.430
3	2.689	2.423	63.67	2.367
4	2.476	2.442	35.52	2.464
5	2.73	2.44	30.45	2.414
6	<b>2.626</b>	<b>2.486</b>	<b>74.71</b>	<b>2.390</b>
7	2.423	2.345	60.04	2.344
8	2.456	2.389	60.59	2.435
9	2.438	2.411	52.02	2.447
10	<b>2.726</b>	<b>2.374</b>	<b>73.21</b>	<b>2.399</b>
11	2.604	2.437	48.81	2.444
12	2.496	2.447	36.24	2.472



The highlighted figures in table 22 show that fibres 11 and 12 have the largest diameters and therefore the closest fit to the light source diameter. These two fibres also had the strongest light intensity measurements recorded at 90.38 mW and 93.76 mW.

Surlyn<sup>®</sup> 9910 fibres also followed the same trend. As shown in table 23, the two fibres highlighted with the greatest diameter ends also had the greatest light intensities. These were 73.21 mW and 74.71 mW. From the results it is clear that the fibre connection with the light source and detector does have an effect on light transmission.

Due to the recorded impact of the fibre connection; methods of connecting the fibres and further light transmission studies on the thin Surlyn<sup>®</sup> fibres were investigated and are reported in the following sections.

#### **5.5.4** *Light Transmission Distance Measurements for Extruded Thin Surlyn<sup>®</sup> fibres*

The following studies investigate the light transmission capabilities of the thin fibres and whether the thin fibres could be used as self-sensing light guides. This initial study on the Surlyn<sup>®</sup> fibres which were hauled off in longer lengths was to investigate the distance the fibre could guide light. Both Surlyn<sup>®</sup> PC2000 and 9910 fibres were studied. The initial set of results collected were on fibres extruded using settings one - three. Fibres were 20 cm in length.

**Table 24** – Average diameter and light guide distance for settings one - three Surlyn<sup>®</sup> PC2000 and 9910 fibres.

<b>Surlyn PC2000<sup>®</sup></b>	Av. Diameter (mm)	S.D	Light Guide Distance (cm)
Setting 1 (33 RPM)	0.472	0.005	> 20 cm
Setting 2 (48 RPM)	0.428	0.004	> 20 cm
Setting 3 (62 RPM)	0.272	0.009	> 20 cm
<b>Surlyn 9910<sup>®</sup></b>			
Setting 1 (33 RPM)	0.294	0.008	~ 5 cm
Setting 2 (48 RPM)	0.309	0.009	~ 5 cm
Setting 3 (62 RPM)	0.248	0.006	~2 cm

Visual analysis was used to detect the light guide distance. The Surlyn<sup>®</sup> PC2000 fibres all guided light efficiently over the 20 cm length and a strong orange glow was apparent at the end of the fibre. This is due to the light reacting with sodium ions present in the material. With reference to table 24, the greatest distance the Surlyn<sup>®</sup> 9910 fibres guided light was ~ 5 cm. The lower light guide results recorded for Surlyn<sup>®</sup> 9910 may be due to the cross-linking present in the Surlyn<sup>®</sup> caused by the presence of the zinc ions. As Surlyn<sup>®</sup> PC2000 fibres showed the potential of transmitting light over distances greater than 20 cm only Surlyn<sup>®</sup> PC2000 fibres were studied further.

<b>Surlyn<sup>®</sup> PC2000</b>	Av. Diameter (mm)	S.D	Light Guide Distance (cm)
----------------------------------	-------------------	-----	---------------------------

Setting 1 (33 RPM)	0.472	0.01	~ 120
Setting 2 (48 RPM)	0.428	0.017	~140
Setting 3 (62 RPM)	0.272	0.011	~ 150
Setting 4 (77 RPM)	0.357	0.008	~ 190
Setting 5 (92 RPM)	0.298	0.018	~ 75
Setting 6 (116 RPM)	0.268	0.01	~ 248.5
Setting 7 (122 RPM)	0.271	0.01	~ 175
Setting 8 (137 RPM)	0.244	0.012	~ 155
Setting 10 (168 RPM)	0.226	0.007	~ 130

**Table 25** - Average diameter and light guide distance for thin Surlyn<sup>®</sup> PC2000 fibres.

Table 25 conveys the results collected and the setting six fibre guided light the longest distance of 248.5 cm. The initial trend showed that as fibre diameter decreased the light transmission distances increased. However fibre five only guided light ~ 75 cm and this was due to the fibre bleeding light along its surface area. From setting seven – ten the fibre diameter began to decrease causing the light guide distance to also decrease. The standard deviation showed that the fibres had a uniform diameter.

Although the thin diameter fibres were not connected with SMA connectors, the results clearly show that the thin Surlyn<sup>®</sup> PC2000 fibres are able to transmit light. The following sections report different methods of connecting the fibre ends and also further investigate the light transmission characteristics of Surlyn<sup>®</sup> PC2000 thin fibres.

### **5.5.5 Fibre Connection Methods using SMA Connectors**

As previously reported in section 5.5.3 the fibre connection does have a significant effect on the recorded light transmission through the Surlyn<sup>®</sup> fibres. Therefore three methods were used to connect the Surlyn<sup>®</sup> PC2000 thin fibres with SMA connectors.

Once fibres were connected using the three methods previously described in section 4.6.5, they were connected to a light source to ensure transmission of light through the fibre.

Following image analysis, methods two and three were unable to transmit light through the fibre when Epotek 310m epoxy resin was used to secure the fibre. However method one was successful when using the UV cure glue and this method was used for the remaining light transmission studies on thin Surlyn<sup>®</sup> PC2000 fibres.

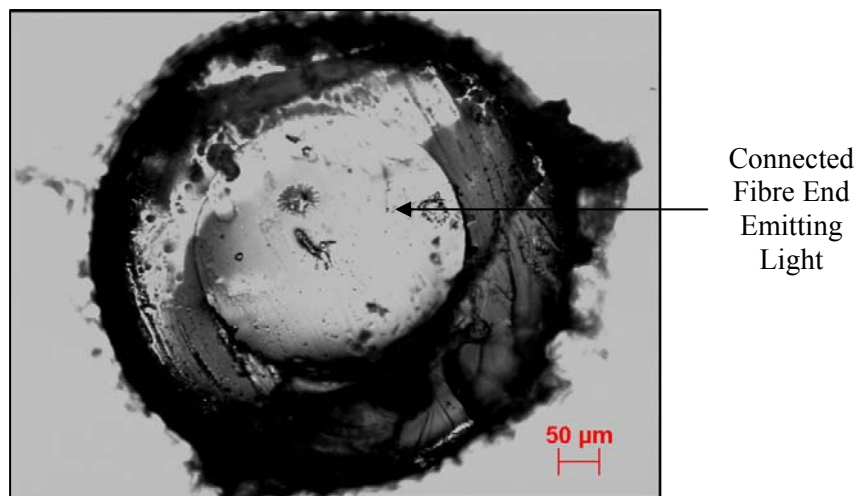


**Figure 51** – 10x magnification image of Surlyn<sup>®</sup> PC2000 fibre transmitting light following method one connection.

#### **5.5.6** *Light Transmission Measurements through Extruded Thin Surlyn<sup>®</sup> fibres*

As Surlyn® PC2000 fibres were able to guide light and a method for connecting the fibre ends was developed, three light transmission studies were carried out on the fibres to further characterize the light transmission and self-sensing capabilities of the Surlyn® PC2000 fibres. Light transmission readings were taken once:

- 1) Both fibre ends were connected.
- 2) Both fibre ends were disconnected and reconnected.
- 3) Each connector was only connected halfway.

Four different lengths of fibre were subjected to each test and included 40 cm, 30 cm, 20 cm and 10 cm fibres.

**Table 26** – Light transmission readings for test one to three (N/R – no reading).

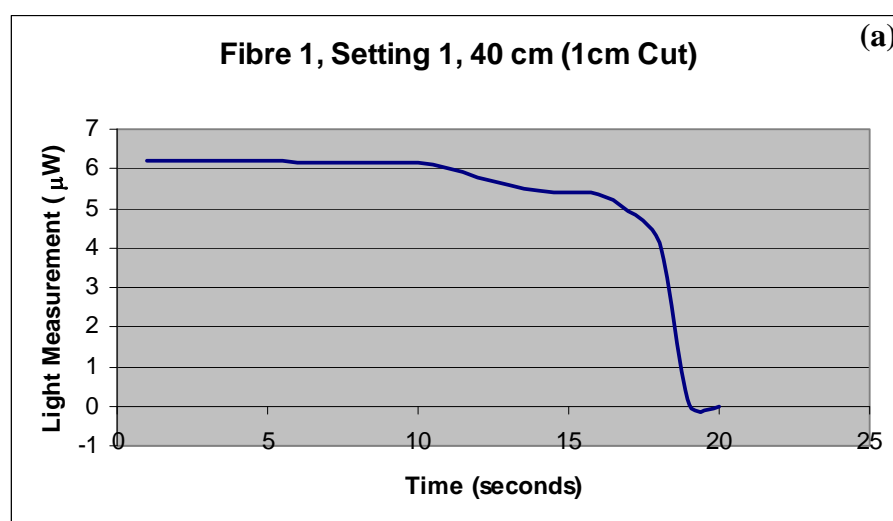
<b>Surlyn® PC2000</b>	<b>Fibre Extrusion Setting/Light Intensity Measurement (µW)</b>								
<b>Test 1</b>	<b>1</b>	<b>2</b>	<b>3</b>	<b>4</b>	<b>5</b>	<b>6</b>	<b>7</b>	<b>8</b>	<b>10</b>
40 cm	6.24	1.26	253.6 nW	543.9 nW	N/R	1.046	780.4 nW	230.9 nW	N/R
30 cm	9.72	14.3	952.9 nW	5.73	N/R	5.501	2.819	1.422	N/R
20 cm	52.3	34.05	3.677	14.28	561.2 nW	6.625	6.442	7.154	129.8 nW
10 cm	95.3	88.2	19.26	21.41	2.431	17.74	25.06	25.61	2.249
<b>Test 2</b>									
40 cm	6.26	1.25	237.3 nW	542.8 nW	N/R	1.081	785.1 nW	234.9 nW	N/R
30 cm	9.77	34.05	0.995	5.882	N/R	5.551	2.824	1.435	N/R
20 cm	52.7	33.97	3.622	14.22	586.9 nW	6.791	6.615	7.249	132.1 nW
10 cm	95.1	90.2	19.68	20.31	2.41	16.51	25.19	25.17	2.253
<b>Test 3</b>									
40 cm	4.95	1.11	187.2 nW	450.9 nW	N/R	0.945	696.4 nW	193.2 nW	N/R
30 cm	7.26	88.2	700 nW	5.233	N/R	5.121	2.423	1.23	N/R
20 cm	42.7	28.22	2.9	11.29	462.4 nW	6.214	5.965	6.471	85.89 nW
10 cm	87.1	77.8	16.22	17.57	1.957	14.62	22.56	22.8	1.891

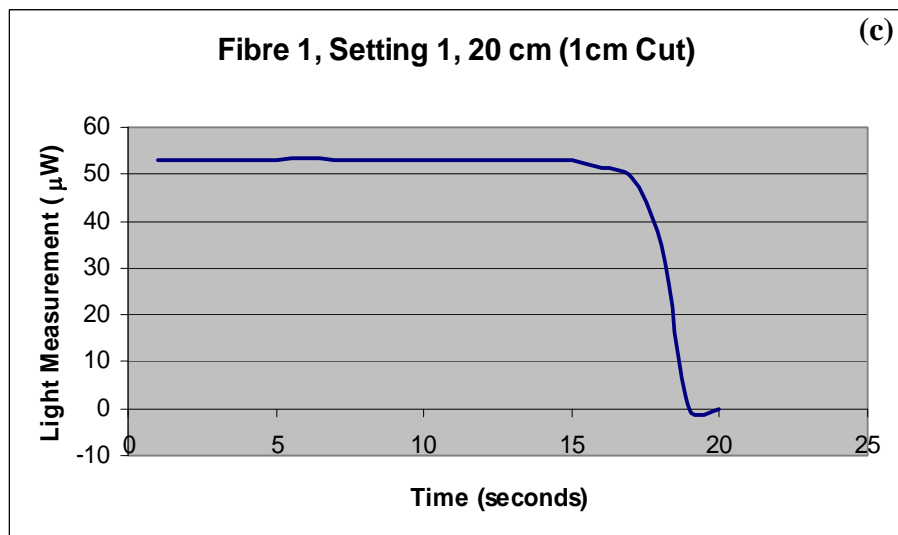
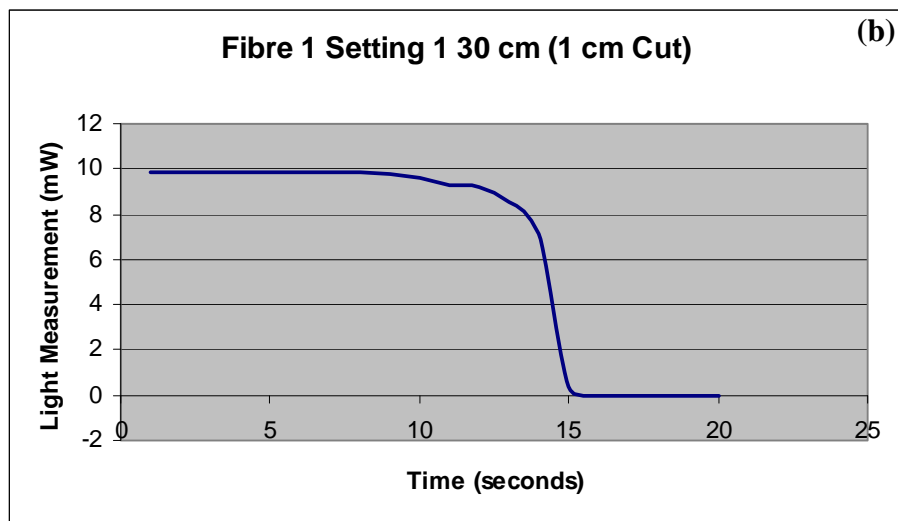
The general trend for tests one, two and three show that as the extrusion setting increases, decreasing the fibre diameter, the light intensity measurements also decrease. Fibre five does not follow the trend and this maybe due to defects in the fibre.

Test two involved disconnecting the fibre at both ends and then reconnecting the fibre before taking a reading. Results show that when the fibre was reconnected there was only a minor change in light transmission highlighting that the light transmission through the fibre is stable.

Test three involved only connecting the fibre halfway. All results were found to decrease in intensity reiterating the importance of the fibre connection to the light source and detector. As the fibre extruded using setting one had the highest light intensity reading, this fibre was subjected to a fourth test. This involved monitoring the light transmission for 20 seconds whilst cutting the fibre 10 mm away from the detector.

Figure 52 contains light transmission curves for 40 cm, 30 cm, 20 cm and 10 cm fibre lengths for setting one extruded fibres.





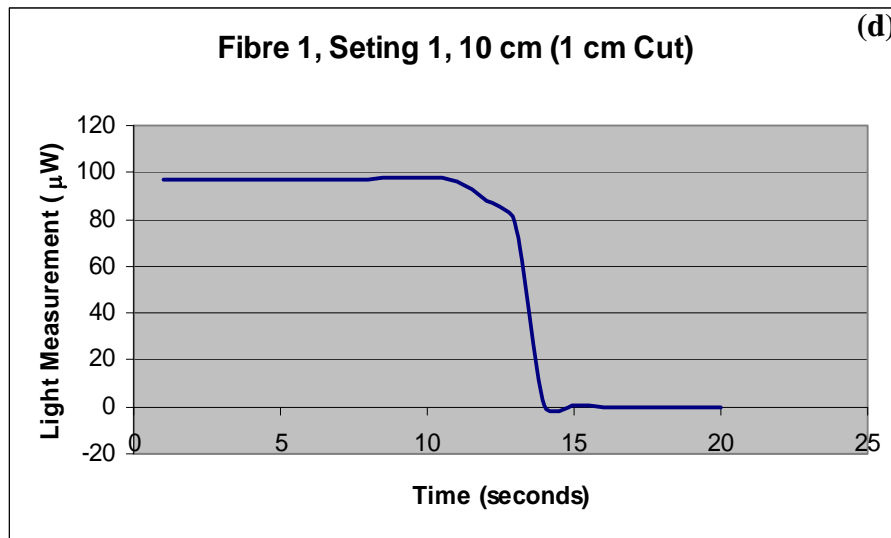


**Figure 52** – Light transmission curves for (a) 40 cm, (b) 30 cm, (c) 20 cm and (d) 10 cm Surlyn<sup>®</sup> PC2000 fibres during the 1 cm cut test.

With reference to figure 52a, the light intensity begins to decrease at around ten seconds when pressure from the blade is applied to the fibre. The near vertical drop in the curve shows where the fibre is cut causing the light transmission to fail.

This trend is present for all fibre lengths. The light intensity of the fibres is shown to be stable until pressure is applied from the blade. Tests show that the small diameter fibres are able to be connected and transmit light. Light transmission through the fibres was stable and the light guide properties were able to provide information when damage was caused to the fibre. This highlights the self-sensing capabilities of thin Surlyn<sup>®</sup> PC2000 fibres and is further explored in the next section during attenuation tests.



### 5.5.7 Attenuation Experiments

These tests were undertaken to further investigate the self-sensing capabilities of the Surlyn<sup>®</sup> fibres. Tests were carried out on the extruded thin Surlyn<sup>®</sup> PC2000 fibres, establishing the attenuation characteristics. Different weights were applied to the centre of the fibre whilst light intensity was monitored.

Surlyn<sup>®</sup> PC2000 fibre, which was hauled off using setting one (33 RPM), was chosen for the test as this fibre was shown to have the greatest light transmission reading. A 20 cm length of fibre was used throughout testing.

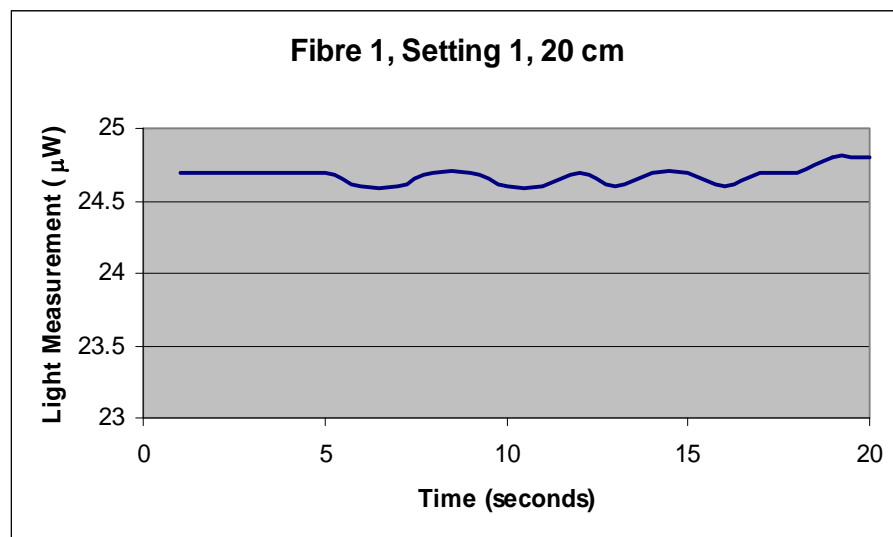


**Figure 53** – Light transmission curve for the Surlyn<sup>®</sup> PC2000, 20 cm fibre hauled off using setting one.

Figure 53 contains the initial light transmission curve for the fibre. The fibre was monitored over a 20 second period and had a light transmission reading of 24.70 µW.

Six different weights were applied to the fibre and the light transmission curves for each test are presented below in figure 54.

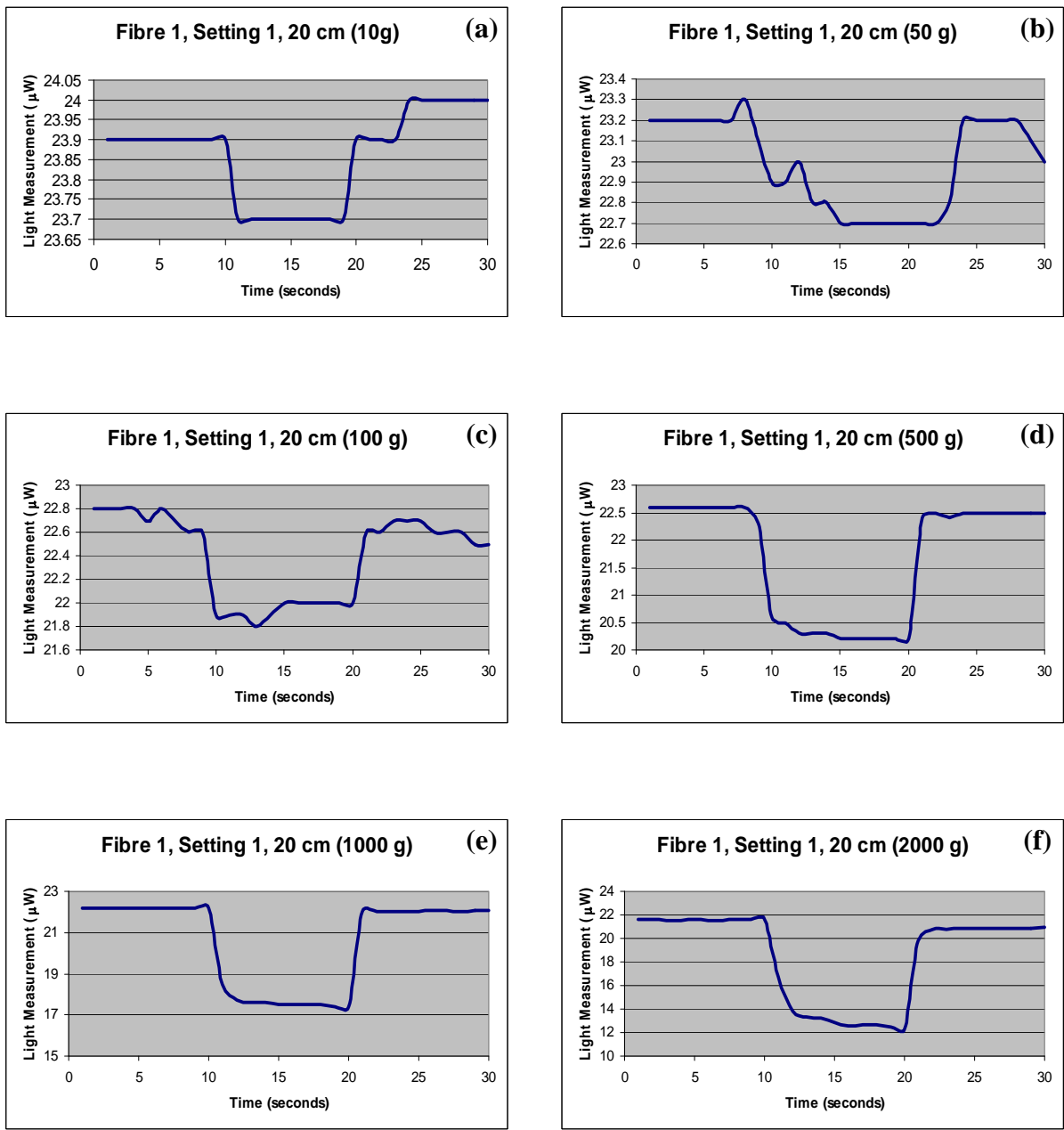


**Figure 54** – Light attenuation curves for Surlyn<sup>®</sup> PC2000 fibre hauled off using setting 1; (a) 10 g, (b) 50 g , (c) 100 g, (d) 500 g, (e) 1000 g and (f) 2000 g.

Light transmission was monitored for 30 seconds and the weight was applied from 11 - 20 seconds. With reference to figure 54a, the light intensity is shown to drop 0.2  $\mu\text{W}$  to 23.7  $\mu\text{W}$  once the 10 gram weight was applied to the fibre. This was a 1 % drop in light transmission for the fibre.

Results show that as the weight applied to the fibre is increased, the percentage loss in light transmission is also shown to increase. The maximum weight that was applied to the fibre was 2000 grams causing a drop of 9.6  $\mu\text{W}$ . This is a 56 % loss in light transmission compared to the 1 % loss when a 10 gram weight was applied.

The light attenuation curves also show that after each test the light transmission reading for each fibre was shown to drop and was caused by the increased weight causing permanent damage to the fibre.

The fibres have demonstrated the ability of sensing damage when used as fibre light guides. Permanent damage to the fibre is caused when increasing weight is applied to the fibre surface. The use of a coating maybe used to prolong the integrity of the fibres and future studies would investigate whether the fibres also have reported self-healing capabilities and are discussed further in the future work section.

## 5.6 Fibre Characterisation

Density and DSC experiments that were carried out on the thin Surlyn<sup>®</sup> plaques in section 4.2 were used to investigate whether extruding the fibre has caused any changes in the density and thermal characteristics of the material.

Surlyn<sup>®</sup> PC2000 fibre (setting six) was the studied fibre as results showed this fibre had the best light guide distance measurements and was involved in further testing during this project.

### 5.6.1 Density Measurements

Table 27 presents the five density measurements, average density and standard deviation for Surlyn<sup>®</sup> PC2000 fibre, setting six.

**Table 27** – Density measurement results for Surlyn<sup>®</sup> PC2000 fibre, setting six.

Surlyn <sup>®</sup> PC2000 Setting 6	Sample Weight(g)	Sample Buoyancy(g)	Density of Liquid	Density(g/cm <sup>3</sup> )
1	0.00077	0.00054	0.68376	0.975
2	0.00077	0.00054	0.68376	0.975
3	0.00089	0.00059	0.68376	1.03
4	0.00078	0.00056	0.68376	1.03
5	0.00083	0.00064	0.68376	0.887
				<b>Average = 0.979</b>
				S.D = 0.06

The average density of the fibre was measured at 0.98 g/cm<sup>3</sup>. The density has increased by 0.01 g/cm<sup>3</sup> after being extruded. The standard deviation for the density measurements was

0.06 showing that the results are not as consistent as those for the plaques. The size of the fibre and difficulty of the measurement may be the cause of the higher standard deviation.

### 5.6.2 Differential Scanning Calorimetry (DSC)

Using the two temperature ramps previously described in section 4.2.3, the thermal characteristics of the fibre were investigated. Figure 55 contains the results from the one cycle temperature ramp.

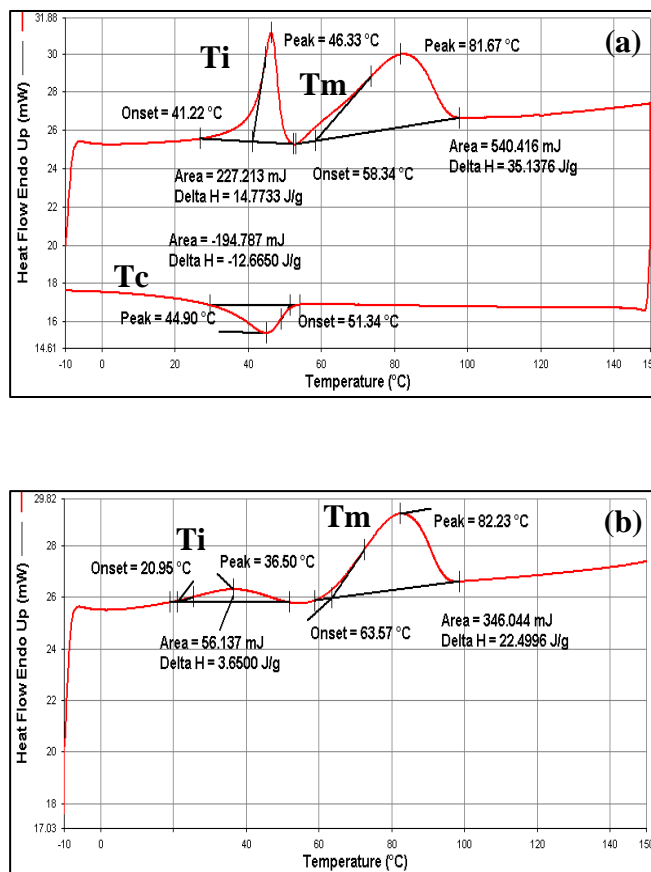


**Figure 55** –DSC of extruded Surlyn<sup>®</sup> PC2000 fibre (setting six); one cycle.

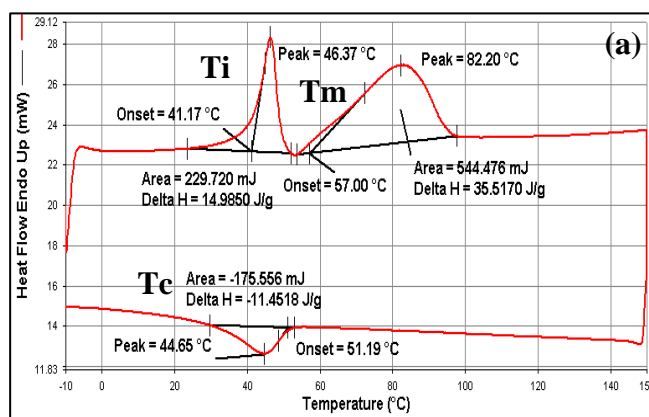
The thermal transitions including the order-disorder transition ( $T_i$ ), melt transition ( $T_m$ ), crystallization transition ( $T_c$ ) and crystallinity % were determined for the fibre.

**Table 28** - Thermal characteristics of extruded Surlyn<sup>®</sup> PC2000 fibre (setting six).

Surlyn <sup>®</sup> PC2000 Setting 6	$T_i$ (°C)	$T_m$ (°C)	$T_c$ (°C)	Crystallinity (%)
	46.33	81.67	44.90	12

The same trend is apparent as previously reported in section 5.1.2 for the Surlyn<sup>®</sup> plaques. However when comparing the two sets of results the temperature of the  $T_i$  and  $T_m$  has decreased and the  $T_c$  has increased. The percentage of crystallinity present in the fibre has increased by 3 % to 12 %. The increase in crystallinity is consistent with the density measurements as the increase in density is due to the increased crystallinity present in the fibre.

With reference to figure 55a, the order disorder peak ( $T_i$ ) is at ~ 46 °C. At this temperature the ionic aggregates become disordered and upon the second heat the transition has become suppressed. The temperature for this transition has once again decreased. Figure 56 contains the thermal traces produced during the three cycle temperature ramp.



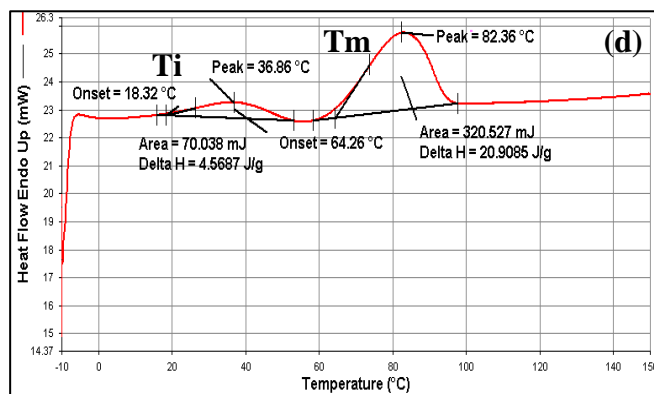
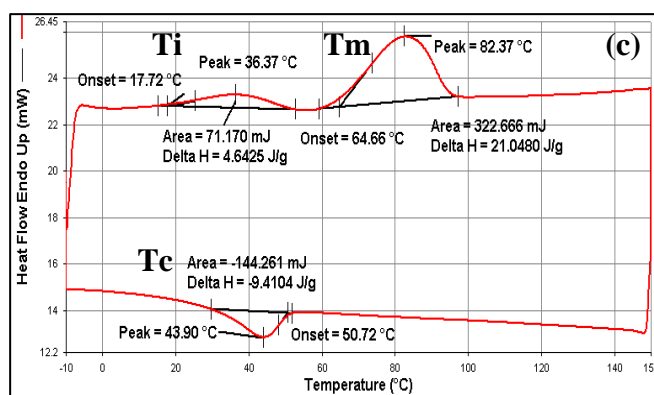
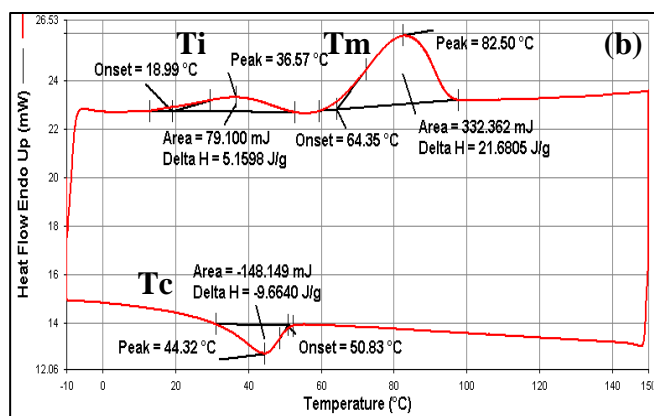


**Figure 56** - DSC of extruded Surlyn® PC2000 fibre (setting six); three cycles.

The results portray the same trend as the plaques where the temperature peaks for the different thermal characteristics have changed and the order-disorder transition has suppressed.

As previous sections have reported a new area of study based on the light guide and self-sensing capabilities of Surlyn<sup>®</sup> fibres, the following sections focus on developing and incorporating both Surlyn<sup>®</sup> fibres and films to form a self-healing and self-sensing composite material.

## **5.7 Self-Healing and Self-sensing Composite Development**

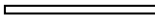

### ***5.7.1 Self-Healing Composite Development***

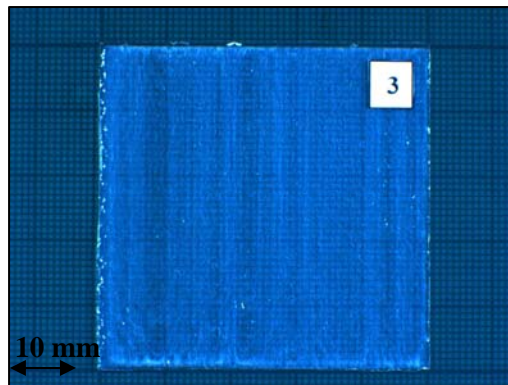
Using Surlyn<sup>®</sup> 1706 film and VTM 264 glass-fibre, different composites were fabricated in order to carry out indentation and ballistic experiments, allowing information to be gathered on the self-healing capabilities of Surlyn<sup>®</sup>. These tests are discussed further in the future work chapter 7.0.

The fabricated samples were 50 mm x 50 mm in size and consisted of single ply, two ply and four ply composites. Figure 57 contains images along with cross-sectional diagrams (not to scale) of a single ply, two ply and four ply sample.

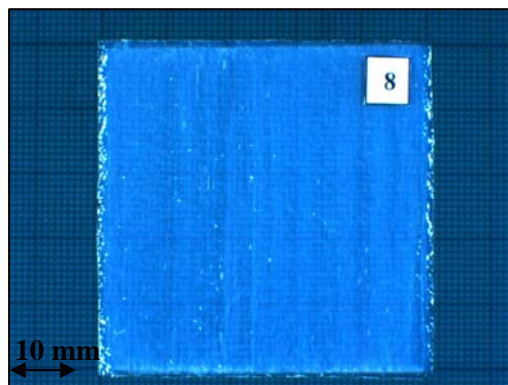
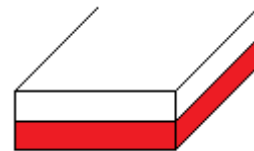


Key:

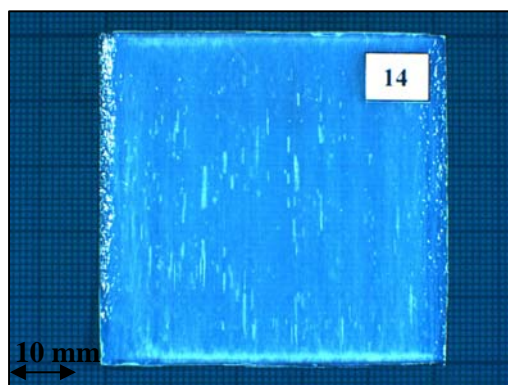
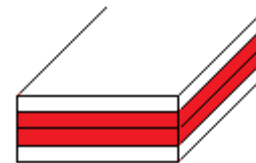
-  - VTM264 glass-fibre pre-preg  
 - Surlyn<sup>®</sup> 1706 film



(a)



(b)



(c)

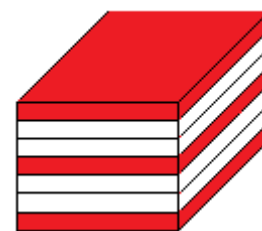


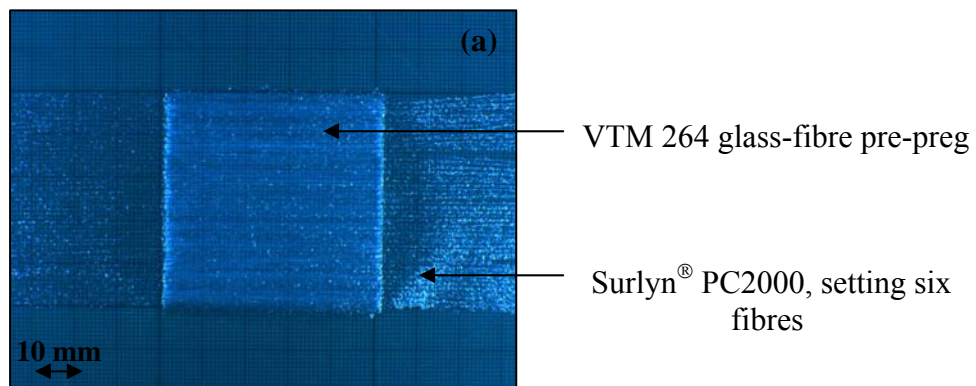
**Figure 57** – Images and schematic diagrams (not to scale) of 50 mm x 50 mm (a) single ply, (b) Two ply and (c) four ply glass-fibre/Surlyn<sup>®</sup> 1706 film composites.

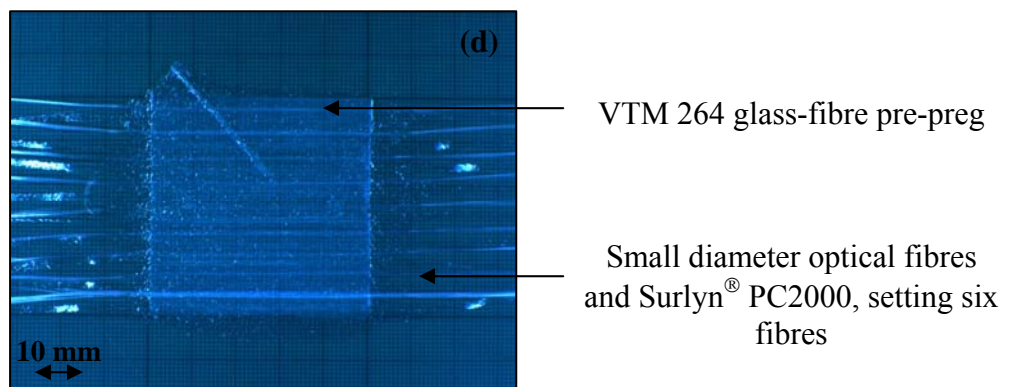
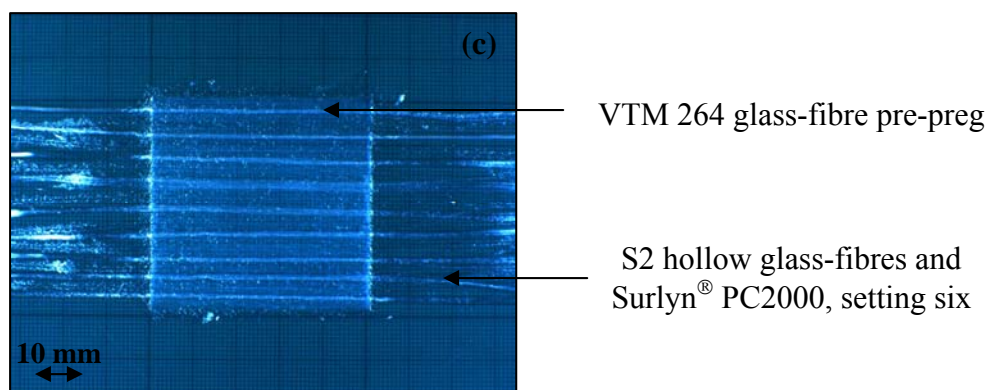
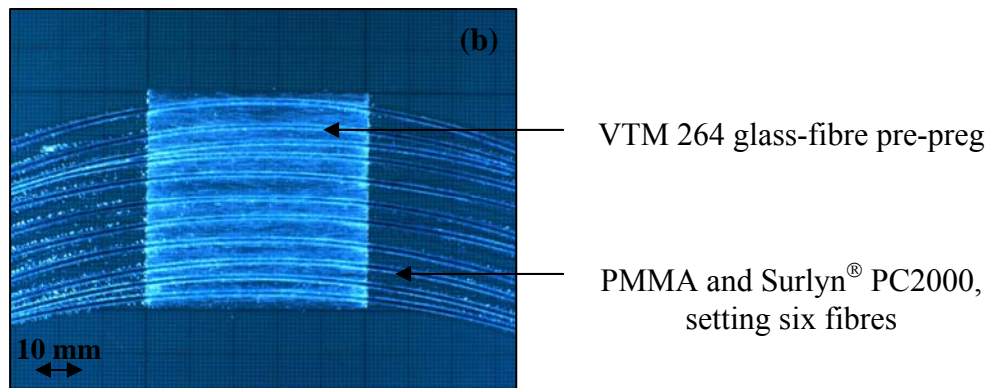
Reference plates were also produced allowing comparisons to be made, highlighting any self-healing properties. Following the development of producing a reported self-healing Surlyn<sup>®</sup> composite, the next section involves the development of producing both a self-healing and self-sensing Surlyn<sup>®</sup> composite.

### *5.7.2 Self-Healing and Self-Sensing Composite Development*

Surlyn<sup>®</sup> PC2000 fibre (setting six) was used as fibre measurements showed that it guided light the furthest distance. Five single ply composite samples were fabricated. All five samples contained Surlyn<sup>®</sup> Fibres.

The intention was to produce a composite with both self-sensing and self-healing capabilities. The different fibres would act as light guides, whilst the reported self-healing ability of Surlyn<sup>®</sup> would help heal the composites when subjected to indentation and ballistic experiments which are further discussed in the future work chapter 7.0. Figure 58 contains images of the different fabricated composites and fibres used.





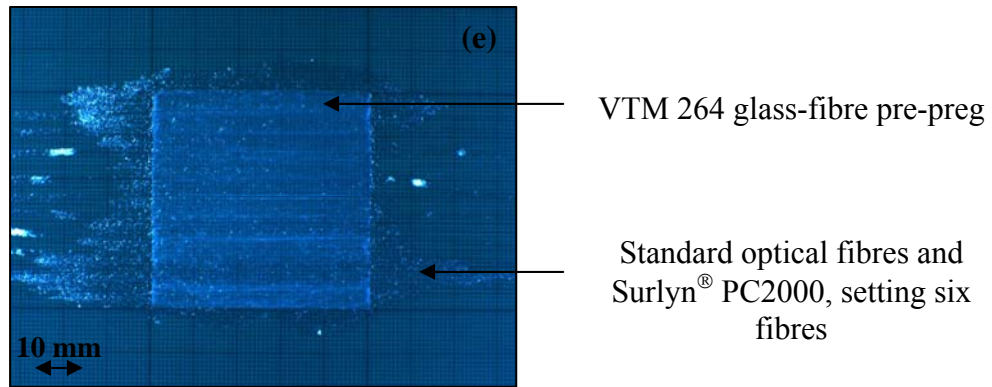


**Figure 58** – Images of (a) Surlyn® fibres and glass-fibre. (b) Surlyn® fibres, PMMA fibres and glass-fibre. (c) Surlyn® fibres, S2 hollow glass-fibres and glass-fibre. (d) Surlyn® fibres, SDOF and glass-fibre. (e) Surlyn® fibres, standard optical fibres and glass-fibre composites.

Following the development of producing a self-healing and self-sensing Surlyn® composite, the final section investigates the ability of Surlyn® acting as a crack arrestor when incorporated into a carbon-fibre composite.

### 5.7.3 Crack Arrestor Composites

Carbon-fibre composites are known for properties such as high strength and low density making them desirable for use in such industries as the aerospace and automotive industries.<sup>93</sup> However they are susceptible to delamination. Delamination is described as interlaminar cracks which are prone to appear and propagate between plies under static or dynamic conditions.<sup>94</sup>

The main aim of this part of the study was to investigate whether Surlyn<sup>®</sup> film and fibres can act as crack arrestors when placed between the centre plies of a 16 ply carbon-fibre composite.

Mode I fracture toughness tests were carried out and are defined as the resistance to the initiation and propagation of a delamination crack in unidirectional reinforced polymer matrix composite laminates under mode I opening load. Fracture toughness is measured in Joules per square metre.<sup>79</sup>

A mode I double cantilever beam specimen was used to determine  $G_{Ic}$ , the critical energy release rate of the fibre reinforced plastic composites.<sup>79</sup>

Three different crack arrestors were examined: extruded Surlyn<sup>®</sup> PC2000, setting six fibres, Surlyn<sup>®</sup> 1706 film and Surlyn<sup>®</sup> 1706 punctured film. Five 16 ply carbon-fibre reference samples were tested enabling a comparison to be made once testing had been carried out on the Surlyn<sup>®</sup> crack arrestors.

#### **5.7.3.1 Reference Samples**

Before testing, image analysis was carried out on a 20 mm x 20 mm section from the reference plate. Figure 59 shows a cross-sectional image showing how all individual carbon-fibres are on the same plane representing the unidirectional lay-up sequence of the reference composite.

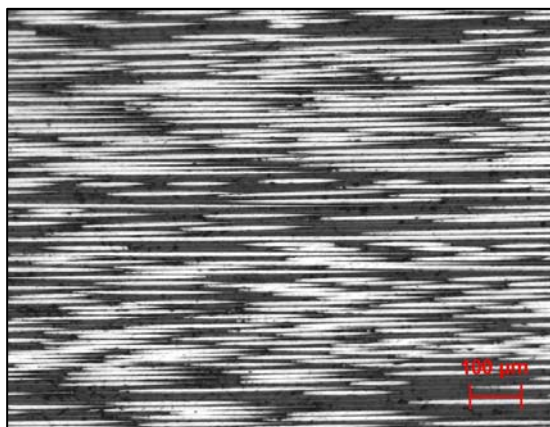


**Figure 59** – Cross-sectional image of  $G_{Ic}$  reference test specimen  
(magnification – 10x).

The interlaminar fracture toughness was determined in terms of the critical strain energy release rate, known as  $G_{Ic}$ . Two data reduction methods (corrected beam theory (CBT) and modified compliance theory (MCC) <sup>79, 95</sup>) as previously described in section 4.10.4.5 were used to calculate the average  $G_{Ic}$ , of the reference samples and are presented in table 29.

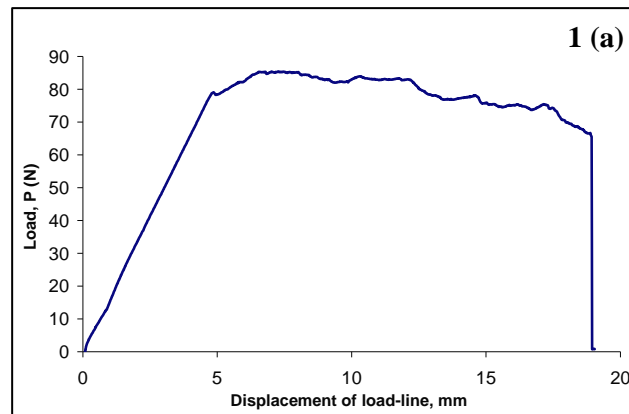
**Table 29** – Average  $G_{Ic}$ , critical energy release rate ( $J/m^2$ ) for reference samples, using both corrected beam (CBT) and modified compliance theory (MCC).

Reference Samples	$G_{Ic}$ Average ( $J/m^2$ )	
	CBT	MCC
1	724	723
2	605	599
3	745	757
4	870	871
5	574	572
<b>Average</b>	<b>703.6</b>	<b>704.4</b>
S.D	118.7	157.7

Using the corrected beam theory the average  $G_{Ic}$  for the reference samples was  $703.6 \text{ J/m}^2$ . The standard deviation was 118.7 showing a wide spread of results. This indicates the unpredictable fracture toughness of the carbon fibre-composites.

Propagation values of  $G_{Ic}$  are dependent on the mechanisms of delamination growth which is affected by such factors as the level of fibre-matrix adhesion, the interlaminar bonding strength and the extent of fibre bridging.<sup>96</sup> Such factors may explain the varied  $G_{Ic}$  values present in table 29.

Figure 60 contains a load-displacement curve collected from the Instron machine and also using the corrected beam theory, the interlaminar fracture toughness ( $G_{Ic}$ ) versus crack length was calculated and plotted for reference sample one (see Appendix Figure 4 for samples two - five).



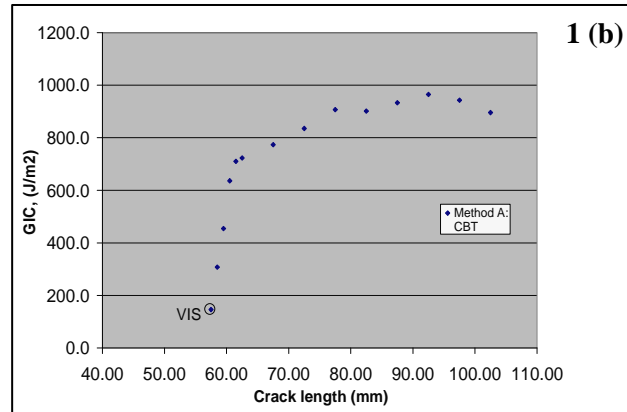


**Figure 60** – (a) Typical Load versus displacement curve and (b) interlaminar fracture toughness ( $G_{Ic}$ ) versus crack length for reference sample one.

The load-displacement curve shows a linear increase in load and displacement until the initial maximum load point was reached, indicating the crack initiation. Stable delamination was present for all reference samples. Instead of the load decreasing rapidly from the onset of delamination, the delamination grew slowly and the load did not decrease.

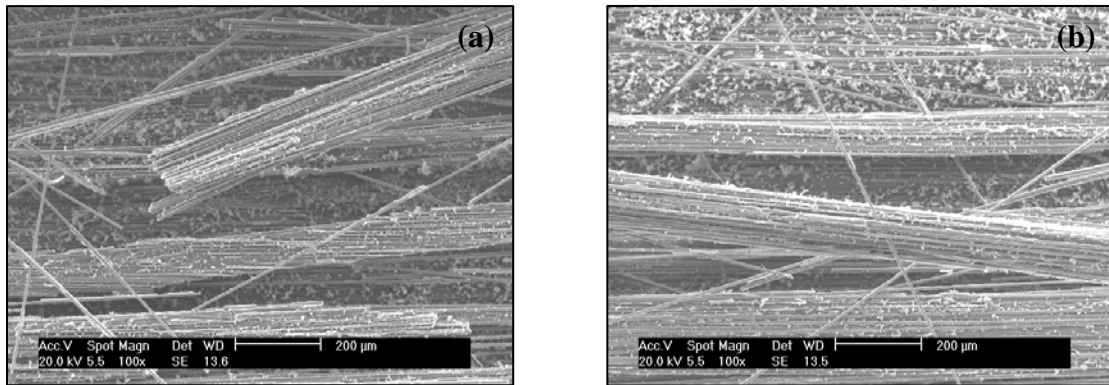
The load-displacement behaviour of the test specimens increases and gradually decreases as the crack begins to propagate, as reported by previous studies.<sup>97</sup> The drop in load at the end of the curve signifies sample failure.

Figure 60b represents the  $G_{Ic}$  versus crack length for reference sample one and the same trend is present for all reference samples. The VIS point indicates the point of onset of delamination. A  $G_{Ic}$  value of 146 J/m<sup>2</sup> and a crack length of 57.5 mm were recorded for the onset of delamination. The  $G_{Ic}$  is shown to increase with increasing crack length and is due to fibre bridging. Fibre bridging occurs as the delamination of the composite occurs, progressing



along the length of the sample and therefore increasing the energy required to propagate the delamination further.<sup>98, 99</sup>

Figure 61 contains S.E.M. images of the reference sample fracture surface following mode I testing.



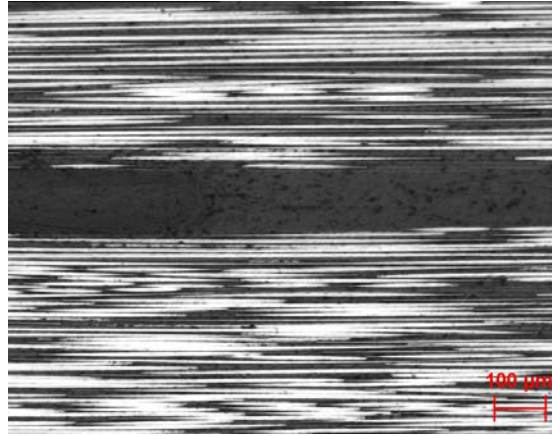
**Figure 61** – S.E.M images of reference sample following Mode I fracture testing.

Figure 61 shows images of fibre bridging resulting in increases in  $G_{Ic}$ . Fibre bridging takes place when delamination occurs, the crack switches from one fibre/matrix interface to another and this leaves behind fibres to bridge the gap, preventing the crack from propagating further. This is a positive attribute of fracture in composites as more energy is needed in order to propagate the bridged gap increasing the  $G_{Ic}$  value of the material.<sup>100</sup>

#### **5.7.3.2** *Surlyn<sup>®</sup> PC2000 Fibre Samples*

Surlyn<sup>®</sup> PC2000 fibres (setting six) were chosen as a crack arrestor as it recorded the greatest distance for guiding light. Figure 62 contains an image of the cross-sectional area of a fibre

sample before testing. The image shows the unidirectional lay-up of the carbon-fibres and the dark section at the centre of the image corresponds to Surlyn<sup>®</sup> PC2000 fibres.



**Figure 62** - Cross sectional image of  $G_{Ic}$  Surlyn<sup>®</sup> PC2000 fibre test specimen (magnification – 10x).

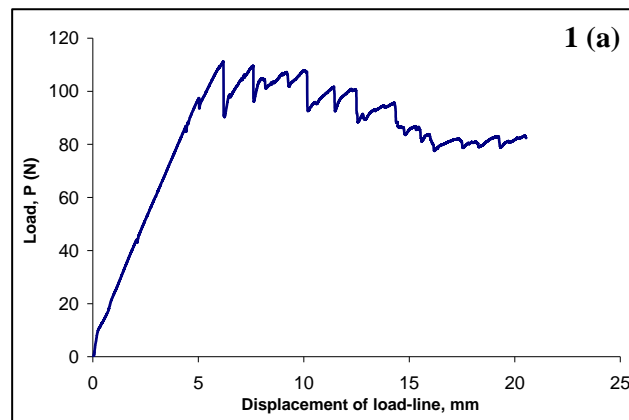
**Table 30** – Average  $G_{Ic}$ , critical energy release rate ( $J/m^2$ ) for Surlyn<sup>®</sup> PC2000 fibre samples, using both corrected beam (CBT) and modified compliance theory (MCC).

<b>Fibre Samples</b>	<b><math>G_{Ic}</math> Average (<math>J/m^2</math>)</b>	
	<b>CBT</b>	<b>MCC</b>
1	876	881
2	928	928
3	917	915
4		
5	983	982
<b>Average</b>	<b>926</b>	<b>926.5</b>
S.D	44.1	41.9

Due to a defect in sample four, only four samples were tested. The PTFE film did not perform as expected and the pre-crack was unable to be triggered before the mechanical test.

The average  $G_{Ic}$  for the fibre samples was  $926 \text{ J/m}^2$ . When compared with the reference samples, the presence of the fibres has increased the strain energy release rate by 31 % showing that the fibres have acted as a crack arrestor. The standard deviation was 44.1 indicating that the fracture toughness for the composite samples has become more consistent after using the fibres as a crack arrestor. The Surlyn<sup>®</sup> fibres have increased the interlaminar bonding strength and the amount of fibre bridging caused during delamination resulting in the increase in average  $G_{Ic}$  value.

Figure 63 contains the load-displacement curve and also the interlaminar fracture toughness ( $G_{Ic}$ ) versus crack length data for Surlyn<sup>®</sup> PC2000 fibres, sample one (see Appendix Figure 5 for samples two, three and five).



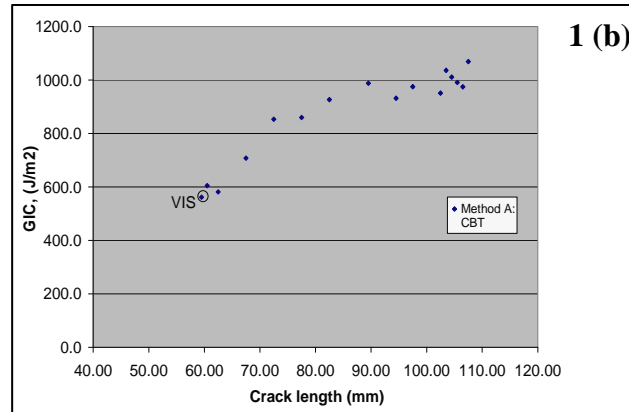


**Figure 63** – (a) Typical Load versus displacement curve and (b) interlaminar fracture toughness ( $G_{Ic}$ ) versus crack length for Surlyn<sup>®</sup> PC2000 fibres, sample one.

The load-displacement curve present in figure 63a indicates a linear increase in load and displacement until the maximum load point is reached, initiating the start of delamination. The maximum load applied to the fibre sample when compared with the reference sample, has increased by 25 (P) N, indicating an increase in interlaminar fracture toughness due to the presence of the fibres increasing the interlaminar bond strength.

The trend in figure 63a shows an increase and decrease in load-displacement for the sample and is attributed to the unstable propagation of the crack along the length of the beam due to the presence of the Surlyn<sup>®</sup> fibres acting as a crack arrestor, preventing delamination. This trend is also present for all other fibre samples.

The second graph shows the  $G_{Ic}$  versus crack length for the Surlyn<sup>®</sup> PC2000 fibre samples. In contrast with the reference sample the VIS point indicated for fibre sample one, shows that a  $G_{Ic}$  value of 562 J/m<sup>2</sup> and a crack length of 59.5 mm were recorded for the onset of

delamination. This shows a significant increase in energy required to cause delamination due to the presence of the fibres.

Figure 63b shows that the value of  $G_{Ic}$  is increasing, with increasing crack length and is due to increased amounts of fibre bridging and bonding strength caused by the presence of the Surlyn<sup>®</sup> fibres.

Figures 64a and 64b show images of fibre bridging that has occurred during testing. Larger sections of fibre bridging were apparent due to the use of fibres acting as crack arrestors, preventing the propagation of the crack.

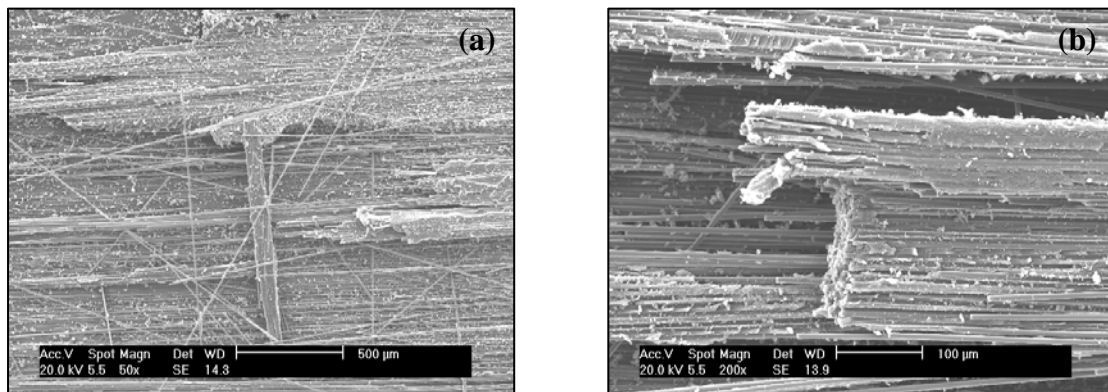


**Figure 64** – S.E.M images of Surlyn<sup>®</sup> PC2000 fibre sample following Mode I fracture testing.

### 5.7.3.3 Surlyn<sup>®</sup> 1706 Film Samples

The second material to be investigated as a crack arrestor was the as received Surlyn<sup>®</sup> 1706 film. The average thickness of the film was 0.06 mm and one layer of the film was incorporated into the centre of the carbon-fibre composite. Figure 65 shows a cross-sectional

image of the composite sample. The dark section found in the centre of the image is the Surlyn<sup>®</sup> 1706 film.

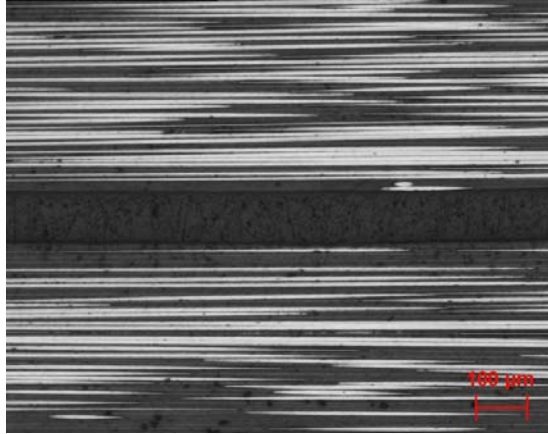


**Figure 65** - Cross sectional image of  $G_{Ic}$  Surlyn<sup>®</sup> 1706 film test specimen (Magnification – 10x).

**Table 31** – Average  $G_{Ic}$ , critical energy release rate ( $J/m^2$ ) for Surlyn<sup>®</sup> 1706 film samples, using both corrected beam (CBT) and modified compliance theory (MCC).

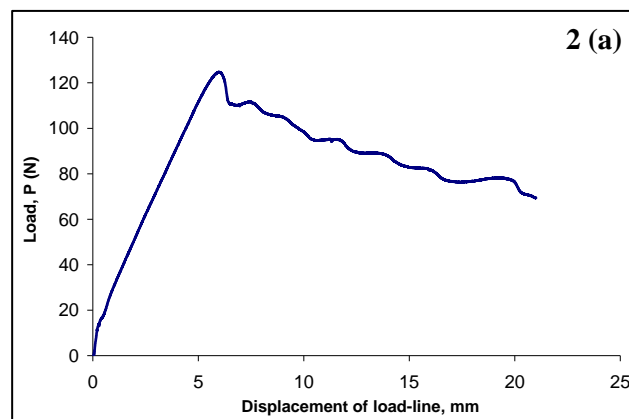
<b>Film Samples</b>	<b><math>G_{Ic}</math> Average (<math>J/m^2</math>)</b>	
	<b>CBT</b>	<b>MCC</b>
1	596	586
2	943	945
3	824	822
4	913	913
5	885	885
<b>Average</b>	<b>832.2</b>	<b>830.2</b>
S.D	139.1	143.8

The average  $G_{Ic}$  value for the film samples was  $832.2 J/m^2$ . This shows an increase in critical release energy rate ( $G_{Ic}$ ) when compared to the reference samples; however the increase is not as significant as the value calculated for the fibre samples.

Sample two has recorded the highest  $G_{Ic}$  value so far and after the initiation of the crack the Surlyn<sup>®</sup> film was shown to increase interlaminar fracture toughness as the crack length increases. Using the film as a crack arrestor has increased the average  $G_{Ic}$  value by 18 %, indicating that the film has acted as a crack arrestor.

The standard deviation for the result was 139.1. When compared with both reference and fibre values the spread of the results for the film is higher. This is due to the low average  $G_{Ic}$  value recorded for sample one. This result was caused by a shift in the crack forming a secondary delamination above the layer of the Surlyn<sup>®</sup> film. This caused unstable delamination as the film was unable to act as a crack arrestor due to the formation of a new crack.

The load-displacement curve and graph plotting the interlaminar fracture toughness ( $G_{Ic}$ ) versus crack length for Surlyn<sup>®</sup> 1706 film, sample two are presented in figure 66 (see Appendix Figure 6 for samples one, three, four and five).



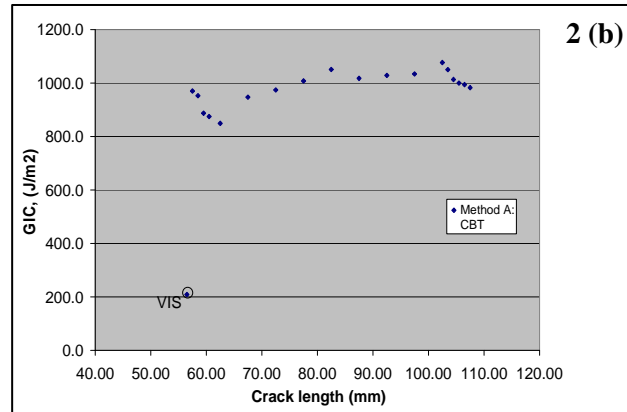


**Figure 66** – (a) Typical Load versus displacement curve and (b) interlaminar fracture toughness ( $G_{Ic}$ ) versus crack length for Surlyn<sup>®</sup> 1706 film, sample two.

When compared with the fibre samples, figure 66a shows an initial linear increase in load and displacement until the maximum load point is reached. A steep rise in load is shown over the first 5 mm of displacement for all five samples until the maximum load point is reached and crack propagation is initiated. Once the crack propagation is initiated the load-displacement behaviour of the samples increases and decreases as the crack begins to propagate. The load-displacement curve shows that crack propagation was stable due to the gradual decrease in applied load.

The maximum load point has increased by 40 (P) N, when compared with the reference sample. This indicates that the film has increased the interlaminar fracture toughness and acted as a crack arrestor; however further propagation of the crack shown by the displacement takes place at lower loads than the fibre samples showing the film is not as efficient as the fibres at arresting the crack.



With reference to figure 66b the point of onset of delamination (VIS) for sample two is shown to have a  $G_{Ic}$  value of  $209 \text{ J/m}^2$  and a crack length of 56.5 mm. When compared with both the reference and fibre samples, the onset of delamination has taken place at lower values. However the critical release energy rate ( $G_{Ic}$ ) does increase significantly in all samples after the initiation of delamination indicating a poor matrix and film adhesion at the edge of the film.

The initial trend observed in figure 66b shows that the  $G_{Ic}$  value does increase with increasing crack length for sample two, however this increase is not stable and drops in critical release energy rate are shown as the crack length increases. This is shown for all film samples. Spacing was present between the Surlyn<sup>®</sup> fibres during fabrication of the composites. The film however covered the entire surface of the pre-preg. This may have caused the amount of fibre bridging across the length of the beam to decrease in parts and is shown by the drops in the critical release energy rate along the length of the beam. The presence of ductile and brittle fracture surfaces caused by the film may have also caused the decrease in  $G_{Ic}$  at certain crack lengths.

Figure 67 contains S.E.M. images of the film sample fracture surface following testing. Figure 67a shows a small area of fibre bridging on top of the film caused during propagation of the crack. Figure 67b shows the ductile and brittle fracture of the film, where the film was acting as a crack arrestor.

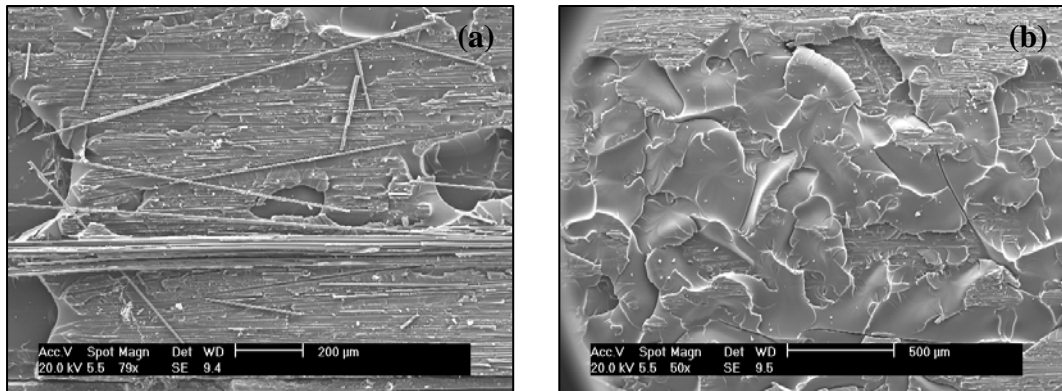


**Figure 67** – S.E.M images of Surlyn<sup>®</sup> 1706 film sample following mode I fracture testing.

#### **5.7.3.4** *Surlyn<sup>®</sup> 1706 Punctured Film Samples*

The final crack arrestor experiment involved using the Surlyn<sup>®</sup> 1706 film, however this time the film was punctured using a custom made device. This was done to investigate whether the punctures would allow the flow of resin through the holes during curing forming bridges between the centre plies enhancing the use of the film as a crack arrestor. Figure 68 contains a S.E.M image of the punctured Surlyn<sup>®</sup> 1706 film.

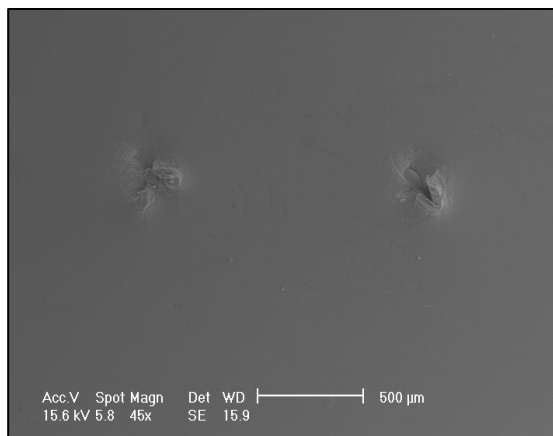


**Figure 68** – S.E.M image of punctured Surlyn<sup>®</sup> 1706 film.

Figure 69 shows a cross sectional image of a punctured film sample before testing. The dark strip at the centre of the image is the punctured film.

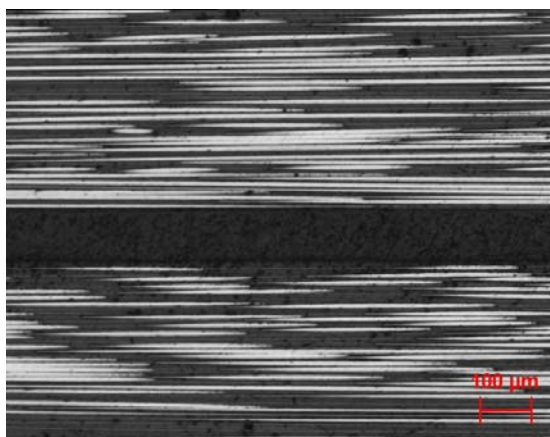


**Figure 69** - Cross sectional image of  $G_{lc}$  punctured Surlyn<sup>®</sup> 1706 film test specimen (Magnification – 10x).

**Table 32** – Average  $G_{Ic}$ , critical energy release rate ( $J/m^2$ ) for punctured Surlyn<sup>®</sup> 1706 film samples, using both corrected beam (CBT) and modified compliance theory (MCC).

<b>P Film Samples</b>	<b><math>G_{Ic}</math> Average (<math>J/m^2</math>)</b>	
	<b>CBT</b>	<b>MCC</b>
1	900	906
2	756	757
3	1013	1011
4	1002	1027
5	814	820
<b>Average</b>	<b>897</b>	<b>904.2</b>
<b>S.D</b>	<b>113.2</b>	<b>117.5</b>

The average  $G_{Ic}$  value for the punctured film samples was measured at 897  $J/m^2$ . The punctured film increased the critical release energy rate by 27 % when compared with the reference samples. After comparing the interlaminar fracture toughness for both the film and punctured film, results showed that puncturing the film increased the interlaminar fracture toughness by a further 9 %.

The results show that two out of the five samples tested, recorded the highest fracture toughness of all crack arrestors tested. This shows that the puncturing of the film has increased the flow of the resin during curing consolidating the sample and forming a bridge between the composite and the film.

The standard deviation was 113.1 showing that the puncturing of the film has made the interlaminar fracture toughness more consistent, when compared with the non punctured film.

Figure 70 contains the load-displacement curve from the Instron machine and the interlaminar fracture toughness ( $G_{Ic}$ ) versus crack length plots for the punctured film sample three (see Appendix Figure 7 for samples one, two, four and five).

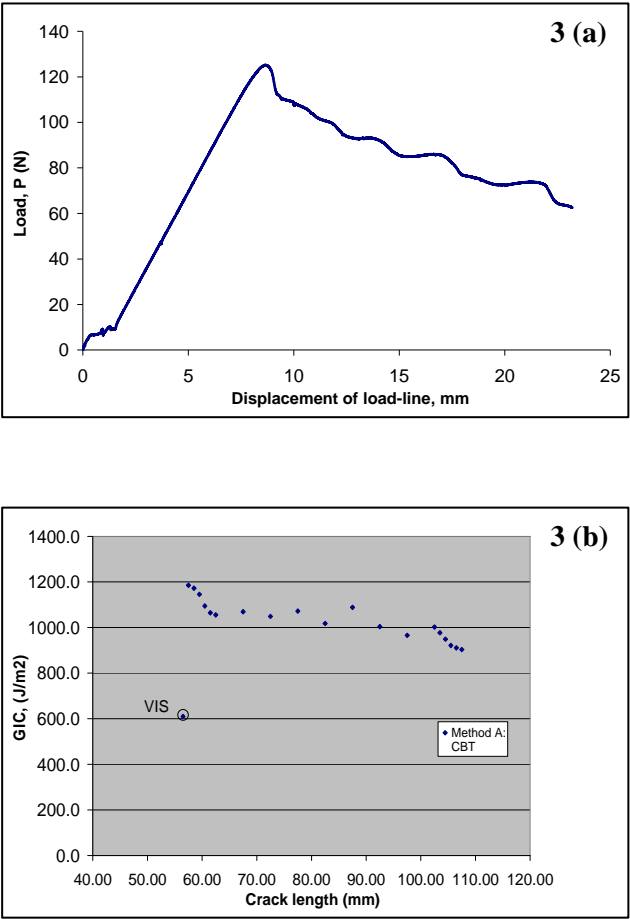


**Figure 70** - (a) Typical Load versus displacement curve and (b) interlaminar fracture toughness ( $G_{Ic}$ ) versus crack length for punctured Surlyn® 1706 film, sample two.

Figure 70a shows a steep increase in load over the first 6 - 8 mm of displacement until the maximum load point is reached. Once the crack was initiated, the results show a significant drop in applied load for all samples. The behaviour of the load-displacement curve for all samples increases and decreases as the crack begins to propagate. As previously described for

the as-received film, the punctured film has acted as a crack arrestor; however further propagation of the crack takes place at lower loads than the fibre samples showing the punctured film is not as efficient as the fibres.

The punctured film has also increased the maximum load point by  $\sim 40$  (P) N and indicates an increase in interlaminar fracture toughness as a higher load is required for onset of the crack propagation. As the load is shown to steadily decrease the crack propagation is stable, however displacement is shown to occur at lower loads indicating the punctured film does not perform as well as the fibres arresting the crack.

Figure 70b shows the  $G_{Ic}$  values plotted against the crack length for punctured Surlyn<sup>®</sup> film sample three. The onset of delamination (VIS) is shown to have a  $G_{Ic}$  value of  $610 \text{ J/m}^2$  and a crack length of 56.5 mm. This indicates that puncture holes present in the film have enabled bridges to form between the film and centre plies increasing the interlaminar fracture toughness.

An initial increase in  $G_{Ic}$  critical release energy rate and increasing crack length is shown for sample three and the other samples. However as with the film samples the  $G_{Ic}$  is shown to decrease with increasing crack length at certain crack lengths along the beam for the punctured sample. This may also be attributed to the amount of bridging present during delamination of the sample leading to a decrease in  $G_{Ic}$ . Ductile and brittle fracture was also present along the fractured film areas of the sample again causing decreases in  $G_{Ic}$ .

Figure 71 contains S.E.M images of the surface area of the punctured film samples following mode I fracture testing. No fibre bridging was present on the samples following testing showing that the punctured film had bonded with both the carbon -fibre laminates. Figures 71a and 71b show the ductile (rough) and brittle (smooth) fracture surfaces of the punctured film that was caused by the crack propagating through the sample.

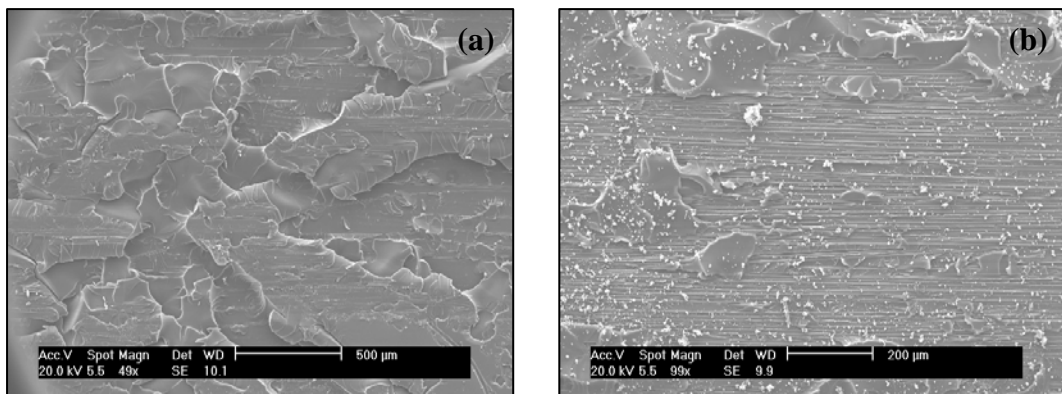


**Figure 71** – S.E.M images of punctured Surlyn® 1706 film sample following mode I fracture testing.

The aim of this section was to investigate whether Surlyn® would act as a crack arrestor. Overall the average  $G_{Ic}$  value was increased for all samples using Surlyn® as a crack arrestor, indicating an increase in interlaminar fracture toughness. The PC2000 fibres increased the average  $G_{Ic}$  value by 31 %. This was the highest average increase in  $G_{Ic}$ . However for the punctured film, two out of the five samples recorded the highest average  $G_{Ic}$  value and puncturing the film increased the interlaminar fracture toughness by a further 9 %, when compared with the as-received film.

Fibre bridging and the added increase of the bonding between the Surlyn<sup>®</sup> and the pre-preg were attributed to the increase in  $G_{Ic}$  values. Fractography demonstrated the different types of fracture and fibre bridging present following delamination.

The main focus of the study was to investigate the ionomer Surlyn<sup>®</sup> as a self-healing and self-sensing composite. The preliminary characterisation techniques showed that Surlyn<sup>®</sup> is a low density amorphous material. The material had a low refractive index of 1.52. Taking these initial properties into account the ionomer is ideal as a composite due to it being light weight. The initial light guide and self-sensing ability was also shown. The thermal characteristics of the three grades of Surlyn<sup>®</sup> also showed the same trends as Surlyn<sup>®</sup> 8940, which was previously reported as having self-healing abilities.

The study then focused on new areas involving the development of Surlyn<sup>®</sup> plaques and Surlyn<sup>®</sup> fibres focusing on the self-healing and self-sensing abilities of Surlyn<sup>®</sup> separately. Although Surlyn<sup>®</sup> plaques were fabricated and shown to have stable thermal characteristics, indentation and ballistics experiments were unable to be carried out.

A new and novel method was designed to extrude Surlyn<sup>®</sup> fibres of varying diameter. Both grades of Surlyn<sup>®</sup> PC2000 and 9910 were shown to transmit light, however once smaller diameter fibres were extruded Surlyn<sup>®</sup> PC2000 showed the highest light transmission results. This fibre then underwent several experiments which showed that Surlyn<sup>®</sup> fibres have the ability to act as a self-sensing light guides. During the attenuation studies on the Surlyn<sup>®</sup> PC2000 fibres, the fibres were shown to undergo permanent damage as the weight applied to



the fibre increased. This shows that a protective coating around the fibre will be needed for further application of the fibres.

Although the self-healing ability of Surlyn<sup>®</sup> was discussed in the literature review section, due to circumstances outside of the authors control indentation and ballistics experiments were not carried out. However the crack healing ability of Surlyn<sup>®</sup> fibres and films was studied during mode I fracture tests. All results showed that the Surlyn<sup>®</sup> was able to act as a crack arrestor increasing the fracture toughness of the carbon-fibre composite and also suggesting that Surlyn<sup>®</sup> is able to self-heal.

Overall Surlyn<sup>®</sup> has shown the ability as both a self-sensing and self-healing material. Joining the self-healing and self-sensing properties together, Surlyn<sup>®</sup> composites were fabricated with varying fibres.

The next step is to demonstrate both the properties together during both indentation and ballistics experiments and also further mode I experiments. Further exploitation of the Surlyn<sup>®</sup> fibres is another key area and is discussed in the future work chapter 7.0.

## 6.0 Conclusion

Initial primary characterisation studies showed that all three grades of Surlyn<sup>®</sup> were low density amorphous materials. They also had a low refractive index of  $\sim 1.51$  and were lightweight and transparent in form. These properties initially suggested that Surlyn<sup>®</sup> would be ideal for incorporation into a composite and contain light guide capabilities. Following the preliminary characterisation studies, the self-healing and self-sensing properties of Surlyn<sup>®</sup> were studied. Novel techniques were developed to produce both thick Surlyn<sup>®</sup> plaques and Surlyn<sup>®</sup> fibres. The thick Surlyn<sup>®</sup> plaques were shown to have stable heat flow properties.

Two methods involving the use of weights and a custom haul off machine were developed to produce Surlyn<sup>®</sup> PC2000 and 9910 fibres of varying diameter. Initial tests showed that Surlyn<sup>®</sup> PC2000 recorded the highest light intensity measurements of up to  $\sim 93$  mW and had the longest light guide properties. Factors such as fibre quality, the cleave angle and metal cation present in the material influenced the light intensity results. Further light transmission experiments showed that Surlyn<sup>®</sup> PC2000 fibres were able to guide light efficiently and readings were stable over short periods of time. The fibres also showed the ability to provide information when damaged proving their ability as a self-sensing material. However during attenuation experiments permanent damage was caused to the fibre suggesting the need for a fibre coating.

Using 16 ply carbon-fibre composite beam samples, Surlyn<sup>®</sup> PC2000 fibres and Surlyn<sup>®</sup> 1706 film were used as crack arrestors during mode I fracture toughness tests. Both grades of Surlyn<sup>®</sup> were shown to act as crack arrestors increasing the fracture toughness of the carbon-

fibre composites and also suggesting that Surlyn<sup>®</sup> is able to self-heal. The Surlyn<sup>®</sup> fibres increased the fracture toughness by 32 % and the Surlyn<sup>®</sup> film and Surlyn<sup>®</sup> punctured film increased the fracture toughness by 18 % and 27 %. The punctures in the Surlyn<sup>®</sup> film enabled increased interlaminar bonding between the film and the fibres.

Following the reported self-healing and self-sensing properties, Surlyn<sup>®</sup> composites were developed and fabricated. VTM264 glass-fibre pre-preg was incorporated with both Surlyn<sup>®</sup> 1706 film and Surlyn<sup>®</sup> PC2000 fibres producing a self-healing and self-sensing Surlyn<sup>®</sup> composite.

## **7.0 Future Work**

Future areas of study include light guide, light intensity, impact and puncture testing. Using the thick Surlyn<sup>®</sup> plaques; heat flow through the samples could be monitored during puncture and ballistics experiments. The optimum temperature for self-healing could then be investigated. Heating the tool used to puncture the sample could be another variable. The use of a high speed camera to monitor the self-healing phenomenon could also be used.

Further indentation tests using the fabricated Surlyn<sup>®</sup> and SDOF composite could also be carried out. The fibres could be connectorised enabling light intensity measurements to be carried out. During indentation tests the self-healing and self-sensing ability of the composite could be studied. During my course of study, Surlyn<sup>®</sup> and glass-fibre composites were produced. Further indentation and ballistic testing could be carried out to investigate the self-healing capacity of the composites. Incorporating different types of fibres could also be examined, further investigating the idea of a self-healing and self-sensing composite.

The fabrication of Surlyn<sup>®</sup> fibres is another important area. Smaller diameter fibres could be produced, enabling further light guide and light intensity measurements. The fibres could then be placed under tension or flexion further investigating the self-sensing capabilities of Surlyn<sup>®</sup> fibres.

Further crack arrestor composites could be fabricated incorporating both Surlyn<sup>®</sup> and different types of fibres. During mode I testing the fibres could be connectorised and light intensity

measurements could be recorded. The experiment could be monitored using a high speed camera, further researching self-healing and self-sensing composites.

Other grades of Surlyn<sup>®</sup> could be added to the above experiments investigating whether the different grades of Surlyn<sup>®</sup> react differently to the ones already studied.

## 8.0 Appendices

**A1.1 Figure 1a** – Raw data for *Surlyn® PC2000* density measurements.

<b>Surlyn® PC 2000</b>	Sample Weight (g)	Sample Buoyancy (g)	Density of Liquid	Density (g/cm <sup>3</sup> )
1	0.22071	0.15607	0.68376	0.967
2	0.18467	0.13044	0.68376	0.968
3	0.22125	0.15636	0.68376	0.967
4	0.22906	0.16165	0.68376	0.969
5	0.18232	0.12872	0.68376	0.968
				Average = <b>0.968</b>

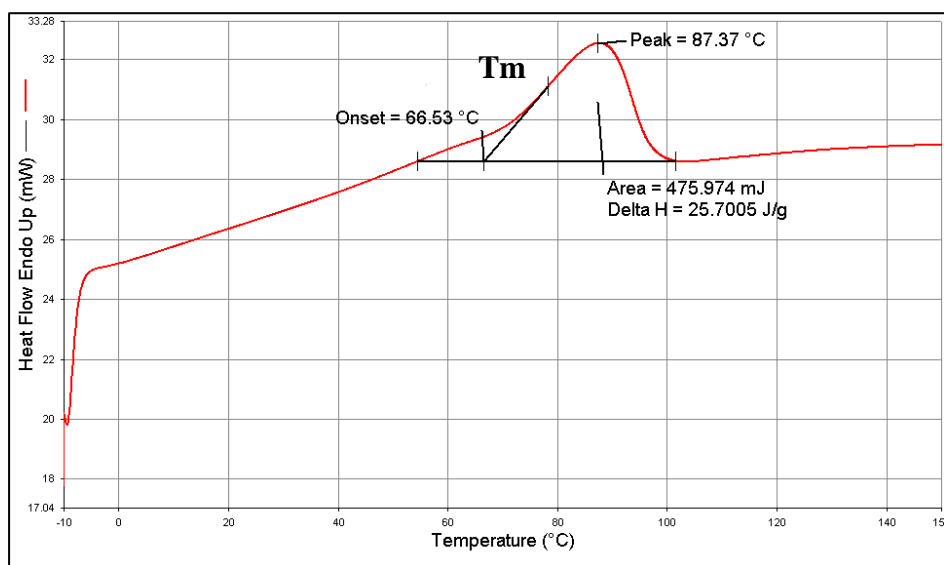
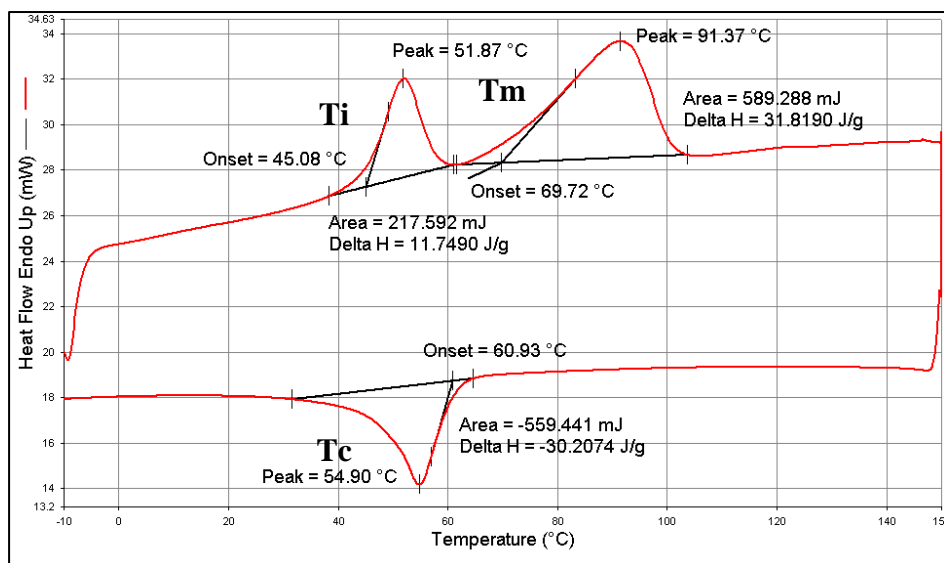
**A1.2 Figure 1b** - Raw data for *Surlyn® 9910* density measurements.

<b>Surlyn® 9910</b>	Sample Weight (g)	Sample Buoyancy (g)	Density of Liquid	Density (g/cm <sup>3</sup> )
1	0.26872	0.18882	0.68376	0.973
2	0.28532	0.20032	0.68376	0.974
3	0.24625	0.17298	0.68376	0.973
4	0.27091	0.19025	0.68376	0.974
5	0.26605	0.18697	0.68376	0.973
				Average = <b>0.973</b>

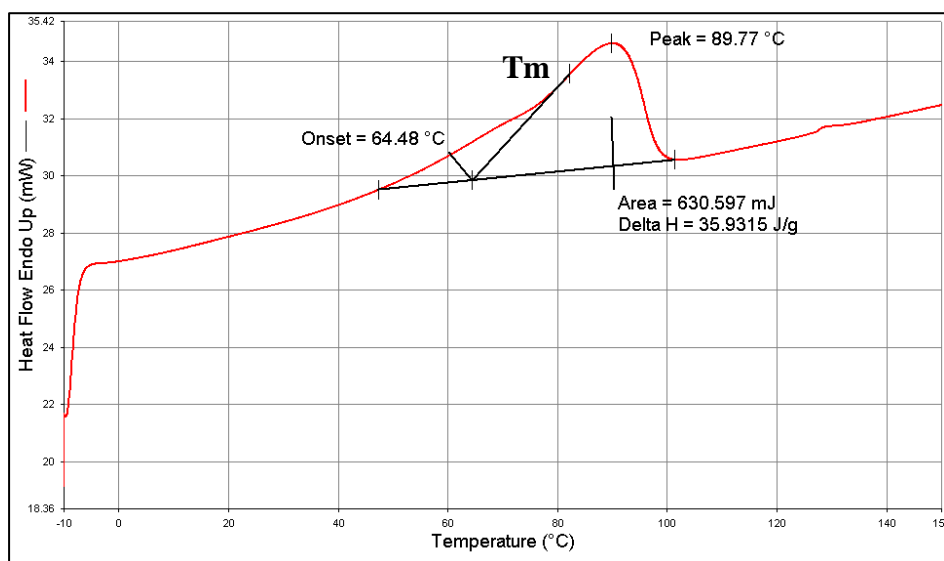
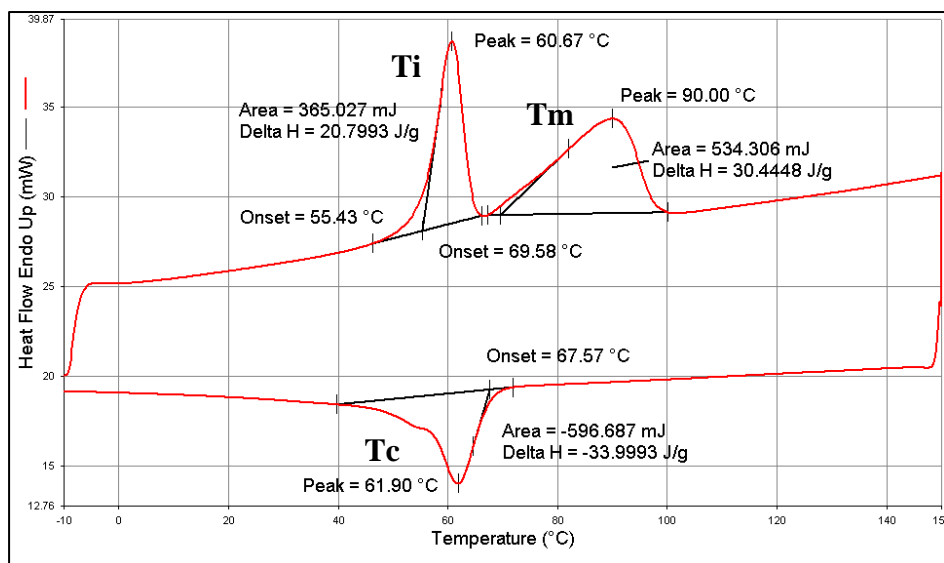
**A1.3 Figure 1c** – Raw data for *Surlyn® 1706* density measurements.

<b>Surlyn® 1706</b>	Sample Weight (g)	Sample Buoyancy (g)	Density of Liquid	Density (g/cm <sup>3</sup> )
1	0.01239	0.00858	0.68376	0.987
2	0.01132	0.00786	0.68376	0.985
3	0.00963	0.00658	0.68376	0.977
4	0.00887	0.00621	0.68376	0.977
5	0.01013	0.00735	0.68376	0.942
				Average = <b>0.974</b>

**A2.1 Figure 2a** – DSC trace of Surlyn<sup>®</sup> 9910; one cycle.

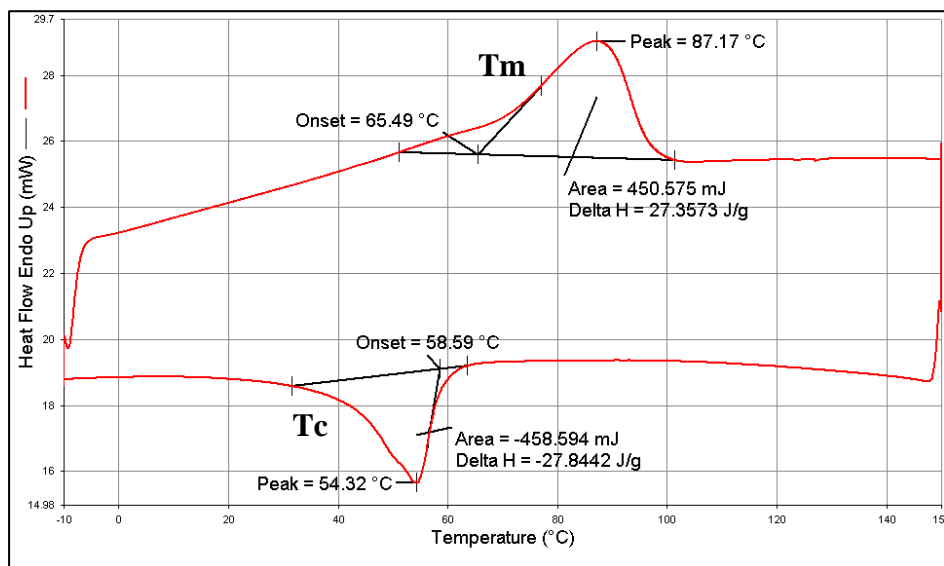
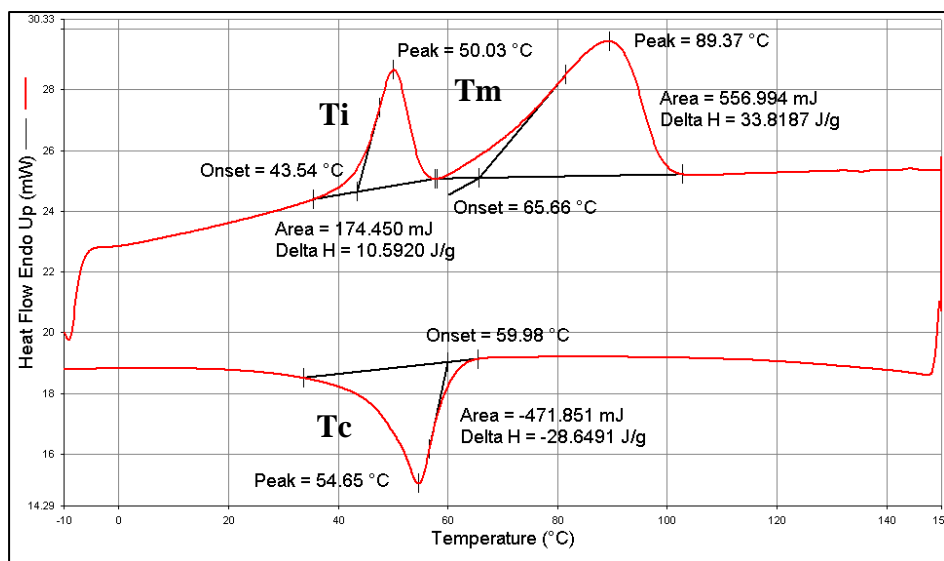


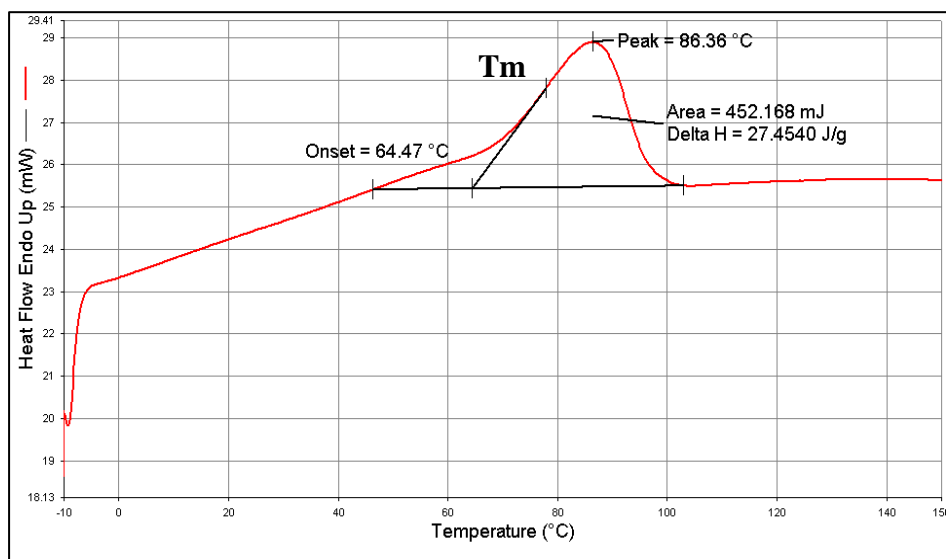
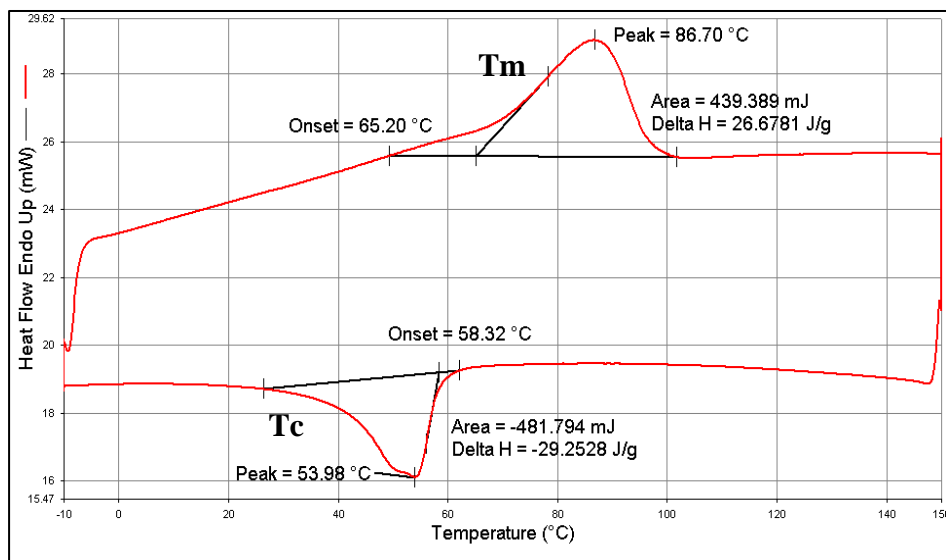
**A2.2 Figure 2b** – DSC trace of *Surlyn*<sup>®</sup> 1706; one cycle.



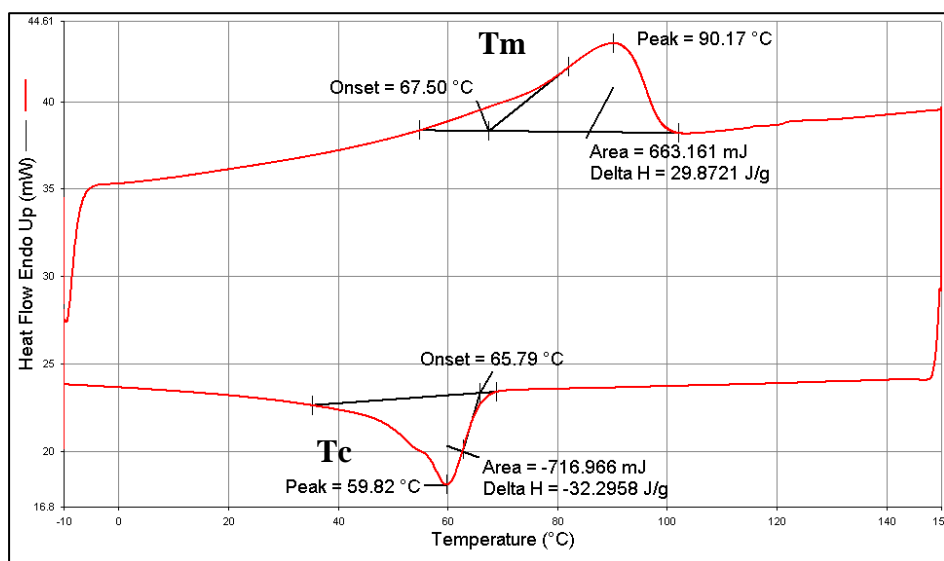
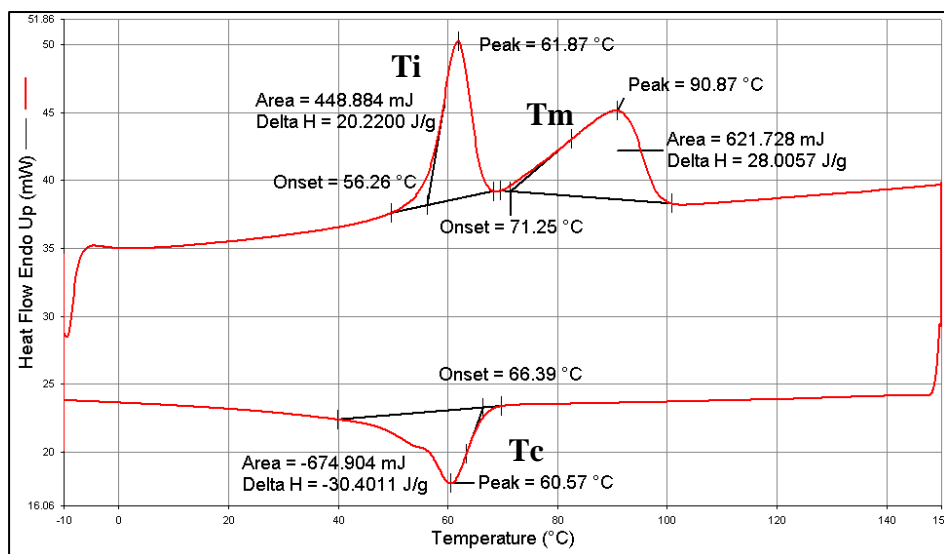


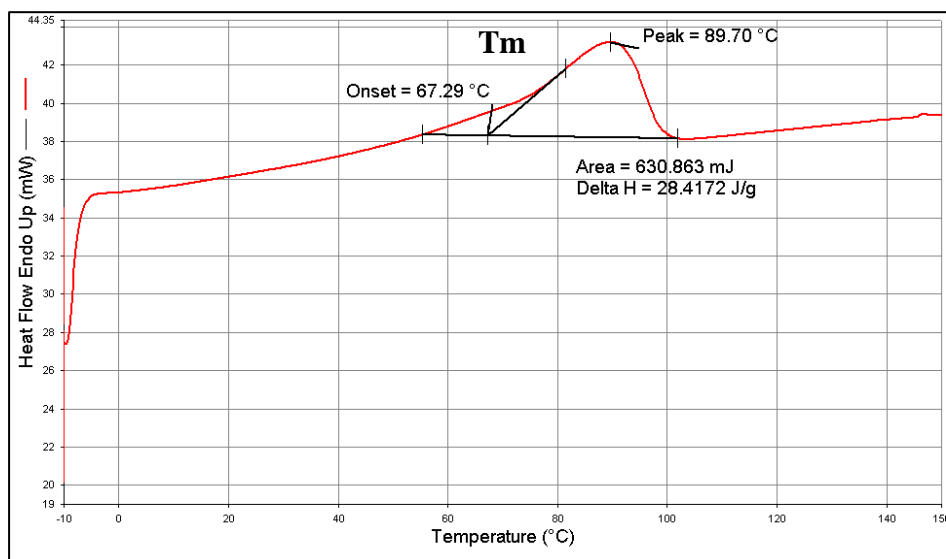
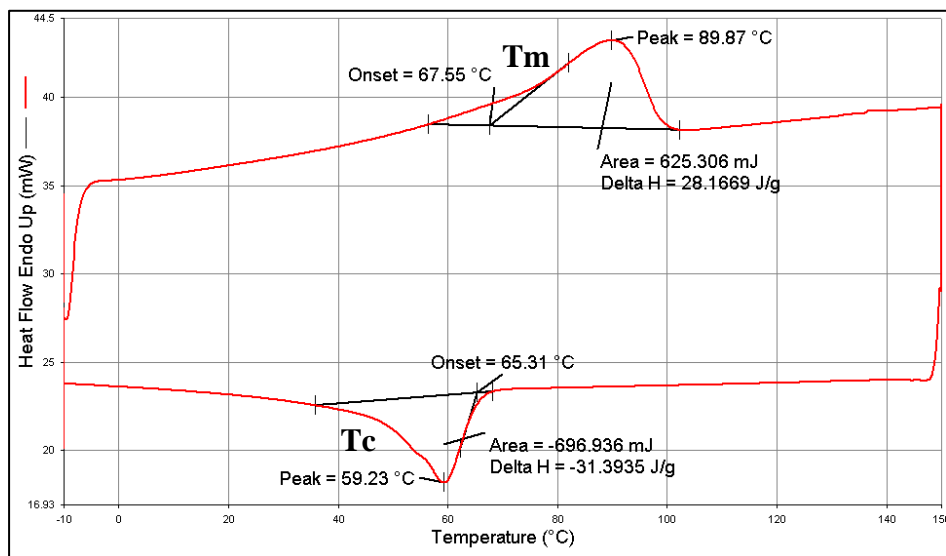
**A3.1 Figure 3a** – DSC trace of Surlyn<sup>®</sup> 9910; three cycles.





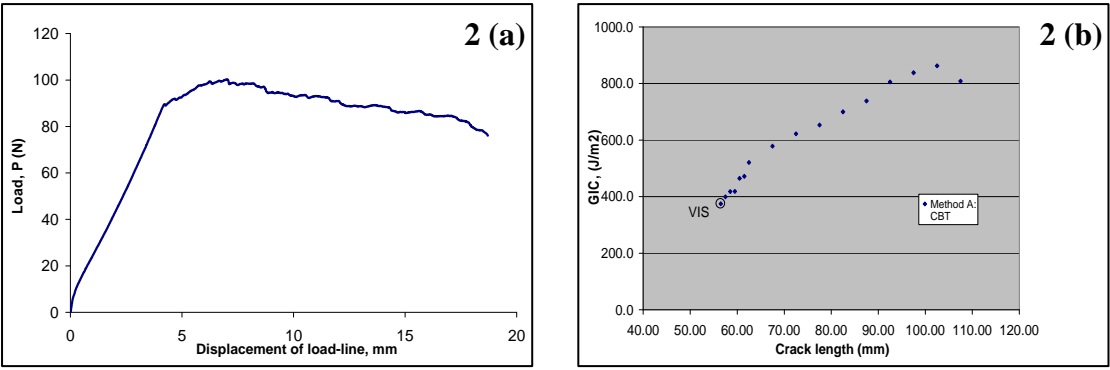
**A3.2 Figure 3b** - DSC trace of Surlyn<sup>®</sup> 1706; three cycles.



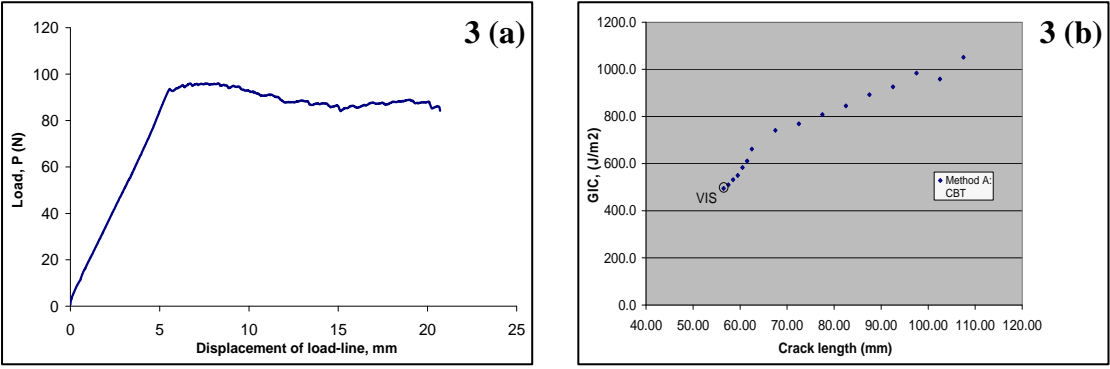


**A4. Figure 4** - (a) Typical Load versus displacement curve and (b) interlaminar fracture toughness ( $G_{Ic}$ ) versus crack length for reference samples two – five.

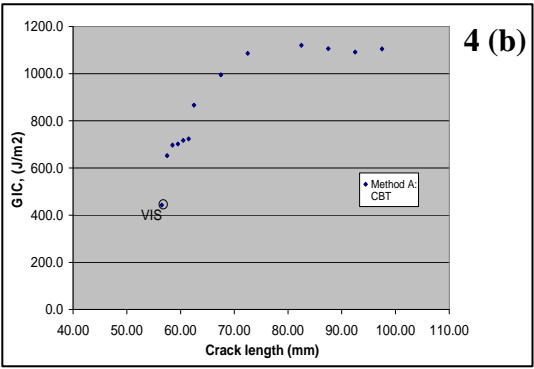
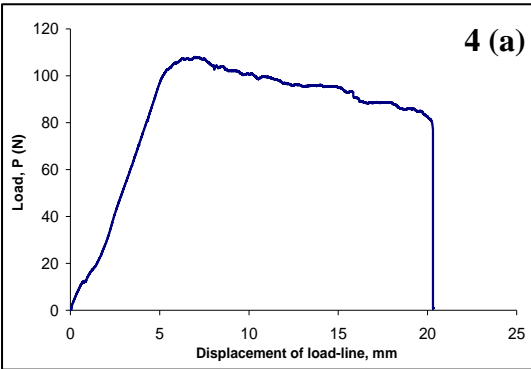
*Sample Two:*



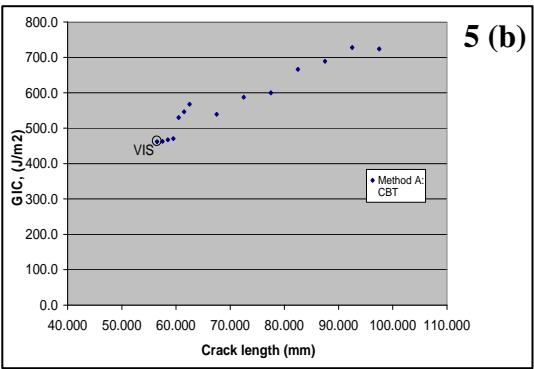
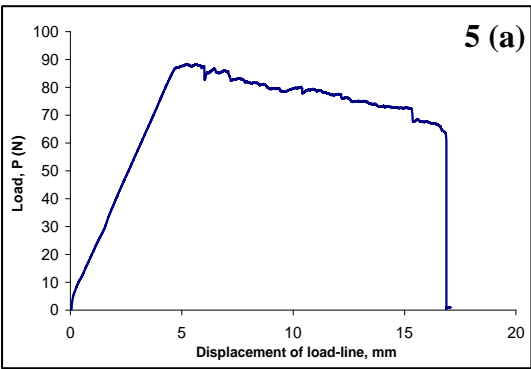
*Sample Three:*



Sample Four:

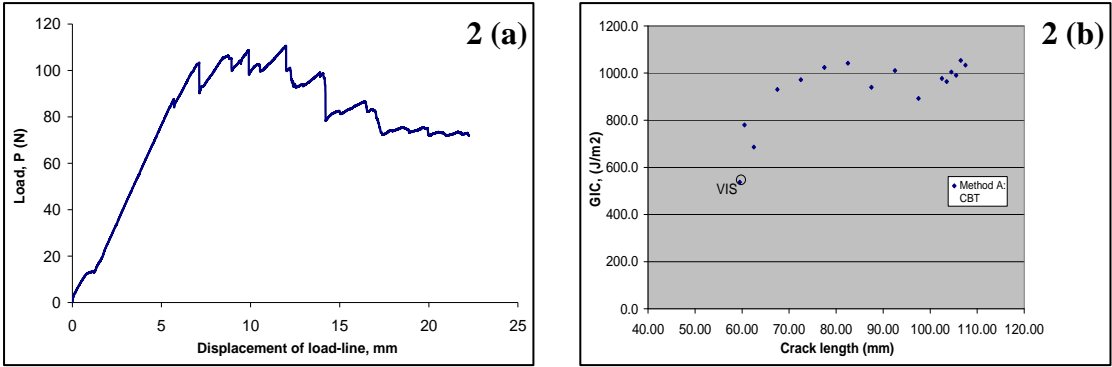


Sample Five:

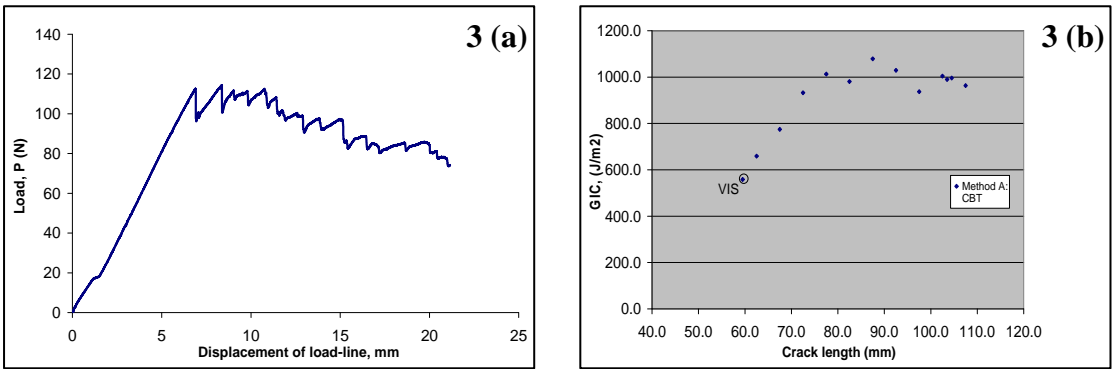


**A5. Figure 5** - (a) Typical Load versus displacement curve and (b) interlaminar fracture toughness ( $G_{Ic}$ ) versus crack length for Surlyn<sup>®</sup> PC2000 fibre samples two, three and five.

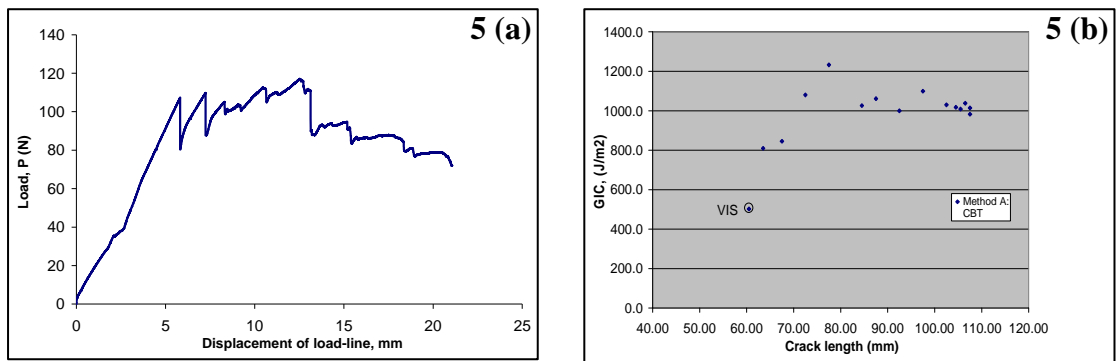
*Sample Two:*



*Sample Three:*

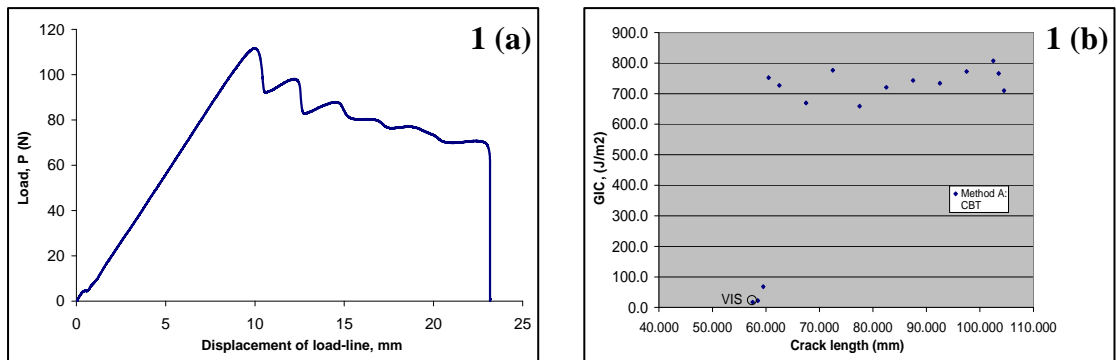


Sample Five:



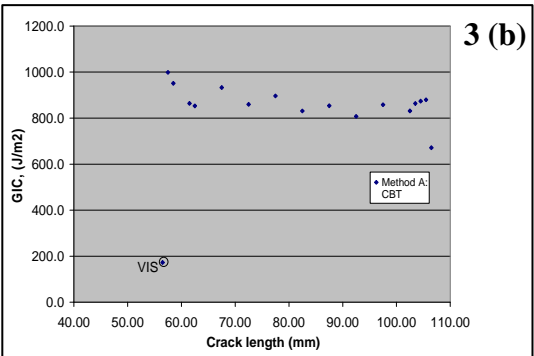
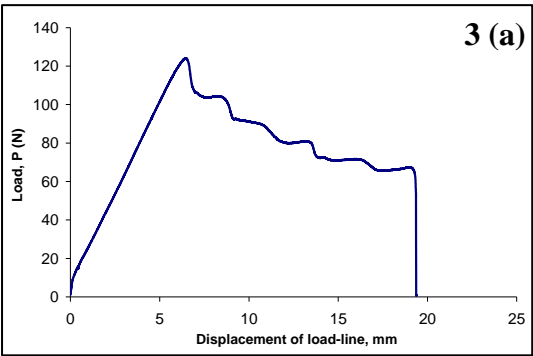
**A6. Figure 6** - (a) Typical Load versus displacement curve and (b) interlaminar fracture toughness ( $G_{IC}$ ) versus crack length for Surlyn<sup>®</sup> 1706 film, samples one, three, four and five.

Sample One:

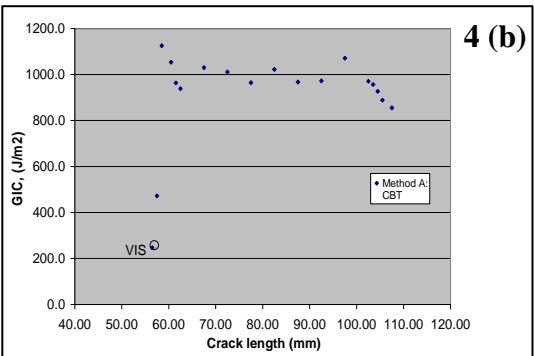
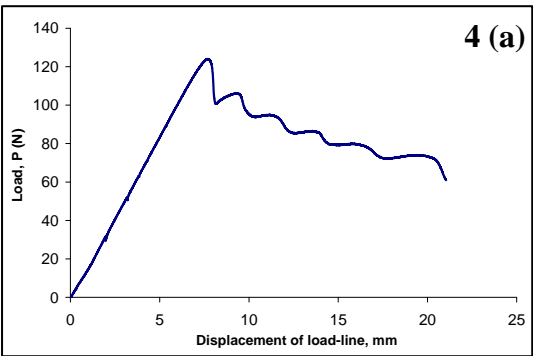




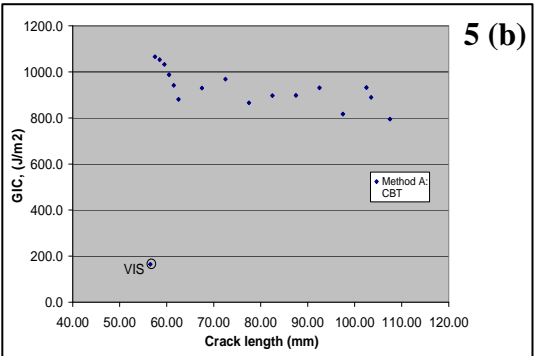
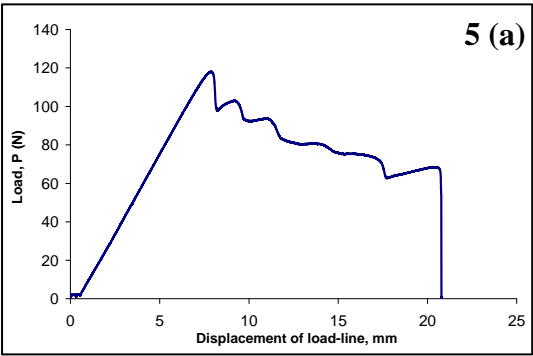
Sample Three:



Sample Four:

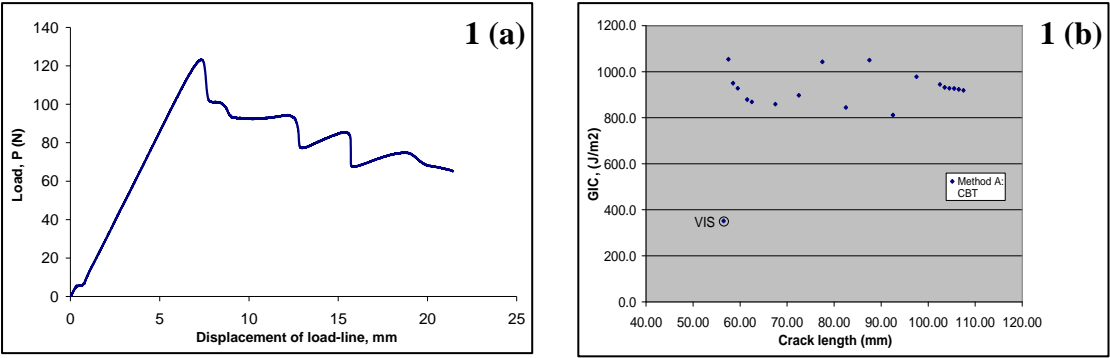


Sample Five:

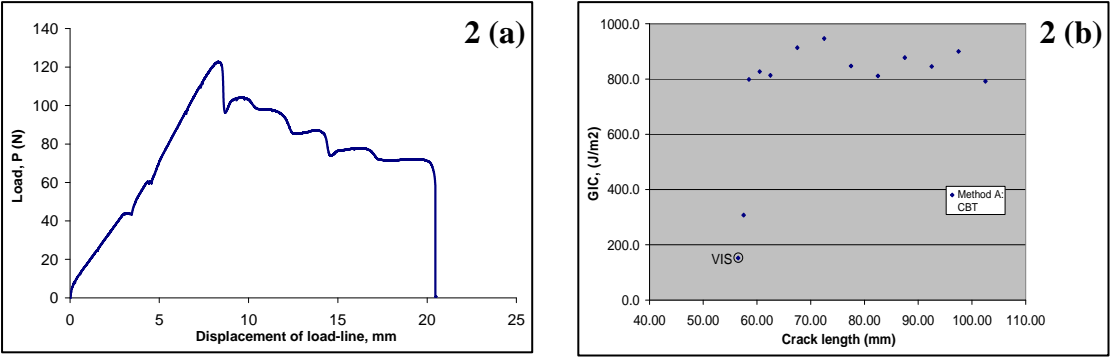


**A7. Figure 7** - (a) Typical Load versus displacement curve and (b) interlaminar fracture toughness ( $G_{Ic}$ ) versus crack length for punctured Surlyn<sup>®</sup> 1706 film, samples one, two, four and five.

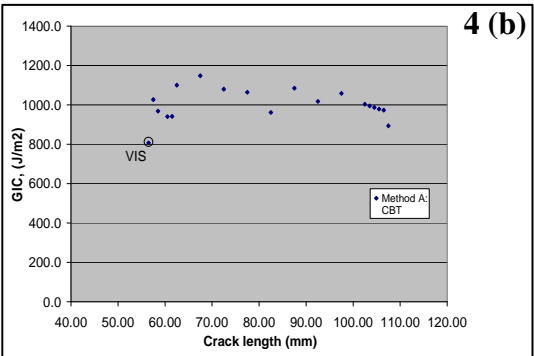
*Sample One:*



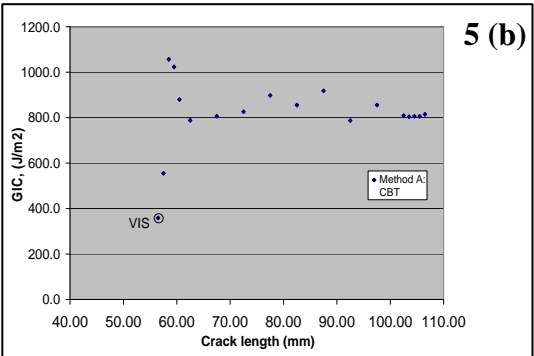
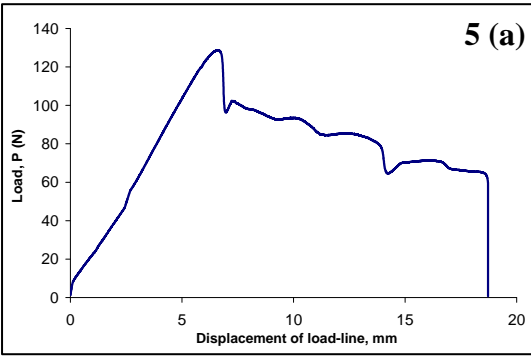
*Sample Two:*



Sample Four:



Sample Five:



## 9.0 References

- 1) DuPont miracles of science, product grades, by family.  
[http://www2.dupont.com/Surllyn/en\\_US/products/index.html](http://www2.dupont.com/Surllyn/en_US/products/index.html).
- 2) Samadzadeh, H., Baura, S. H., Peikari, M., Kashiriha, S. M, and Ashrafi, A, *A review of self-healing coatings based on micro/nancapsules*. Progress in organic coatings, 2010, 68 (3) p: 159-164.
- 3) Hager, M. D., Greil, P., Leyans, C., van der Zwaag, S, and Schubert, U. S, *Self-healing materials*. Advanced Materials, 2010, 22 (47) p: 5424-5430.
- 4) Kalista, Jr., S. J, *Self-healing of Thermoplastic Poly(ethylene-co-methacrylic Acid) Copolymers Following Projectile Puncture*. Masters Thesis, Virginia Tech. 2003.
- 5) Coughlin, C. S., Martinelli, A. A, Boswell, R. F, *Mechanism of Ballistic Self-healing in EMAA Ionomers*. Polymeric Materials science and Engineering, 2004, 91 (228): p. 261 – PMSE.
- 6) Huber, A, and Hinkley, J. A, *Impression Testing of Self-healing Polymers*. NASA, 2005, p. 1-12.
- 7) Rees, R, and Vaughan, D. J, *Polymer Preprints*. American Chemical Society, Division of Polymer Chemistry, 1965, (6): p. 287-295.

- 8) Ma, X., Sauer, J. A, and Hara, M, *Dynamic Mechanical Properties and Morphology*. Macromolecules, 1995, 28 (11): p. 3953 – 3962.
- 9) Tant, M.R, and Wilkes, G. L, *Viscoelastic Behaviour of Ionomers in Bulk and Solution*, in *Structure and Properties of Ionomers*. A. Eisenberg, Editor. 1987, D. Reidel Publishing Co.: Dordrecht. p. 191-226.
- 10) Eisenberg, A, and Kim J – S, *Introduction to Ionomers*. John Wiley and Sons, Inc. New York, 1998.
- 11) Eisenberg, A, and Rinaudo, M, *Polyelectrolytes and Ionomers*. Polymer Bulletin, 1990. 24 (6): p. 671-671.
- 12) Farrell, K. V, and Grady, B. P, *Effects of Temperature on Aggregate Local Structure in a Zinc Neutralized Carboxylate Ionomer*. Macromolecules, 2000. 33 (19): p. 7122- 7126.
- 13) Grady, B. P., Floyd, J. A., Gennetti, W. B., Vanhoorne, P, and Register, R. A, *X-ray absorption spectroscopy studies of zinc neutralized ethylene-methacrylic acid ionomers*. Polymer, 1999. 40 (2): p. 283 – 288.
- 14) Kuwabara, K, and Horii F. J, *Solid-state NMR analyses of the crystalline-noncrystalline structure and its thermal changes for ethylene ionomers*. Polymer Physics, 2002. 40 (11): p. 1142 – 1153.

- 15) Grady, B. P, *Effect of Co-neutralization on Internal Aggregate Structure in Ethylene Based Ionomers*. Macromolecules, 1999. 32 (9): p. 2893 – 2988.
- 16) Zhong, X. F, and Eisenberg, A, *Aggregation and Critical Micellization Behaviour of Carboxylate Terminated Monohelic Polystyrene*. Macromolecules, 1994. 27 (7): p. 1751 – 1758.
- 17) Cowan, J. C. and Teeter, H. M, Ind. Eng. Chem. 1994, 36: p. 48-152.
- 18) Eisenberg, A., Hird, B, and More, R. B, *A New Multiplet-Cluster Model for the Morphology of Random Ionomers*. Macromolecules, 1989. 23 (18): p. 4098 – 4107.
- 19) Lantman, C. W, and Macknight, W. J, *Structural Properties of Ionomers*. Annual Review of Material Science, 1989. 19: p. 295 – 317.
- 20) Kim, J-S., Nah, Y. H., Jarng, S-S., Kim, W., Lee, Y, and Kim, Y-W, *Clustering in poly(methyl acrylate) ionomers*. Polymer, 1999. 41 (8): p. 3099 – 3102.
- 21) Varley, R. J, and van der Zwaag, S, *Towards an understanding of thermally activated self-healing of an ionomer system during ballistic penetration*. Acta Materialia, 2008. 56 (19): p. 5737 – 5750.
- 22) Fall, R, *Puncture Reversal of Ethylene Ionomers – Mechanistic Studies*. Masters of Science in Chemistry, Blacksburg, Virginia, 2001.

- 23) Holiday, L, *Ionic Polymers*. Applied Science, London, 1975.
- 24) Eisenberg, A, and King, M, *Ion Containing Polymers: Polymer Physics*. Academic: New York, Volume 2, 1977.
- 25) Kutsumizu, S., Nagao, N., Tadano, K., Tachino, H., Hirasawa, E, and Yano S, *Effects of water sorption on the structure and properties of ethylene ionomers*. *Macromolecules*, 1992. 25 (25): p. 6829 – 6835.
- 26) Tadano, K., Hirasawa, E., Yamamoto, H, and Yano, S, *Order-disorder transition of ionic clusters in ionomers*. *Macromolecules*, 1989. 22 (1): p. 226 – 233.
- 27) Bellinger, M.A., Sauer, J. A, and Hara, M, *Tensile Fracture Properties of Rigid-Rigid Blends made of Sulfonated Polystyrene Ionomer and Polystyrene*. *Macromolecules*, 1994. 27 (21): p. 6147 – 6155.
- 28) Statz, R, *Ethylene Copolymer Ionomers, in History of Polyolefin's; The World's Most Widely Used Polymers*. R. B. Seymour, and T. Cheng, Editors. 1986, p. 177-182.
- 29) Rees, R, *Ionomeric thermoplastic elastomers early research-Elastomers: A Comprehensive Review*. N. R. Legge, G. Holden, and H. E. Schroeder, Editors. 1987, p. 231-243.

- 30) Varley, R, *Ionomers as Self-healing Polymers*. Self Healing Materials, S. van der Zwaag, Editor. 2007, p. 95-114.
  
- 31) Surlyn Product Sheets, <http://www.dupont.com/packaging/products/resins/E-48623-2/E48623-2.html>.
  
- 32) Jerome, R, and Mazurek, M, *Ionomers: Synthesis, Structure, Properties and Applications*. M. R. Tant, K. A. Mauritz, and G. L. Wilkes, Editors. Blackie Academic and Professional: London. 1997.
  
- 33) Kalista, Jr., S. J, and Ward, T. C, *Thermal characteristics of the self-healing response in poly (ethylene-co-methacrylic acid) copolymers*. Journal of the Royal Society, 2007, 4 (13): p. 405-411.
  
- 34) Van der Zwaag, S, *Self-Healing Materials; An Alternative Approach to 20 Centuries of Materials Science*. R. Hull, R. M. Osgood, Jr. J. Parisi, and H. Warlimont, Editors. 2007.
  
- 35) Kamphaus, J. M., Rule, J. D., Moore, J. S., Sottos, N. R, and White, S. R, *A new self-healing epoxy with tungsten (VI) chloride catalyst*. Journal of the Royal Society, 2007, 5: p. 95-104.



- 36) Brown, E. N., White, S. R, and Sottos, N. R, *Retardation and repair of fatigue cracks in a microcapsule toughened epoxy composite-part II: In situ self-healing*. Composites Science and Technology, 2005, 65: p. 2474-2480.
- 37) Yuan, Y. C., Yin, T., Rong, M. Z, and Zhang, M. Q, *Self-healing in polymers and polymer composites. Concepts, realization and outlook: A review*. Express Polymer Letters, 2008, 2 (4): p. 238-250.
- 38) Bergman, S. D, and Wudl, F, *Mendable Polymers*. Journal of Materials Chemistry, 2007, 18: p. 41-62.
- 39) Kessler, M. R, *Self-healing: a new paradigm in materials design*. Proceedings of the Institution of Mechanical Engineers, Part G: Journal of Aerospace Engineering, 2007, 221 (4): p. 479-495.
- 40) Ghosh, S. W, *Self-healing Materials: Fundamentals, Design Strategies, and Applications*. WILEY-VCH Verlag GmbH & Co. 2009.
- 41) Bergman, S. D, and Wudl, F, *Re-Mendable Polymers*. Self Healing Materials, van der Zwaag, Editor. 2007, p. 45-68.
- 42) Chujo, Y., Sada, K., Naka, A., Nomura, R, and Saegusa, T, *Synthesis and redox gelation of disulfide-modified polyoxazoline*. Macromolecules, 1993, 26 (5): p. 883-887.

- 43) Chung, C. M., Rob, Y. S., Cho, S. Y, and Kim, J. G, *Crack healing in polymeric materials via photochemical cyclo-addition*. Chemistry of Materials, 2004, 16 (21): p. 3982-3984.
  
- 44) Yin, T., Rong, M. Z., Zhang, M. Q, Yang, G. C, *Self-healing epoxy composites – Preparation and effect of the healent consisting of microencapsulated epoxy and latent curing agent*. Composites Science and Technology, 2007, 67 (2): p. 201-212.
  
- 45) Rule, J. D., Sottos, N. R., White, S. R, and Moore, J. S, *The chemistry of self-healing polymers*. Education in Chemistry, 2005, 42 (5): p. 130-132.
  
- 46) Dry, C, *Passive tuneable fibres and matrices*. International Journal of Modern Physics B, 1992, 6 (15-16): p. 2763-2771.
  
- 47) Dry, C, and McMillan, W, *Three-part methyl metha-crylate adhesive system as an internal delivery system for responsive concrete*. Smart Materials Structures, 1996, 5 (3): p. 297-300.
  
- 48) Dry, C, *Procedures developed for self repair of polymer matrix composite materials*. Composite Structures, 1996, 35 (3): p. 263-269.
  
- 49) Bleay, S. M., Loader, C. B., Hawyes, V. J, Humberstone, L, and Curtis, V, *A smart repair system for polymer matrix composites*. Composites Part A: Applied Science and Manufacturing, 2001, 32 (12): p. 1767-1776.

- 50) Pang, J. W. C, and Bond, I. P, *A hollow fibre reinforced polymer composite encompassing self-healing and enhanced damage visibility*. Composite science Technology, 2005, 65 (11-12): p. 1791-1799.
- 51) Pang, J. W. C, and Bond, I. P, *Bleeding Composites – damage detection and self-repair using a biomimetic approach*. Composite science Technology, 2005, 36 (2): p. 183-188.
- 52) Trask, R. S, and Bond, I. P, *Biomimetic self-healing of advanced composite structures using hollow glass fibres*. Smart Materials Structures, 2006, 15 (3): p. 704-710.
- 53) Williams, G, *A self-healing carbon fibre reinforced polymer for aerospace applications*. Composites Part A: Applied Science and Manufacturing, 2007, 38 (6): p. 1525-1532.
- 54) Trask, R. S, and Bond, I. P, *Self-healing of Composite Structures in a Space Environment*. 15<sup>th</sup> International Conference on Composite Materials (ICCM-15), Durban, SA, 27<sup>th</sup> June-1<sup>st</sup> July 2005.
- 55) Dry, C. M, *Self-repairing reinforced matrix materials*. Pub. No.: US 2008/0107888 A1. Pub. Date: May 8, 2008.

- 56) White, S. R., Sottos, N. R., Geubelle, P. H., Moore, J. S., Kessler, M. R., Sriram, S. R., Brown, E. N, and Viswanathan, S, *Autonomic healing of polymer composites*. Nature, 2001, 409: p. 794-797.
- 57) Brown, E. N., Kessler, M. R., Sottos, N. R, and White, J, *Microencapsul*. 2003, (20), 719.
- 58) Brown, E. N., Sottos, N. R, White, S. R, *Fracture Testing of a Self-healing Polymer Composite*. Experimental Mechanics, 2002, 42 (4): p. 372-379.
- 59) Kessler, M. R., Sottos, N. R, and White, S. R, *Self-healing structural composite materials*. Composites Part A: Applied Science and Manufacturing, 2003, 34 (8): p. 743-753.
- 60) Brown, E. N., White, S. R, and Sottos, N. R, *Microcapsule induced toughening in a self-healing polymer composite*. Journal of Materials Science, 2004, 39 (5): p. 1703-1710.
- 61) Rule, J. D, Sottos, N. R, and White, S. R, *Effect of microcapsule size on the performance of self-healing polymers*. Polymer, 2007, 48 (12): p. 3520-3529.
- 62) Li, H., Wang, R., Hu, H, and Liu, W, *Surface modification of self-healing poly (urea-formaldehyde) microcapsule using silane-coupling agent*. Applied surface Science, 2008, 255 (5): p. 1894-1900.

- 63) Blaiszik, B. J., Sottos, N. R., White, S. R., *Nanocapsule for self-healing materials*. Composite Science and Technology, 2008, 68 (3-4): p. 978-986.
  
- 64) Cho, S. H., Anderson, H. M., White, S. R., Sottos, N. R., and Braun, P. V., *Polydimethylsiloxane-Based Self-healing Materials*. Advanced Materials, 2006, 18 (8): p. 997-1000.
  
- 65) Keller, M. W., White, S. R., and Sottos, N. R., *A Self-healing poly (dimethyl Siloxane) Elastomer*. Advanced Functional Materials, 2007, 17 (): p. 2399-2404.
  
- 66) Yin, T., Rong, M. Z., Zhang, M. Q., and Yang, G. C., *Self-healing epoxy composites – Preparation and effect of the healent consisting of microencapsulated epoxy and latent curing agent*. Composite Science and Technology, 2007, 67 (2): p. 201-212.
  
- 67) Yin, T., Zhou, L., Rong, M. Z., and Zhang, M. Q., *Self-healing woven glass fabric/epoxy composites with healent consisting of micro-encapsulated epoxy and latent curing agent*. Smart Material Structures, 2008, 17 (1).
  
- 68) Yin, T., Rong, M. Z., Wu, J., Chen, H., and Zhang, M. Q., *Healing of impact damage in woven glass fabric reinforced epoxy composites*. Composites Part A: Applied Science and Manufacturing, 2008, 39 (9): p. 1479-1487.
  
- 69) Toohey, K. S., Sottos, N. R., Lewis, J. A., Moore, J. S., and White, S. R., *Self-healing materials with microvascular networks*. Nature, 2007 6: p. 581-585.

- 70) Williams, H. R., Trask, R. S, and Bond, I. P, *Self-healing composite sandwich structures*. Smart Material Structures, 2007, 16: p. 1198.
- 71) Williams, H. R., Trask, R. S, and Bond, I. P, *Self-healing sandwich panels: Restoration of compressive strength after impact*. Composites Science and Technology, 2008, 68 (15-16): p. 3171-3177.
- 72) Toohey, K. S., Hansen, C. J., Lewis, J. A., White, S. R, and Sottos, N. R, *Delivery of Two-Part Self-Healing Chemistry via Microvascular Networks*. Advanced Functional Materials, 2009, 19 (9): p. 1399-1405.
- 73) Hansen, C. J., Wu, W., Toohey, K. S., Sottos, N. R., White, S. R, and Lewis, J. A, *Self-Healing Materials with Interpenetrating Microvascular Networks*. Advanced Materials, 2009, 21 (41): p. 4143-4147.
- 74) Collins, D. J, *Damage Detection in Composite Materials using Acoustic Emission and Self-sensing Fibres*. Masters Thesis, University of Birmingham. 2009.
- 75) Wang, S., Chung, D. D. L, and Chung, J. H, *Self-sensing of damage in carbon fiber polymer-matrix composite by measurement of the electrical resistance or potential away from the damaged region*. Journal of Materials Science, 2005. (40): p. 6463 – 6472.

- 76) Hayes, S., Liu, T., Brooks, D., Montheith, S., Ralph, B., Vickers, S, and Fernando, G. F, *In situ self-sensing fibre reinforced composites*. Smart Material Structures, 1997. (6): p. 432 – 440.
- 77) Kister, G., Ralph, B, and Fernando, G. F, *Damage detection in glass fibre-reinforced plastic composites using self-sensing E-glass fibres*. Smart Material Structures, 2004. (13): p. 1166 – 1175.
- 78) Wang, S., Kowalik, D. P, and Chung, D. D. L, *Self-sensing attained in carbon-fiber-polymer-matrix structural composites by using the interlaminar interface as a sensor*. Smart Material Structures, 2004. (13): p. 570 -592.
- 79) British Standard, *Fibre-reinforced plastic composites — Determination of mode I inter laminar fracture toughness, GIC, for unidirectional reinforced materials*. BS ISO 15024: 2001.
- 80) DuPont Packaging and Industrial Resins; Surlyn Resins. *DuPont<sup>tm</sup> Surlyn<sup>®</sup> PC2000 data sheet*. Miracles of Science, March 2004.
- 81) DuPont Packaging and Industrial Resins; Surlyn Resins. *DuPont<sup>tm</sup> Surlyn<sup>®</sup> 9910 data sheet*. Miracles of Science, March 2004.
- 82) DuPont Packaging and Industrial Resins; Surlyn Resins. *DuPont<sup>tm</sup> Surlyn<sup>®</sup> 1706 data sheet*. Miracles of Science, March 2004.

- 83) Hirasawa, E., Yamamoto, Y., Tandano, K, and Yano, S, *Formation of ionic crystallites and its effect on the modulus of ethylene ionomers*. Macromolecules, 1989, 22 (6): p. 2776 – 2780.
- 84) Painter, P. C., Brozoski, B. A, and Coleman, M. M, *FTIR studies of calcium and sodium ionomers derived from an ethylene-methacrylic acid and copolymer*. Journal of Polymer Science: Polymer Physics Edition, 1982, 20 (6): p. 1069 – 1080.
- 85) Kutsumizu, S., Hara, H., Tachino, H., Shimabayashi, K, and Yano, S, *Infrared Spectroscopic Study of the Binary Blends of Sodium and Zinc Salt Ionomers Produced from Poly (ethylene-co-methacrylic acid)*. Macromolecules, 1999, 32 (19): p. 6340 – 6347.
- 86) Fukuda, K, *Infrared spectroscopic study for decalcification in the dentine*. Histochemistry and Cell biology, 1986, 6 (2): p. 127 – 130.
- 87) Siuzdak, D. A., Start, P. R, and Mauritz, K. A, *Surlyn/Silicate Hybrid Materials. I. Polymer In Situ Sol–Gel Process and Structure Characterization*. Journal of Applied Polymer Science, 2000, 77 (13): p. 2882 – 2844.
- 88) Lawson, E. E., Edwards, H. G. M, and Johnson, A. F, *FT Raman spectroscopic study of the wavenumber region 2800 – 2630  $\text{cm}^{-1}$  of selected organic compounds*. Spectrochimica Acta Part A: Molecular and Biomolecular Spectroscopy, 1995, 51 (12): p. 2057 – 2066.



- 89) Forsel, M., Fuson, N, and Josien, M, *Infrared band assignments for 2900 cm<sup>-1</sup> region methyl group vibrations in XC<sub>6</sub>H<sub>4</sub>OOCH<sub>3</sub>, XC<sub>6</sub>H<sub>4</sub>CH<sub>3</sub> and Xc<sub>6</sub>H<sub>4</sub>COCH<sub>3</sub>*. JOSA, 1960, 50 (12): p. 1228 – 1231.
  
- 90) Private communication with DuPont, *Surlyn® Refractive Indices*. ishtiaq.kaleem@gbr.dupont.com.
  
- 91) Miller, S. E., Marcatilli, E. A. J, and Li, T, *Research toward optical-fiber transmission systems. I. The transmission medium; II. Devices and System considerations*, 1973, 61: p. 1703-1751.
  
- 92) McCarthy, D., O’Keefe, S., Leen, G, and Lewis, E, *Optical fibre radiation for low dose applications*. Optical fibre research centre, University of Limerick, 2010.
  
- 93) Chung, D. D. L, *Carbon Fiber Composites, Materials Science/composites*, Butterworth and Heinmann, 1994.
  
- 94) Salmoriaa, G. V., Ahrens, C. H., Fredel, M., Soldi, V, and Pires, A. T. N, *Stereolithography somos 7110 resin: mechanical behavior and Fractography of parts post-cured by different methods*. Polymer Testing, 2005, 24 (2): p. 157–162.
  
- 95) Bonhomme, J., Arguelles, A., Vina, J, and Vina, I, *Fractography and failure mechanisms in static mode I and mode II delamination testing of unidirectional carbon fibre reinforced composites*. Polymer Testing, 2009, 28: p. 612-617.

- 96) Zhang, J, and Brownwyn, Fox, *Manufacturing process effects on the mode I interlaminar fracture toughness and nanocreep properties of CFRP*. Victorian centre for advanced materials manufacturing, School of Engineering and Technology, 2005.
- 97) Mathews, J. M, and Swanson, R. S, *Characterisation of the interlaminar fracture toughness of a laminated carbon/epoxy composite*. Composites science and technology, 2007, 67 (7-8): p. 1489-1498.
- 98) Baral, N., Davies, P., Baley, C, and Bigourdan, B, *Delamination behaviour of very high modulus carbon/epoxy marine composites*. Composite Science and technology, 2008, 68: p. 995-1007.
- 99) Mathews, M. J, and Swanson, S. R, *A numerical approach to separate the modes of fracture in interface crack propagation*. Journal of Composite Materials, 2007, 39 (3): p. 247-264.
- 100) Gregory, J. R, and Spearing, M. S, *A fiber bridging model for fatigue delamination in composite materials*. Acta Materialia, 52 (19): p. 5492-5502.